

In presenting this thesis in partial fulfillment of the requirements for an advanced degree at Idaho State University, I agree that the Library shall make it freely available for inspection. I further state that permission for extensive copying of my thesis for scholarly purposes may be granted by the Dean of the Graduate School, Dean of my academic division, or by the University Librarian. It is understood that any copying or publication of this thesis for financial gain shall not be allowed without my written permission.

Signature _____

Date _____

Physical and Numerical Modeling of a
Wave Impact Simulation Device
(WISD)

by
Rojin Tuladhar

A thesis
submitted in partial fulfillment
of the requirements for the degree of
Master of Science in the Department of Civil & Environmental Engineering
Idaho State University
Spring 2018

To the Graduate Faculty:

The members of the committee appointed to examine the thesis of Rojin Tuladhar find it satisfactory and recommend that it be accepted.

Dr. Bruce Savage
Major Advisor

Dr. Arya Ebrahimpour
Committee Member

Dr. Chad Pope
Graduate Faculty Representative

Dedication

This thesis work is dedicated to my wife, Priyanka, who has been a constant source of support and encouragement during the challenges of graduate school and life. This work is also dedicated to my parents, Rajesh and Rajani, who have always loved me and taught me the value of hard work.

Acknowledgments

I would like to express my gratitude to my thesis advisor Dr. Bruce Savage for his continuous support, motivation, and immense knowledge. Furthermore, I would like to thank Dr. Chad Pope for the opportunity to be a part of the Component Flooding Evaluation Laboratory team and for his encouragement and guidance on the research.

I thank my fellow mates, Soumadipta Jash and Larinda Nichols for the stimulating discussions, the time we spent working together, and all the fun we had on this journey.

Vita

Rojin Tuladhar was born on May 9, 1993, in Kathmandu, Nepal. In 2014 he received his undergraduate degree in Civil Engineering from Kathmandu University, Nepal. After working for 18 months in Total Management Services Pvt. Ltd., an engineering firm in Nepal, he was then accepted into the Civil Engineering master's program at ISU. He plans to pursue a professional career in water resources upon completion of his master's degree.

Table of Contents

| | |
|---|------|
| List of Figures | viii |
| List of Tables | xii |
| List of Equations | xiii |
| List of Abbreviations | xiv |
| Physical and Numerical Modeling of a Wave Impact Simulation Device (WISD) | xv |
| Abstract | xv |
| Introduction..... | 1 |
| Literature Review..... | 5 |
| Wave Theory | 5 |
| Tsunami Waves | 7 |
| Wave Impacts | 8 |
| Water Jets | 9 |
| Kinematics | 10 |
| Artificial Wave Generation | 11 |
| Physical Modeling..... | 15 |
| Computational Fluid Dynamics (CFD) | 16 |
| Governing Equations | 17 |
| Computational Grid | 18 |
| Fluid Surface..... | 18 |
| Solid Geometry | 19 |
| Boundary Conditions | 19 |
| General Moving Objects (GMO) | 20 |

| | |
|--|----|
| Methodology | 21 |
| Numerical Modeling..... | 21 |
| WISD (with gates) | 26 |
| WISD (without gates) | 28 |
| Kinematics | 30 |
| Physical Model Design (Sectional Model)..... | 32 |
| Physical Experimental Study..... | 35 |
| Component 1 (Air pressure chamber):..... | 36 |
| Component 2 (Solenoid Valves)..... | 37 |
| Component 3 (U-tube) | 39 |
| Results..... | 41 |
| WISD (with gates)..... | 41 |
| Design 1 (WD-45-1) | 41 |
| Design 2 (WD-45-2) | 42 |
| Design 3 (WD-45-3) | 43 |
| Design 4 (WD-35-1) | 44 |
| Design 5 (WD-35-2) | 45 |
| Design 6 (WD-35-3) | 46 |
| Design 7 (WD-25-1) | 47 |
| Design 8 (WD-25-2) | 48 |
| Design 9 (WD-25-3) | 49 |
| WISD (without gates)..... | 52 |
| Design 10 (WD-45-1-WG) | 53 |

| | |
|--|----|
| Design 11 (WD-45-2-WG) | 54 |
| Design 12 (WD-35-1-WG) | 55 |
| Design 13 (WD-35-2-WG) | 56 |
| Design 14 (WD-25-1-WG) | 56 |
| Design 15 (WD-25-2-WG) | 57 |
| Design 16 (WD-55-1-WG) | 58 |
| Design 17, 18, & 19 (WD-45-1-WG-1C, 2C, & 3C)..... | 60 |
| Design 20 (WD-45-1-WG-PHY)..... | 62 |
| Physical Experimental Study..... | 64 |
| Conclusions and Future work | 69 |
| References..... | 71 |
| Appendix A : Artificial wave generation references | 75 |
| Appendix B: Drawings for sectional physical model | 80 |
| Appendix C: Pressure transducers | 94 |
| Appendix D: Additional Wavefront Images from the physical experiment | 96 |

List of Figures

| | |
|---|----|
| Figure 1: Design J (Isometric View)..... | 3 |
| Figure 2: Wave section – Design J (Isometric View)..... | 3 |
| Figure 3: Areas of wave theory validity | 6 |
| Figure 4: Wave flume – Pump driven wavemaker | 12 |
| Figure 5: Large wave flume at Oregon State University | 13 |
| Figure 6: Directional wave basin at Oregon State University | 14 |
| Figure 7: Deltares delta flume..... | 15 |
| Figure 8: WISD Design J (Isometric view) | 22 |
| Figure 9: Mesh boundaries..... | 24 |
| Figure 10: Design 2, WD-25-2 (Isometric view)..... | 24 |
| Figure 11: Representation of gate opening | 27 |
| Figure 12: Prescribed motion for the gate..... | 27 |
| Figure 13: WD-45-1-WG (side view)..... | 29 |
| Figure 14: WD-35-2-WG (side view)..... | 29 |
| Figure 15: WD-55-1-WG (side view)..... | 29 |
| Figure 16: Control volume..... | 30 |
| Figure 17: General layout of the sectional physical model..... | 34 |
| Figure 18: Layout of the physical experiment study | 36 |
| Figure 19: Component 1- Air pressure chamber..... | 37 |
| Figure 20: Diagram of pneumatic system for pipe model. | 38 |
| Figure 21: Solenoid valves arrangement..... | 39 |
| Figure 22: Physical experiment study (orthographic view)..... | 40 |

| | |
|---|----|
| Figure 23: Component 3 (U-tube)..... | 40 |
| Figure 24: Velocity sensors | 40 |
| Figure 25: Design 8 (WD-25-2), orthographic view | 41 |
| Figure 26: Design 1 (WD-45-1)..... | 42 |
| Figure 27: Design 1 (WD-45-1) – wave profile at t = 0.8 seconds..... | 42 |
| Figure 28: Design 2 (WD-45-2)..... | 43 |
| Figure 29: Design 2 (WD-45-2) – wave profile at t = 0.8 seconds..... | 43 |
| Figure 30: Design 3 (WD-45-3)..... | 44 |
| Figure 31: Design 3 (WD-45-3) – wave profile at t = 0.8 seconds..... | 44 |
| Figure 32: Design 4 (WD-35-1)..... | 45 |
| Figure 33: Design 4 (WD-35-1) – wave profile at t = 0.4 seconds..... | 45 |
| Figure 34: Design 5 (WD-35-2)..... | 46 |
| Figure 35: Design 5 (WD-35-2) – wave profile at t = 0.4 seconds..... | 46 |
| Figure 36: Design 6 (WD-35-3)..... | 47 |
| Figure 37: Design 6 (WD-35-3) – wave profile at t = 0.6 seconds..... | 47 |
| Figure 38: Design 7 (WD-25-1)..... | 48 |
| Figure 39: Design 7 (WD-25-1) – wave profile at t = 0.8 seconds..... | 48 |
| Figure 40: Design 8 (WD-25-2)..... | 49 |
| Figure 41: Design 8 (WD-25-2) – wave profile at t = 0.85 seconds..... | 49 |
| Figure 42: Design 9 (WD-25-3)..... | 50 |
| Figure 43: Design 9 (WD-25-3) – wave profile at t = 0.9 seconds..... | 50 |
| Figure 44: Velocity vs time..... | 51 |
| Figure 45: Velocity vs time (25 degrees inlet – 2 ft. depth) | 52 |

| | |
|--|----|
| Figure 46: Design 10 (WD-45-1-WG)..... | 54 |
| Figure 47: Design 10 (WD-45-1-WG) – wave profile at t = 0.4 seconds..... | 54 |
| Figure 48: Design 11 (WD-45-2-WG)..... | 54 |
| Figure 49: Design 11 (WD-45-2-WG) – wave profile at t = 0.4 seconds..... | 55 |
| Figure 50: Design 12 (WD-35-1-WG)..... | 55 |
| Figure 51: Design 12 (WD-35-1-WG) – wave profile at t = 0.45 seconds..... | 55 |
| Figure 52: Design 13 (WD-35-2-WG)..... | 56 |
| Figure 53: Design 13 (WD-35-2-WG) – wave profile at t = 0.48 seconds..... | 56 |
| Figure 54: Design 14 (WD-25-1-WG)..... | 57 |
| Figure 55: Design 14 (WD-25-1-WG) – wave profile at t = 0.4 seconds..... | 57 |
| Figure 56: Design 15 (WD-25-2-WG)..... | 58 |
| Figure 57: Design 15 (WD-25-2-WG) – wave profile at t = 0.45 seconds..... | 58 |
| Figure 58: Design 16 (WD-55-1-WG)..... | 59 |
| Figure 59: Design 16 (WD-55-1-WG) – wave profile at t = 0.42 seconds..... | 59 |
| Figure 60: Velocity – vs – time (without gates) for geometries with: (a) 45 degrees; (b) 35 degrees; (c) 55 degrees and 25 degrees..... | 60 |
| Figure 61: Wave profile at t = 0.39 seconds | 61 |
| Figure 62: Wave profile at t = 0.39 seconds with 1 cell of fluid depth downstream..... | 61 |
| Figure 63: Wave profile at t = 0.39 seconds with 2 cell of fluid depth downstream..... | 61 |
| Figure 64: Wave profile at t = 0.39 seconds with 3 cell of fluid depth downstream..... | 61 |
| Figure 65: Design 20 (WD-45-1-WG-PHY) | 62 |
| Figure 66: Design 20 (WD-45-1-WG-PHY) – wave profile at t = 0.42 seconds | 63 |
| Figure 67: Velocity vs time – Design 20 (WD-45-1-WG-PHY)..... | 63 |

Figure 68: Wave profile generated by an inlet pressure of 2.75 psi 64

Figure 69: Velocity Results 66

Figure 70: Tongue produced by the wave..... 67

Figure 71: Chamber pressure vs U-tube pressure 67

List of Tables

| | |
|--|----|
| Table 1: Model – Prototype relations..... | 16 |
| Table 2: Various simulations conducted in FLOW 3D | 23 |
| Table 3: Varying pressure boundary | 25 |
| Table 4: Additional simulations conducted (without gates) | 29 |
| Table 5: Sectional physical model parameters..... | 32 |
| Table 6: Components of the physical model..... | 33 |
| Table 7: Motive pressures for each simulation | 53 |
| Table 8: Results from the physical experimental study | 65 |
| Table 9: Physical vs theoretical results for a chamber pressure of 2.75 psig (run 5) | 68 |

List of Equations

| | |
|---|----|
| Equation 1: Expression for horizontal speed of sinusoidal wave on the ocean | 6 |
| Equation 2: Shallow water wave celerity..... | 7 |
| Equation 3: Morison's equation..... | 8 |
| Equation 4: Newton's second law of motion | 10 |
| Equation 5: General pressure equation | 10 |
| Equation 6: Shear stress | 10 |
| Equation 7: Kinematic equation..... | 10 |
| Equation 8: Acceleration in terms of initial and final velocity..... | 10 |
| Equation 9: Continuity equation | 17 |
| Equation 10: Momentum equation..... | 17 |

List of Abbreviations

| | |
|-------|--|
| NPP | Nuclear Power Plant |
| CFEL | Component Flooding Evaluation Laboratory |
| CFD | Computational Fluid Dynamics |
| WISD | Wave Impact Simulation Device |
| FAVOR | Fractional Area/Volume Obstacle Representation |
| GMO | General Moving Objects |
| RANS | Reynolds-Average Navier Stokes |
| VOF | Volume of Fluid |
| LWF | Large Wave Flume |
| SPH | Smoothed Particle Hydrodynamics |
| FEM | Finite Element Method |
| RNG | Renormalized Group |
| STL | Stereolithographic |
| PVC | Polyvinyl Chloride |

Physical and Numerical Modeling of a Wave Impact Simulation Device (WISD)

Thesis Abstract – Idaho State University (2018)

Flooding is a huge concern to Nuclear Power Plants (NPPs) as experienced by the recent Fukushima Daiichi NPP failure. To improve probabilistic risk modeling of these circumstances, water rise, spray, and wave impact testing capabilities are being developed for the Component Flooding Evaluation Laboratory (CFEL) at Idaho State University.

This study concentrates on improving the previous design and analysis of a Wave Impact Simulation Device (WISD) by numerically generating steady waves and investigating further designs with different inlet angles and water depths. An experimental study is also conducted to analyze the influence of air pressure and behavior of water under these circumstances.

Steady-state and near vertical waves are successfully generated using kinematic theories via numerical and physical experimentations. The U-tube design with 45 degrees inlet and one-foot water depth produced the best results, and the concept of using air pressure as a motive force is deemed feasible through physical experiment.

Key Words: Wave, Wave Simulation, WISD, Numerical modeling, FLOW-3D

Introduction

Component Flooding Evaluation Laboratory (CFEL), a research laboratory at Idaho State University, concentrates on developing a better understanding of the risks and measures to be taken against potential threats posed by flood hazards to Nuclear Power Plants (NPPs). As part of the research for CFEL, this study focuses on improvements in the existing numerical model for a Wave Impact Simulation Device (WISD) and to conduct a physical experimental study to help validate the concept.

The WISD is an air driven wave generator capable of generating a wave traveling at 25.4 feet per second that is 10 foot high and 10 foot wide. It uses ten similar sections, each with a depth of one foot, stacked one on top of the other. After the air pressure is activated, the wave produced by each section combines to form a 10-foot wave section. Initially, the gates hold the water at rest and open quickly after the air pressure is activated. The design is based on the characteristics of a numerically simulated 20 foot tsunami wave studied by Roberts (2017).

Tsunamis are one of the most catastrophic natural events, generating floods that have proven to be a threat to nuclear facilities in the past. The March 2011 tsunami at the Fukushima Nuclear Power Plant (NPP) has clearly exposed the risk associated with flooding incidents in NPP's (Pool, 2011). The goal of the WISD is to allow testing and collecting information that can be applied to risk modeling studies of NPP components and facilities.

Most wave generators around the world use large wave basins and flumes which are expensive to construct and require large experimenting areas. These wave generators use solitary wave equations to produce tsunami-like wave behavior, however, some researchers believe solitary waves underestimate the total energy of a tsunami (Qu, Ren, & Kraatz, 2017). The WISD, instead of generating an artificial wave for impact testing, produces a high-velocity jet as

an alternative to simulate a high-velocity wave impact. Using high-velocity jets instead of waves avoids this debate and can economize available resources at the same time.

Roberts (2017) used a commercially available computational fluid dynamics (CFD) program, FLOW- 3D, which solves the Reynolds-averaged Navier-Stokes equations, to simulate tsunami waves and tsunami wave impacts. Tsunami waves with a height of 20 feet were simulated approaching a solid model, recording flow data such as peak impact forces, pressures, and velocities. This information was then used to direct the design of the WISD. The flow behavior of the tsunami wave was replicated in the numerical code using solitary wave assumptions. To provide a wide range of testing capability for wave impact tests, the maximum horizontal fluid velocity for a 20-foot tsunami wave, 25.4 feet per second, was the criteria used to meet CFEL requirements concluding Roberts's study on tsunami waves.

In addition, Roberts studied ten distinct designs to generate a wave in the laboratory traveling at a maximum velocity of 25.4 feet per second. A primary criteria for the design was to maintain a near vertical wavefront to imitate a tsunami wave traveling up an inclined beach. Roberts proposed Design J as the most viable WISD option for validation and further study. Design J used air pressure to provide the motive force for the water retained behind the bottom-hinged gates. Figure 1 and Figure 2 show the isometric view of Design J and the resulting wave section, respectively (Roberts, 2017).

Graphical plots for the velocity of the wave versus time from Roberts's simulations indicated the velocities are unsteady. However, one of the objectives for CFEL was to generate a steady wave that would conserve the maximum velocity of 25.4 feet per second for a considerable fraction of the total simulation. This study concentrates on developing a steady wave in addition to Roberts's research and design.

Different geometries, in terms of fluid depth and approach angle, are tested in quest of the best geometry to produce a steady velocity. To retain water in the storage tank, diverse options have been explored with and without gates. Furthermore, the results from the numerical simulations will be used in a physical model study to validate the concept. Results from the physical experimental study will be used to build a scaled down model of the WISD.

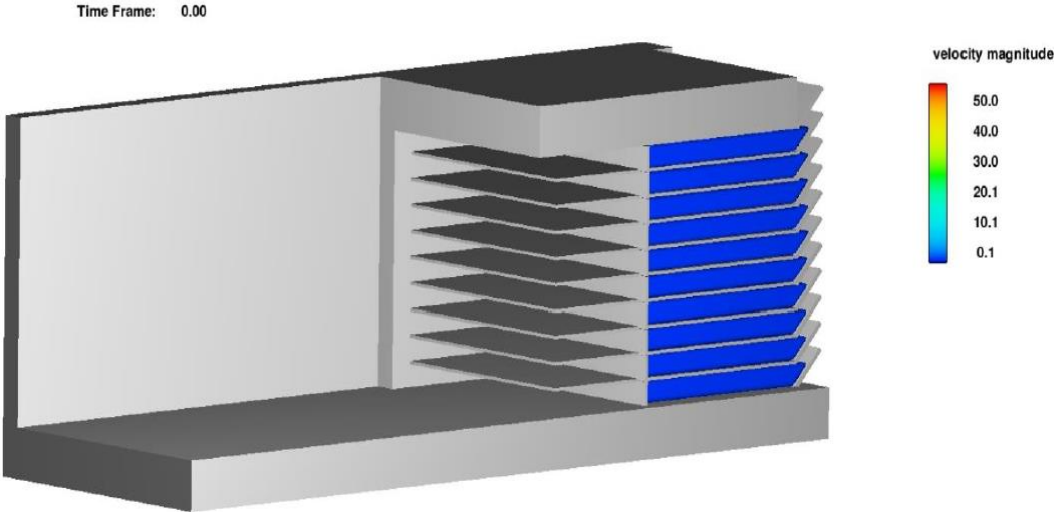


Figure 1: Design J (Isometric View)

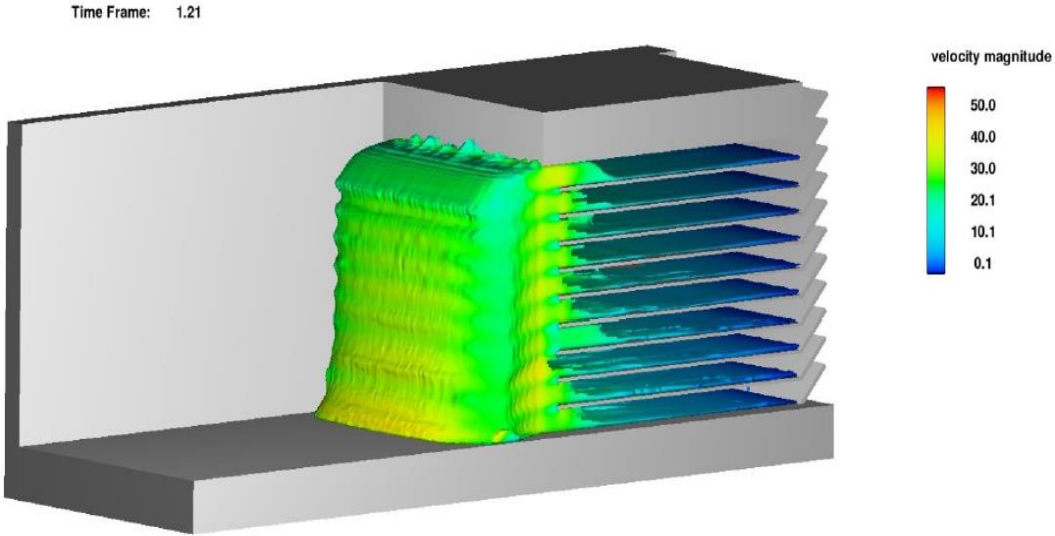


Figure 2: Wave section – Design J (Isometric View)

The scaled physical model of the prototype will be designed in a 1:5 scale ratio. The physical model will provide further insights of the selected design. Generating a 10 ft. high wavefront in a laboratory, conveying the energy of a tsunami wave, opens a new dimension of full-scale nuclear components and facilities testing under extreme flooding conditions. Most importantly, further improvements in the components and facilities can be developed to sustain such drastic events.

Literature Review

Numerous researches have been conducted to generate a laboratory scale wave with an objective to study the behavior, impacts, inundation flows and other aspects of an oceanic wave (Rabinovich, Geist, Fritz & Borrero, 2015). Concentrating on the physical and numerical modeling of a tsunami-like wave, laboratory generation techniques and modeling methodologies were investigated. Fluid kinematics and air pressure variability were explored to generate a steady state fluid motion. Existing wave flumes and basins around the world are also briefly discussed in this section.

Wave Theory

The foundation of ocean research is characterized by the identification of natural formation of waves and their behavior. Numerous wave theories have been developed to define the behavior of waves. Waves are characterized by their relative height and wavelengths. To describe these characteristics, the wave type that best represents the natural conditions is identified and represented by mathematical equations. The validity of these theories is limited to different ranges of wave parameters (height and wavelengths) and water depth as represented in Figure 3 (Apelt and Piorewicz, 1987).

The appropriate waveform can be identified to represent a model simply by using Figure 3. It can be observed that for shallow water close to the breaking zone, the linear theory cannot be used. Beyond the range of its validity, sinusoidal waves are commonly used to describe wave behavior because of its simplicity.

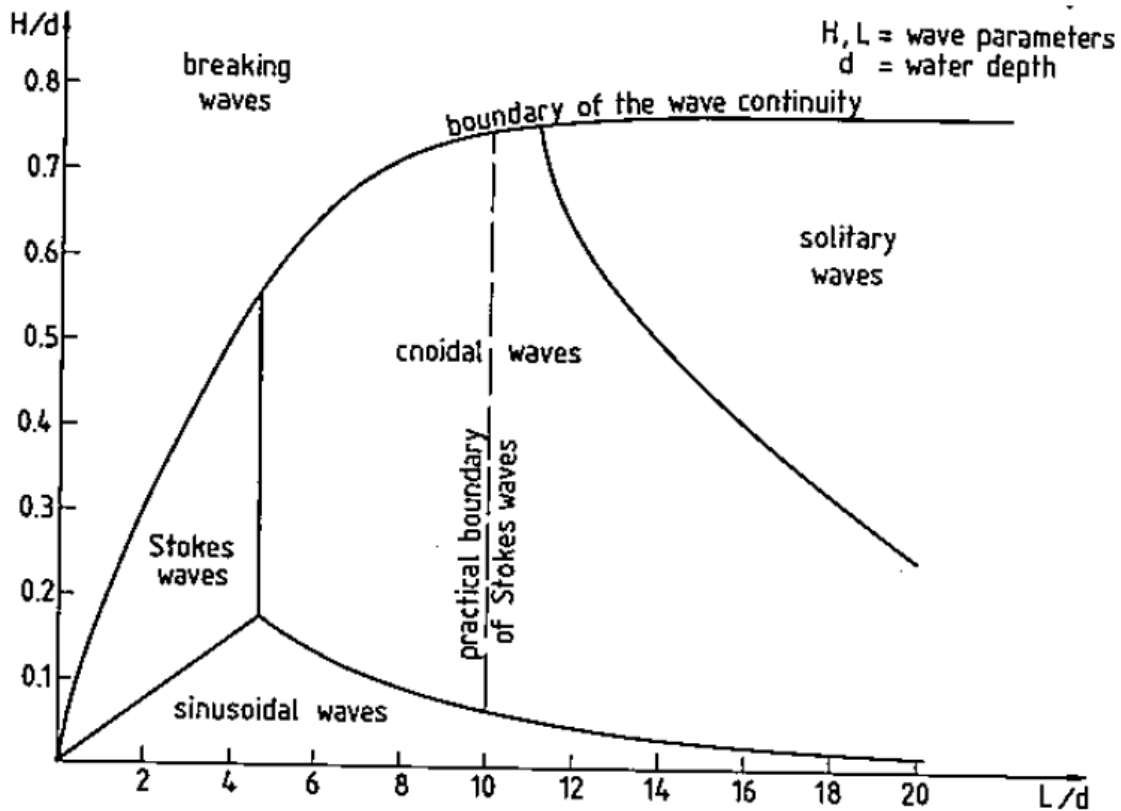


Figure 3: Areas of wave theory validity

An ocean wave can be represented as a periodic sinusoidal waveform as it travels and transfers the energy along its path (Mayo, 1997). The horizontal speed of a sinusoidal wave on the ocean is given by Equation 1.

$$c = \frac{\lambda}{T} = \sqrt{\frac{g \lambda}{2 \pi} \tanh\left(2 \pi \frac{d}{\lambda}\right)}$$

Equation 1: Expression for horizontal speed of sinusoidal wave on the ocean

Where “c” is the wave speed/wave celerity (meter per second), “λ” is the wavelength (meters), and “T” is the period (seconds); “d” is the fluid depth including the wave height (meters), and “g” is the gravitational field strength (meters per second square or newton per kilogram).

Speed is a function of both wavelength and depth of the water. Waves traveling in deep water, where the depth is compared to the wavelength, the ratio of d/λ in the hyperbolic tangent is large and can be approximated by unity. Thereby, the speed only depends on the wavelength in such cases.

In events where the wavelength is greater than the fluid depth by a factor of 20 or more, the equation serves only as a function of the fluid depth. This behavior of the flow is also known as shallow water wave behavior. Equation 2 is the modified form of Equation 1 that shows the wave celerity equation for shallow water waves (Mayo, 1997).

$$c = \sqrt{gd}$$

Equation 2: Shallow water wave celerity

Where “c” is the wave speed/wave celerity (meter per second), “g” is the gravitational field strength (meters per second square or newton per kilogram), and “d” is the fluid depth including the wave height (meters).

Tsunami Waves

The primary objective of this study was to conduct a physical experimental study and a numerical model study of a wave impact simulation device (WISD) that generates an extreme wave impact. To characterize a worst-case scenario, a tsunami wave was chosen by previous researchers in the project because of its capability for large wave heights and high wave celerity (Roberts, 2017).

Stressing on the limitations to generate a tsunami in a laboratory scale, researchers often use solitary waves to resemble tsunami waves (Goseberg, Wurpts & Schlurmann, 2013). A solitary wave has no trailing or preceding waves associated with it and has a long wavelength. At the same time, Goseberg et al. (2013) compared a prototype tsunami wavelength at the coast

with the laboratory-scale solitary waves that revealed a discrepancy of at least one order of magnitude which may misinterpret the results of an experiment while considering physical quantities like pressure or velocity. Goseberg et al. (2013) conducted tests using long waves to represent a tsunami wave. Madsen, Fuhrman, and Schaffer (2008) also questioned the use of solitary waves to replicate a tsunami in a laboratory along with Qu, Ren, and Kraatz (2017) who stated that solitary waves underestimate the total energy of a tsunami wave and the run-up distance. Alternatively, he recommended N-shaped waves give a more realistic approximation of the tsunami wave profile. As of present, it is still unclear, the type of wave that best resembles most characteristics of a tsunami.

Wave Impacts

The extensive use of coastal and offshore structures makes wave impact on shorelines important. The complexity involved with these wave-induced flow urges the use of empirical coefficients to expand the theoretical formulation. Broadly used calculations for forces generated by the wave is developed with the assumption that wave forces can be expressed as the sum of a drag force and an inertia force. Morison was the first to develop a mathematical formula for this assumption. An essentially horizontal force exerted by the wave on a vertical cylinder can be calculated from the general form of Morison's equation as shown in Equation 3 (Apelt and Piorewicz, 1987).

$$f = \frac{1}{2} \rho C_d D u |u| + \rho \pi \frac{D^2}{4} C_I \frac{du}{dt}$$

Equation 3: Morison's equation

Where ρ is the fluid density, C_d is the drag coefficient, D is the pier diameter, C_I is the inertia coefficient, u is wave velocity, and $\frac{du}{dt}$ is the wave acceleration (Apelt and Piorewicz, 1987). Apelt et al. (1987) has mentioned that this mathematical equation is acceptable, however,

choosing the empirical drag and inertia coefficients, C_d , and C_I , amongst a wide range of published values has made it particularly difficult.

Morison's equation was used by Apelt and Piorewicz to study the wave impacts on cylinders situated in the breaking zone and offshore zone close to the breaking point. Two cylinders and three different wave channels were used to carry out the experiment. The empirical coefficients for the object being impacted were determined data from using previous wave impact studies. It was concluded by this study that approximate values for the wave impact forces could be estimated, but Reynold's number regime and specific cylinder drag coefficients had to be developed for test conditions (Apelt and Piorewicz, 1987).

Water Jets

Generating waves in a laboratory requires large space and resources as learned from previous studies (Gent, 2015; Kirby, Ozkan-Haller, & Haller, 2007; Nimmala, Yim, & Grilli, 2013). With this in mind, previous researchers of CFEL opted for using ten rectangular jets of unit length height and 10 feet width, stacked one on top of the other, to simulate a wave section that is 10 feet high and 10 feet wide. It was also numerically simulated stacking up five jets with a depth of 2 feet which would not produce the desired wavefront. For the fluid to achieve a maximum speed of 25.4 feet per second, methods of developing the motive force were also studied (Roberts, 2017). Among the two techniques, air pressure and piston type, the air pressure was preferred over piston plates because of its practicality and affordability. Huge actuators tend to be expensive and the size of the actuators that would be required is not viable for this study.

In general, free water jets are used for other aspects of engineering. Free water jets from orifices are primarily described by empirical laws that involve energy equations. Flammer, Jeppson, and Keedy (1986) described the application of energy equation by solving free water jet

problems. The high velocities of a water jet would mostly denote a turbulent flow (Kraatz, 1965), which is the expected type of flow in this study as well.

Kinematics

Stacking up rectangular conduits to generate a wave using water jets can be challenging considering the lack of research that has been done so far. Roberts (2017) study presented its feasibility using numerical simulations. However, an objective of the CFEL is to produce a wave with a steady velocity which is studied further in this research. Kundu & Cohen (2008) excellently defined the general kinematics laws which were referred to solve for shear stress and wall friction that would ultimately result in stabilizing the celerity of the free jet. The following equations provided the foundation for the calculations:

$$F = m \cdot a$$

Equation 4: Newton's second law of motion

$$P = F/A$$

Equation 5: General pressure equation

$$\tau = \gamma \cdot R_H \cdot S_F$$

Equation 6: Shear stress

$$u_f^2 = u_i^2 + 2 \cdot a \cdot S$$

Equation 7: Kinematic equation

$$u_f = u_i + a \cdot t$$

Equation 8: Acceleration in terms of initial and final velocity

Where, “F” is the force exerted, “m” is the fluid mass and, “a” is the acceleration; “ τ ” is the shear stress, “ γ ” is the unit weight, “ R_H ” is the hydraulic radius and, “ S_F ” is the frictional

slope; “ u_i ” is the initial velocity, “ u_f ” is the final velocity, “ t ” is the time and “ S ” is the distance traveled by the fluid.

Kinematic theories were adapted to compute the ideal variation in air pressure using Equation 4, Equation 5, Equation 6, Equation 7, and Equation 8 mentioned in this particular section. Two pressures were generated, the initially applied pressure displaced the fluid to the design velocity and also dealt with the frictional resistance acted on the fluid by the solid. The second pressure was applied only to overcome the frictional resistance which would help maintain the constant velocity. The first pressure was applied for a certain amount of time as calculated by Equation 8, and the second pressure was applied for the remaining portion of the simulation.

Artificial Wave Generation

Goseberg et al. (2013) presented several wave generation techniques; piston-type wave generation, dam-break analogy, pump driven wave, vertical wave board motion, and volume driven wave generation. Among these, his paper concentrated on using pump driven waves to solve standard coastal engineering problems only requiring basic control theories. Figure 4 is the technical drawing of the closed-circuit flume at the Franzius-Institute for Hydraulic, Waterways, and Coastal Engineering in Germany (Goserberg et al., 2013).

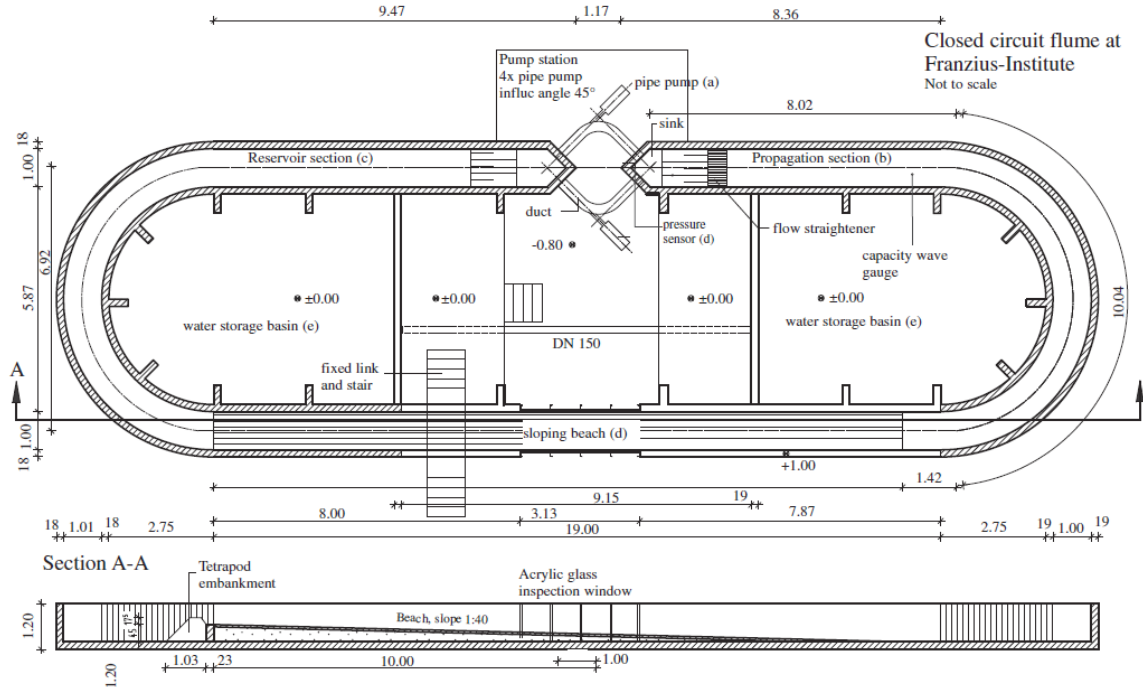


Figure 4: Wave flume – Pump driven wavemaker

The Large Wave Flume (LWF), located in Oregon State University, is the largest of its kind in North America. The LWF can generate tsunami waves and long waves, along with scaled shallow water hurricanes and storm waves. This LWF is 343 feet long, and 12 feet wide with a depth of 15 feet. Using a piston-type wavemaker, it can produce solitary wave heights up to 5.6 feet. It can generate a maximum stroke of 13.1 feet at a velocity of 13.1 feet per second (Kirby, Ozkan-Haller, & Haller, 2007). Figure 5 includes snapshots of the Large Wave Flume and a data sheet can be found in Appendix A for further information (Large Wave Flume, 2017).



Figure 5: Large wave flume at Oregon State University

Previously known as Tsunami Wave Basin, the Directional Wave Basin at Oregon State University was designed with a purpose to study the fundamental nature of a tsunami wave and its impact. This machine can produce regular, irregular, tsunami, and other user-defined waves with its unique snake-type piston wavemaker. With a length of 160 feet, a width of 87 feet, and a depth of 4.5 feet, this wave basin can produce waves up to a height of 4.5 feet and a maximum velocity of 6.6 feet per second (Nimmala et. al, 2013). Figure 6 includes images of the Directional Wave Basin and a data sheet can be found in Appendix A for additional information (Directional Wave Basin, 2017).



Figure 6: Directional wave basin at Oregon State University

The new Delta Flume, located at the Deltares Research Institute, Delft, Netherlands, is the world's largest artificial wave generator. It has a length of about 300 meters, a width of 5 meters, and a height of 9.5 meters, with the ability to generate waves up to 4.5 meters (14.8 feet). A piston-type wave board is used in this flume because of its superior performance on coastal applications (Gent, 2015). Figure 7 shows wave generations in Delta Flume and further information can be referred in Appendix A.

These wave basins and wave generators are simply outstanding considering their uniqueness and vast testing capabilities. However, none of these can fulfill CFEL's objective to produce a wave section that mimics a 20-foot wave traveling at a velocity of 25.4 feet per second for nuclear component testing.



Figure 7: Deltares delta flume

Physical Modeling

The world has already witnessed the possible threats posed by a tsunami. It has been necessary to gain an insight into the mechanisms of a tsunami formation highlighting its risks and life-changing events; especially on large energy plants costing billions to build and operate. Physical models of these types of waves help to understand tsunami formation and thus develop an early warning system to reduce casualties (Goseberg et al., 2013). Also, numerical modeling has been gaining wide popularity for its accuracy and flexibility. The ever-reliable physical models can be used to verify the results of the optimum designs from numerical models. Flammer et al. (1986) presented a step-by-step method with real-world examples to generate a model-prototype relationship, which was studied in depth for the design of the scaled down physical model of the prototype. Table 1 represents the model – prototype relationship from force ratio equations (Flammer et al., 1986).

Table 1: Model – Prototype relations

| | Froude's No. | Reynolds No. | Mach No. | Weber's No. |
|--------------------------------|--------------------------------|----------------------|------------------------------------|---|
| | $Fr_p = Fr_m$ | $Re_p = Re_m$ | $M_p = M_m$ | $We_p = We_m$ |
| Velocity_r = | $L_r^{1/2} g_r^{1/2}$ | V_r/L_r | $\sqrt{E_{v_r}/\rho_r}$ | $\sigma_r^{1/2}/\rho_r^{1/2} L_r^{1/2}$ |
| Time_r = | $L_r^{1/2}/g_r^{1/2}$ | L_r^2/v_r | $L_r \rho_r^{1/2}/E_{v_r}^{1/2}$ | $L_r^{3/2} \rho_r^{1/2}/\sigma_r^{1/2}$ |
| Flow Rate_r = | $L_r^{5/2} g_r^{1/2}$ | $L_r v_r$ | $L_r^2 E_{v_r}^{1/2}/\rho_r^{1/2}$ | $L_r^{3/2} \sigma_r^{1/2}/\rho_r^{1/2}$ |
| Force_r = | $\gamma_r L_r^3$ | $\rho_r v_r^2$ | $E_{v_r} L_r^2$ | $\sigma_r L_r$ |
| Pressure_r = | $\gamma_r L_r$ | $\rho_r v_r^2/L_r^2$ | E_{v_r} | σ_r/L_r |
| Power_r = | $g_r^{1/2} \gamma_r L_r^{7/2}$ | $\rho_r v_r^3/L_r$ | $E_{v_r}^{3/2} L_r^2/\rho_r^{1/2}$ | $\sigma_r^{3/2} L_r^{1/2}/\rho_r^{1/2}$ |

The subscript “r” denotes the ratio of the model and the prototype, subscript “p” and “m” denote model and prototype respectively. It is necessary to accurately follow principles from the literature to acquire quantities for a prototype from a model or vice-versa. Depending on the nature of the study, either of the dimensionless quantities mentioned in the columns of Table 1 is assumed to be the same for the model and the prototype. In some cases, more than one dimensionless parameters are assumed to be the same.

Computational Fluid Dynamics (CFD)

Numerical modeling is widely gaining popularity for its efficient nature and ability to model complex fluids problems. There are several methods for modeling and computing numerical models; some of which are Finite Volume Method (Versteeg & Malalasekera, 2007), Smoothed Particle Hydrodynamics (SPH) method (Monaghan, 1992) and Finite Element Method (FEM) (Dhatt, Lefrançois & Touzot, 2012). The Computational Fluid Dynamics (CFD) code, FLOW-3D, which uses a Finite Volume Method, is used for this study. Because it uses a finite volume method in a regular hexagonal grid, the form of the employed discrete equations is

similar to discrete equations in finite difference method (Taghavi & Ghodousi, 2016). This numerical code is well known for modeling flows with free water surface and complex geometries. A unique post-processing tool named Flow-Sight has excellent abilities to portray the results of a simulation.

Governing Equations

Equations governing fluid flow are based on the law of conservation of mass and the law of conservation of momentum for incompressible flow as shown in Equation 9 and Equation 10. These equations are a modification of the Reynolds-Average Navier- Stokes (RANS) equations including variables that allow algorithms to track the free surface and to model the geometry as a flow obstruction. The equations simulate three-dimensional flow including continuity relations and movement size in x, y and z directions.

$$\frac{\partial}{\partial x}(uA_x) + \frac{\partial}{\partial y}(vA_y) + \frac{\partial}{\partial z}(wA_z) = 0$$

Equation 9: Continuity equation

$$\frac{\partial U_i}{\partial t} + \frac{1}{V_F} \left(U_j A_j \frac{\partial U_i}{\partial x_j} \right) = -\frac{1}{\rho} \frac{\partial P'}{\partial x_i} + g_i + f_i$$

Equation 10: Momentum equation

The variables u, v and w denote the velocities in the x, y, and z directions; V_F is the volume fraction of fluid in each cell; A_x , A_y , and A_z indicate the fraction of open level in x, y, and z directions.; ρ is the density; P' is defined as the pressure, and g_i is the gravitational force in the subscript direction. The variable f_i represents the Reynolds stresses, provided by the selected turbulence model (Johnson & Savage, 2001). There are eight available turbulence options in FLOW-3D such as the standard k- ϵ model (Harlow & Nakayama, 1968) and Renormalized Group (RNG) k- ϵ model (Yakhot & Smith, 1992).

Computational Grid

Most Computational Fluid Dynamics (CFD) codes depend on the subdivision of space into a grid of discrete volume elements in which average values of flow variables can be defined. FLOW-3D uses the simplest kind of grid composed of rectangular-shaped elements defined by a set of planes perpendicular to each of the coordinate axes generating a hexahedron around the domain. Difference equations are simpler in comparison to non-structured grids. Numerical approximations to partial differential equations include the rate of change of spatial and temporal values of physical quantities, which improves the accuracy associated with finite difference equations when uniform grid elements are used. However, it is difficult to accommodate complex geometries using a rectangular mesh limiting their usefulness.

Different rectangular mesh blocks can be used to define a domain using various cell sizes. Defining mesh planes at desired locations generate a variable spaced block allowing more efficiency in the gridding of complex geometric regions. Finer meshes can be embedded into a coarser mesh depending on the problem setup and precision of the desired result. These rectangular meshes could be efficiently used to open up memory and urges solver routines to basically run through a list of active grid elements to further save computational time (FLOW-3D user manual, 2017).

Fluid Surface

To analyze, describe, and apply appropriate boundary conditions on a free surface, FLOW-3D uses the Volume of Fluid (VOF) method (Hirt & Nichols, 1981). This method operates by determining the volume of fluid within each discretized cell. An empty cell receives a value of zero, and, a value of one is assigned if a cell is full. A free surface is represented in a cell with a value between 0 and 1 that correlates to the ratio of fluid volume to cell volume.

Solid Geometry

FLOW-3D uses a grid porosity technique called Fractional Area/Volume Obstacle Representation (FAVOR) method to define the solid geometries in 3D using computational cells (Hirt & Sicilian, 1985). A porosity of zero is assigned to solid regions and a porosity of one is assigned to nonsolid regions. Like the VOF method, cells with both obstacle and flow volume are assigned a value per the ratio of the volume of the obstacle to the volume of the cell (FLOW-3D user manual, 2017).

Boundary Conditions

The boundary conditions defined by the user must accurately represent the physical occurrence of a flow. It is very important in every simulation as it directly affects the simulation results. Since a hexahedron is used to define the flow domain in Cartesian coordinates, there are six different boundaries on the mesh, in addition to the obstacle surface (Johnson & Savage, 2001; Babaali, Shamsai & Vosoughifar, 2015). Ten different boundary conditions are possible in FLOW-3D which are well defined by Flow Science, Inc. in the software user manual (2017).

A continuative boundary sets a zero-gradient condition at a boundary. This zero-derivative condition is intended to represent a smooth continuation of the flow through a boundary.

A grid overlay boundary is used to apply the solution derived from a restart source simulation as a boundary condition in a restart simulation.

A Sommerfeld radiation condition to dynamically estimate the conditions at the boundary can be defined using an outflow boundary. It can be used for incompressible flows that are confined or even for a free surface flow. It can also be used for entirely compressible flows.

Periodic boundaries are applied in pairs, meaning two boundaries have to be defined as a periodic boundary. Any fluid that exits through one boundary is re-entered through the other boundary that is defined in the pair.

If it is desired to define a specific pressure on a boundary, specific pressure boundary can be used. If the fluid elevation is also specified, a hydrostatic distribution is followed by the pressure at the boundary.

Specified velocity boundary condition defines a specific velocity at the boundary. Similarly, volume flow rate boundary specifies a flow at the selected boundary.

A zero-gradient condition at the boundary, along with a zero velocity condition normal to the boundary can be defined by a symmetry boundary.

Wall boundary applies the no-slip condition at the boundary and a zero velocity condition normal to the boundary.

Wave boundary generates a velocity field associated with the desired wave type. Solitary waves, Stokes waves, Cnoidal waves are few of many types of waves that can be applied to a boundary using this boundary condition

General Moving Objects (GMO)

If a rigid body requires being in any kind of motion, a six-degrees-of-freedom or motion constraints such as a fixed axis/point can be prescribed in FLOW-3D. Two types of motion, either a user-defined or a dynamically coupled motion is offered by this code. User-defined forces and torques on a general moving object can define a desired motion, whereas, independent motions including collision and continuous contact can also be used for multiple rigid bodies (FLOW-3D user manual, 2017).

Methodology

Generating a wave in a laboratory that characterizes a tsunami can be challenging with respect to multiple aspects. For example, the laboratory space available at Idaho State University and the number of resources that would be spent on building this device could be cost prohibitive. So, meticulous design and rigorous pre-testing are necessary. Numerical model study and physical experimental study would identify any defects in the design of the Wave Impact Simulation device (WISD).

Previous researchers for CFEL have brilliantly designed the mechanism of the WISD. However, for better performance of the device, these questions remain unanswered: How should the air pressure be varied to produce a constant velocity in the jet? Which geometry, in terms of fluid entrance depth and approach angles, will yield a near vertical wave profile? Does a system with gates produce a near vertical wave profile, or does the system without gates yield a near vertical wave profile? This study was engineered to determine the optimum set of air pressures and geometry to create the ideal tsunami-like wave for component and facilities testing.

Numerical Modeling

To solve for the optimal geometry and the most favorable air pressure pattern, the Reynolds-averaged Navier-Stokes (RANS) equations were solved numerically with a commercially available Computational Fluid Dynamics (CFD) code from Flow Science, Inc., FLOW-3D, which uses the finite volume technique.

Using CFD simulations, Roberts (2017) concluded the best motive force to be air pressure over other options like pistons. He tested the different designs of a general geometry for the WISD with the goal to produce a maximum velocity of 25.4 feet per second. A major advantage of using air pressure over another possible method to generate the motive force,

pistons, was the flexibility to use different fluid depths by dividing it into discrete channels. Figure 8 shows the best-proposed design (Design J) from Roberts's numerical modeling (Roberts, 2017).

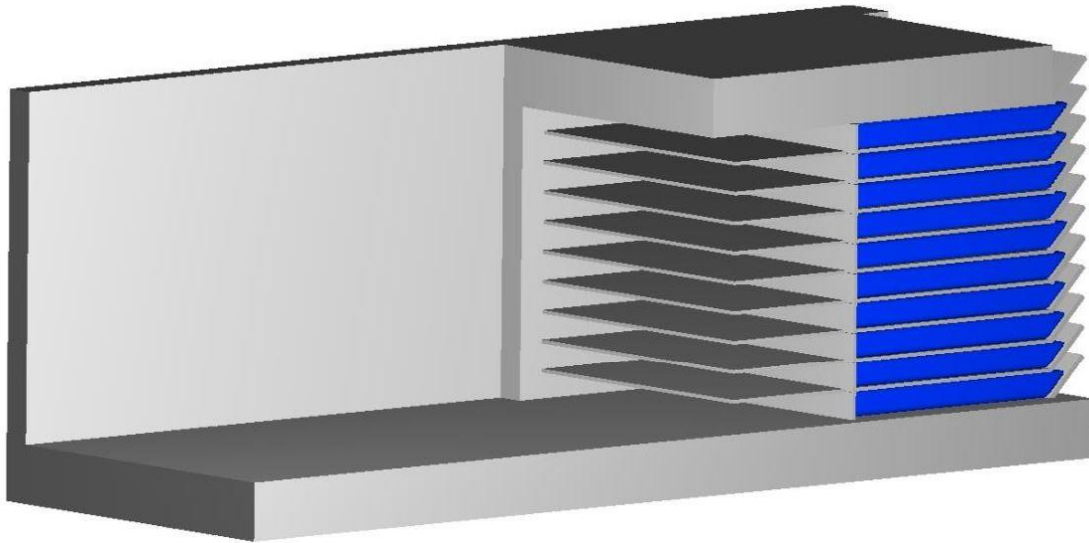


Figure 8: WISD Design J (Isometric view)

The motive force needs to provide a large force to initiate motion in water and then reduce to maintain a steady fluid velocity by overcoming the frictional forces. To reduce the computational time to compute a transient motive force, a sectional model was considered using only one section of the jet. In addition, modifications to the section were made, looking for the most effective arrangement to apply air pressure to displace the water by considering differently angled inlets and fluid depths. Table 2 shows the various simulations that were conducted in search of the optimum geometry. Parameters like wave profile and velocity were considered to compare the different geometries.

Table 2: Various simulations conducted in FLOW 3D

| Design No. | Design ID. | Inlet Angle (In degrees) | Fluid Depth (ft.) |
|------------|------------|--------------------------|-------------------|
| 1 | WD-45-1 | 45 | 1 |
| 2 | WD-45-2 | 45 | 2 |
| 3 | WD-45-3 | 45 | 3 |
| 4 | WD-35-1 | 35 | 1 |
| 5 | WD-35-2 | 35 | 2 |
| 6 | WD-35-3 | 35 | 3 |
| 7 | WD-25-1 | 25 | 1 |
| 8 | WD-25-2 | 25 | 2 |
| 9 | WD-25-3 | 25 | 3 |

3-D solid geometries of the WISD were designed in AutoCAD, and, a stereolithographic file format was used to import it into Flow-3D. A rectangular grid, with a mesh size of 0.02 feet defined the flow domain in Flow-3D which divides one foot into 50 cells. Grid convergence tests were not conducted in this study as it has already been tested in previous research (Roberts, 2017). The pressure was applied through the top boundary, i.e. Z_{max} boundary. The adjacent side boundaries, and the bottom boundary, Y_{min} , Y_{max} , and Z_{min} , respectively, were defined as walls and the downstream boundary, X_{max} , was set as outflow to allow free flow out of the simulation. The X_{min} boundary was also defined as a wall. Figure 9 represents the definitions of each boundary. Also, Figure 10 shows the initial setup for an inlet inclined at 25 degrees with a depth of 2 foot. The fluid moves from the right boundary to the left direction.

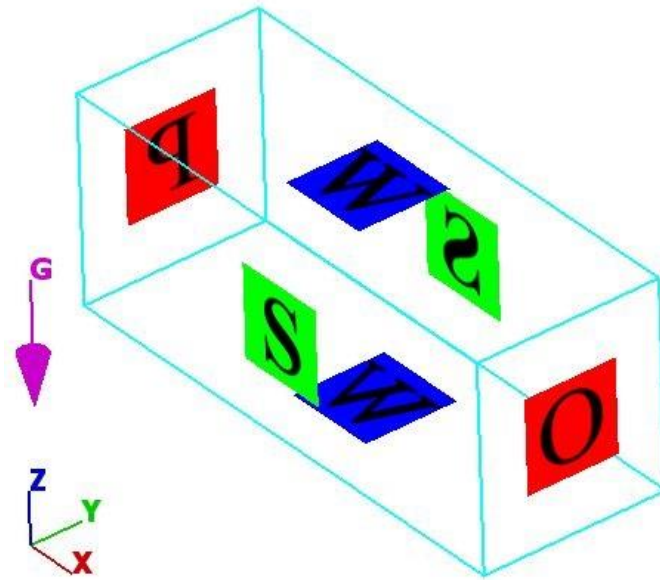


Figure 9: Mesh boundaries

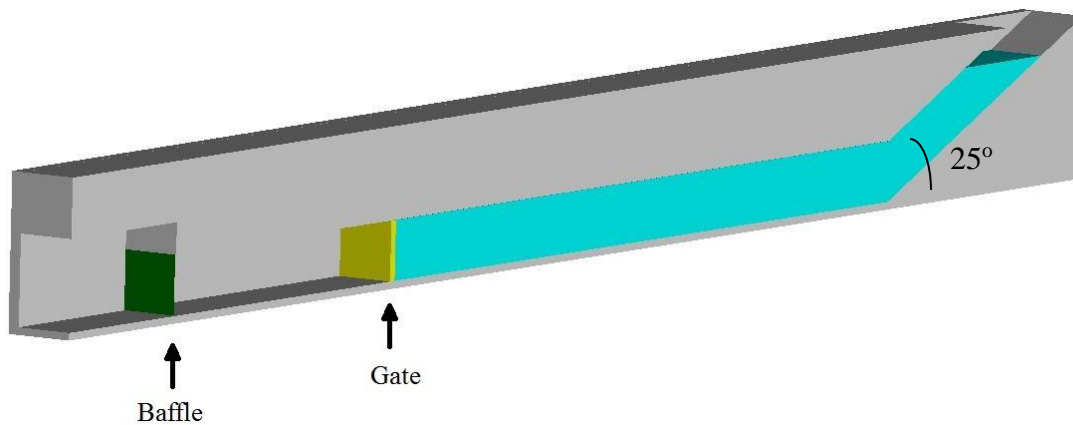


Figure 10: Design 2, WD-25-2 (Isometric view)

A bottom hinged watertight gate was placed downstream to retain the water in the reservoir. To measure the flow rate exiting the chamber, a baffle was placed at the same location for all arrangements. These numerical baffles do not impede or change the flow, rather they were used to better understand the fluid behavior. The yellow component on the left end in Figure 10 represents the baffle. Immediately downstream of the baffle, the height of the channel was increased to replicate an open channel flow where the wave profile was observed. The

motive air pressure was set to 625 psf. (lbs. /ft²) for the simulations from an initial time, t = 0 seconds to 1.5 seconds; 1.5 seconds being the total time of the simulation (Roberts, 2017). All the simulations behaved quite similar. Results show that the fluid would rapidly accelerate at t = 0.8 seconds to a maximum velocity without maintaining it.

Although these simulations provide good information on the behavior of the motive force, one of the goals of the WISD is to have a fairly constant velocity for a considerable portion of the total time frame, which did not occur. To modify the flow behavior, at approximately t = 0.8 seconds, the motive air pressure was decreased sharply starting from t = 0.8 seconds. This was applied to one simulation with an inlet depth of one foot and a 45 degrees angle. The varying inlet air pressure is shown in Table 3. The resulting velocity was fairly constant.

Table 3: Varying pressure boundary

| Time (secs.) | Pressure (psf.) |
|---------------------|------------------------|
| 0 | 625 |
| 0.3 | 625 |
| 0.6 | 625 |
| 0.8 | 625 |
| 0.9 | 75 |
| 1.2 | 50 |
| 1.5 | 0 |

Using the assumption that the water moves as a solid block through the conduit and applying general kinematic equations and Newton’s second law of motion which are mentioned in the literature, it was determined that a certain pressure force of 2144.1 lbs. /ft² was required to accelerate the water to a velocity of 25.4 feet per second. This supplies the necessary inertial force to start the water moving. And, once the water “block” achieved the desired velocity, the only the force needed to maintain this velocity was a force to match the shear stress of the water acting on the structure walls. Computing Equation 6 for a geometry with a 25 degrees inlet angle

and a fluid depth of 2 feet showed that a pressure of 30.0 lbs. /ft² will maintain the motion. It is expected that this will be applied over a time frame 0.39 seconds to 1.5 seconds.

The motive pressure force and the shear stress required is a function of the volume of water and the cross-section of the conduit, respectively. Hence, it is different for various geometries and fluid depths.

WISD (with gates)

Another important component for the WISD was the gates. These mechanical sections have to withstand the hydrostatic pressure from the retained fluid behind it with minimum possible leakage. Also, these gates had to be designed in such a way that at the exact moment when the air pressure would hit the water, they have to open quickly allowing the fluid to move. This principle was adopted so that the air pressure behind the fluid would not add forces on to the gate, and thinner gates could be used with strength enough to withstand the hydrostatic pressure of the resting water. These gates on opening were supposed to merge on to the plates underneath, without influencing the wave profile, so thick gates are not an option. Nichols (2018) designed and analyzed the gates, fulfilling all the standards and criteria of the research. A snapshot of the gate holding water is shown in Figure 10.

Using the general feature of FLOW-3D to assign the gate as a moving object, it was hinged at its bottom and was assigned to rotate at the gate axis in the flow direction. Figure 11 shows the gate opening on its bottom axis, allowing the fluid to move upon the action of air pressure.

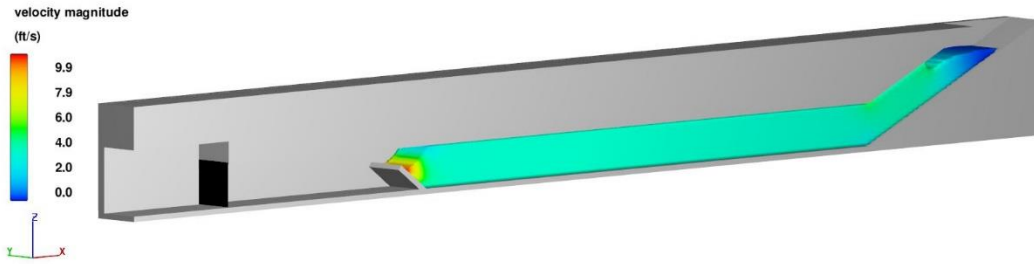


Figure 11: Representation of gate opening

A motion was prescribed to the gate component manually, and directional limitations were assigned to the gate so that it would merge with the solid plate located below. An angular velocity of magnitude -31.416 radians per second was assigned as shown in Figure 12.

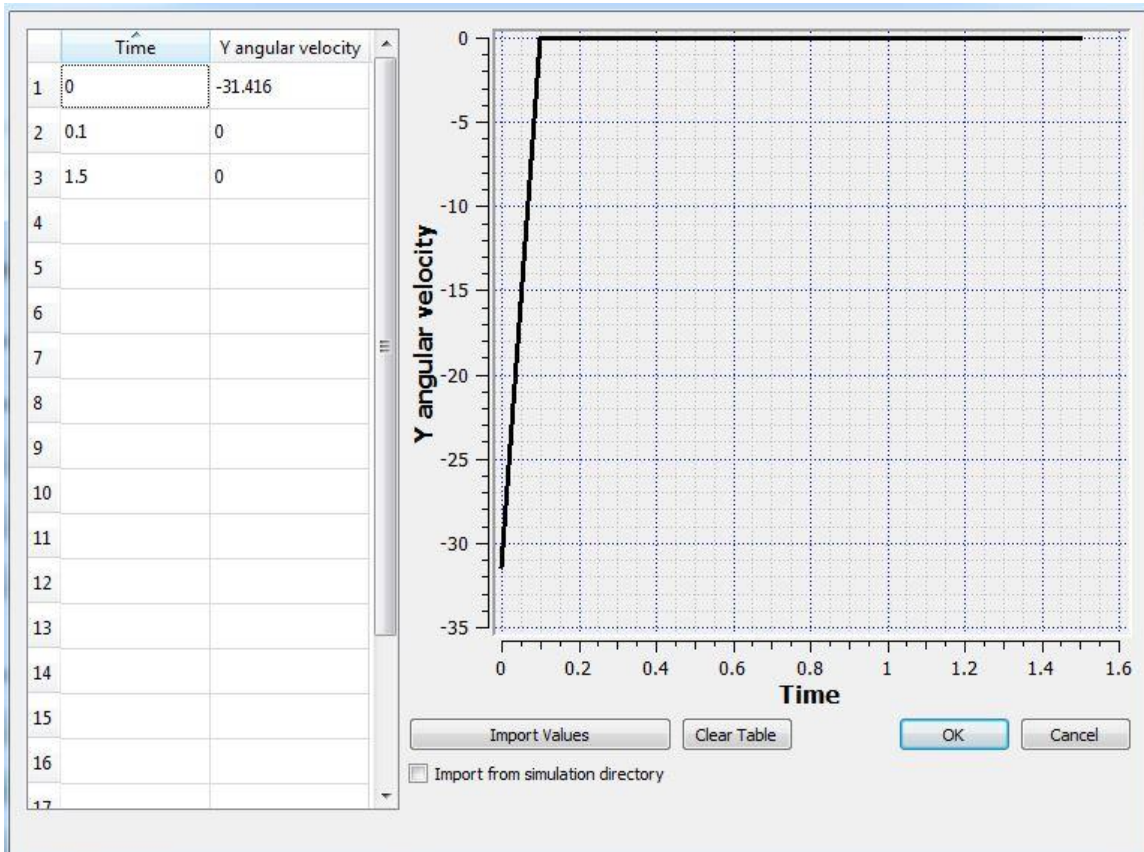


Figure 12: Prescribed motion for the gate

WISD (without gates)

The gates used in the WISD produced excellent results, however, another option was also explored excluding the gate. For this case, a U-tube shape was used to retain the fluid and similar to the option with the gate, air pressure was used to apply the motive force. The inlet and outlet were inclined, and different angles and depths were adopted to produce a steady state water jet with a near vertical wave profile. It was necessary for the inlet and outlet to be inclined but not at 90 degrees, as a larger space would be required in the laboratory for construction of the full-scale prototype. If U-tubes with vertical inlets or outlets would have been used, when stacked one on top of the other, the lower tubes would require being longer than the ones on top. This was deemed unfeasible due to this constraint.

Similar to the models with the gate, 3-D solid geometries of the U-tube model were designed in AutoCAD, and, a stereolithographic file (STL) format was used to import it into FLOW-3D. A rectangular grid defined the flow domain with a mesh size of 0.02 feet. The pressure was applied through the X_{\min} boundary. Simulating these settings as a 2-D simulation, the adjacent boundaries, Y_{\min} and Y_{\max} , were defined as symmetry boundaries and the top and bottom boundary, Z_{\min} , and Z_{\max} were defined as walls with the downstream boundary, X_{\max} , set as outflow to allow free flow out of the simulation. The Z_{\min} boundary was also defined as a wall. Table 4 is a list of simulations that were conducted without gates in the WISD. Figure 13, Figure 14, and Figure 15 are side views of some two-dimensional WISD simulations without gates.

Table 4: Additional simulations conducted (without gates)

| Design No. | Design ID | Inlet Angle (In degrees) | Fluid Depth (ft.) |
|------------|----------------|--------------------------|-------------------|
| 10 | WD-45-1-WG | 45 | 1 |
| 11 | WD-45-2-WG | 45 | 2 |
| 12 | WD-35-1-WG | 35 | 1 |
| 13 | WD-35-2-WG | 35 | 2 |
| 14 | WD-25-1-WG | 25 | 1 |
| 15 | WD-25-2-WG | 25 | 2 |
| 16 | WD-55-1-WG | 55 | 1 |
| 17 | WD-45-1-WG-1C | 45 | 1 |
| 18 | WD-45-1-WG-2C | 45 | 1 |
| 19 | WD-45-1-WG-3C | 45 | 1 |
| 20 | WD-45-1-WG-PHY | 45 | 1 |



Figure 13: WD-45-1-WG (side view)



Figure 14: WD-35-2-WG (side view)



Figure 15: WD-55-1-WG (side view)

After observing the wave profiles from the simulation results in FLOW-3D, the 45 degrees inlet/outlet with a water depth of 1 feet produced the best uniform velocity and vertical faced wavefront. To make improvements in the wave profile, additional simulations were completed on Design 10 (WD-45-1-WG) with a thin layer of water placed downstream of the

gate. The rationale was that the water layer would impede the lower portion of the wavefront, helping to maintain the upper portion of the wave by decelerating the lower portion, thus, producing a near vertical wave better than the preliminary simulation. Three simulations were run including a thin film of water with depths of one cell, two cells, and three cells; the cell size of the FLOW-3D setup being 0.02 ft.

Kinematics

As mentioned before, water was assumed to be a solid block which does not change its shape under application of forces. Using Equation 4, Equation 5, Equation 6, Equation 7, and Equation 8, the motive force required to displace the fluid was calculated. In addition, the force required to maintain the expected velocity was also calculated. Example calculation for Design 20 is shown below. Figure 16 shows the forces applied to the control volume.

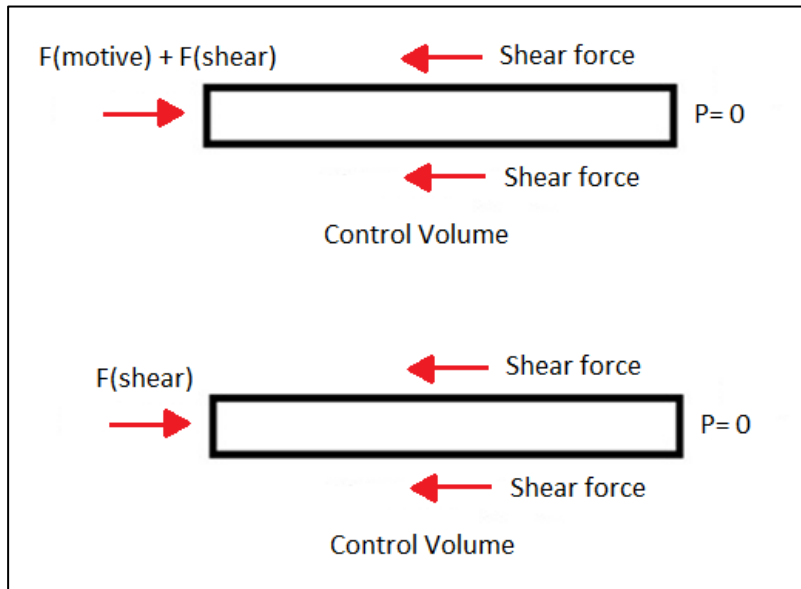


Figure 16: Control volume

Known Parameters:

| | | |
|--|------------------------------|-------------------------------------|
| Diameter of Pipe (D): | 4 in. | |
| Volume of water (V): | 0.32 ft. ³ | Calculated from AutoCAD drawing |
| Area: $A = \pi r^2 =$ | 0.087 ft. ² | |
| Wetted Perimeter (P) = $\pi \cdot D =$ | 1.05 ft. | |
| Initial velocity (u _i): | 0 ft. /s | |
| Final velocity (u _f): | 11.3 ft. /s | Scaled down velocity from prototype |
| Development Length (S): | 3 ft. | |
| Surf. Roughness for PVC (f): | 0.012 | |
| Fluid Density (ρ): | 62.29 lbm. /ft. ³ | |
| Fluid Mass = $\rho \cdot V =$ | 19.93 lbm. | |
| Acceleration due to gravity (g) | 32.2 ft. /s ² | |
| Friction Loss (S _f) = $\frac{4 \cdot f \cdot u_f^2}{A \cdot P \cdot 2g} =$ | 1.14 | |

Calculations:

Equation 4: Newton's Law of Motion

$$F = m \cdot a = 13.17 \text{ lbf.}$$

Equation 5: General pressure equation

$$P = F/A = 150.96 \text{ psf.} = 1.05 \text{ psi.} \quad (\text{A})$$

Equation 6: Shear stress

$$\tau = \gamma \cdot \left(\frac{A}{P}\right) \cdot S_F = 5.93 \text{ psf.} = 0.04 \text{ psi} \quad (\text{B})$$

$$\text{Total Pressure needed for Motive Force} = A + B = 156.9 \text{ psf.} = 1.09 \text{ psi}$$

$$\text{Total Pressure needed to overcome Friction} = B = 5.93 \text{ psf.} = 0.04 \text{ psi}$$

Physical Model Design (Sectional Model)

The sectional physical model of the WISD was designed in a 1:5 scale ratio assuming the Froude's number to be same for the model and the prototype. Similar to the numerical model, only one tube was designed out of total 10 tubes as each tube was defined to have exact same characteristics. Plexiglass was proposed as the material to construct the physical model to observe the behavior of the fluid. The model was designed to be watertight. Using the physical model, possible discrepancies for both gate and motive force systems could be investigated, along with the flow behavior and the workability of mechanical components. Parameters for the sectional model using a 1:5 scale ratio are presented in Table 5.

Table 5: Sectional physical model parameters

| Model Scale Ratios and Prototype Equivalence | | |
|---|-----------------------|---------------------------------------|
| Scale | Scale Value | Model to Prototype Equivalence |
| Length scale | $L_r = 5$ | 1 ft = 5 ft. |
| Time scale | $t_r = 2.24$ | 1 s = 2.24 s. |
| Velocity scale | $V_r = 2.24$ | 1 ft/s = 2.24 ft/s. |
| Pressure Scale | $P_r = 5$ | 1 psig = 5 psig. |
| Design Parameters (For small scaled Model) | | |
| Scale factor | 1:5 | |
| Prototype-Model Similarity | Froude Number | |
| Velocity | 11.36 fps. | |
| Pressure | 125 psf. (0.87 psig.) | |
| Materials to be used (Model) | | |
| Outer Walls | Plexiglass | |
| Inner plates & gates | Steel | |

The physical model was designed as a module with the ability to change the channel length as deemed necessary for different scenarios. The inclined entrance was the first component providing a bend at different angles; 25 degrees, 35 degrees, and 45 degrees totaling at three in numbers. Air pressure would be applied in the first component with the help of an air compressor. The second component lies between the inclined entrance and the third component. This component consists of a bottom-hinged gate and one foot of length to allow the fluid motion

to develop. The velocities would be measured at selected locations after the gate. The third component is a cuboidal box where the wavefront would be observed and the velocities would also be measured. The additional length segments that could alter the length of the reservoir and the development length was named as component four. Component five was the flange attached to other components for connecting/disconnecting capabilities. Table 6 is a list of components for the physical model and Figure 17 depicts the general layout of the sectional model for a 45 degrees inlet angle. Additional drawings for the sectional physical model are presented in Appendix B.

Table 6: Components of the physical model

| Component No. | Description | Quantity | Drawing No. |
|----------------------|-----------------------------|-----------------|--------------------|
| 1 | Inclined Inlet | | 2-10 |
| | 25 ° | 1 | |
| | 35 ° | 1 | |
| | 45 ° | 1 | |
| 2 | Gate Channel | 1 | 11-13 |
| 3 | Outlet box | 1 | 14-17 |
| 4 | Additional Length component | | 18-26 |
| | 0.2' | 2 | |
| | 0.4' | 4 | |
| | 1' | 2 | |
| 5 | Flanges | 22 | 27-28 |

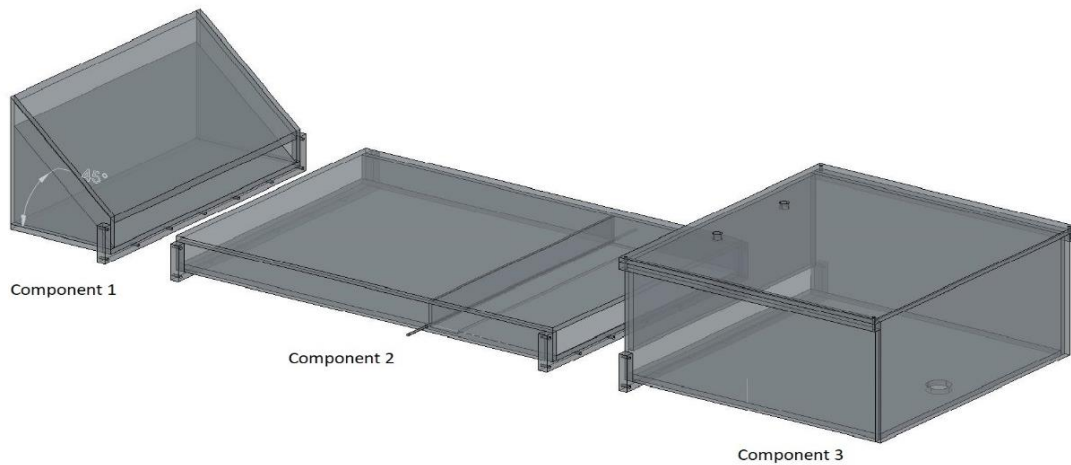


Figure 17: General layout of the sectional physical model

Component two is two feet wide, 0.2 feet high and three feet long with a gate located one foot from the exit. As mentioned earlier, using component 4 the lengths upstream and downstream could be increased. Note that only the length, entrance angle, and the motive air pressure were allowed to change for variation in data collection.

Velocity sensors would be strategically placed in longitudinal and lateral directions to capture velocities at selected locations. Highly precise and accurate instruments would be used to record the air pressure in at least every 100th of a second, the total simulation time being 1.5 seconds. A high-speed camera would also be used to observe the wavefront downstream of the gate (Jash, 2018).

This study includes the design and drawings for the 1:5 scaled down physical model. Actual construction and data collection via this model was not a part of this study. It was necessary to understand the workability of air pressure and velocity sensors beforehand. Only then, the study for the 1:5 scaled physical model would be conducted. A physical experimental study was constructed instead to validate these mentioned parameters which are described in the next section.

Physical Experimental Study

Another small-scale physical experiment study was proposed to verify the usability of air pressure and velocity measurement devices on a small-scale physical model before it was applied to a larger model. This allowed us to identify potential drawbacks on the mechanism of the air pressure system and hence, make possible improvements for larger models. The possibility of using U-tubes in lieu of the gates could also be verified via this physical experiment study. The proposed conduit was a schedule 40 clear Polyvinyl chloride (PVC) pipe with a diameter of four inches. Using a clear PVC pipe, the fluid behavior could be observed upon application of the air pressure. Whereas, common PVC fittings were used for the elbows as clear PVC elbows were relatively expensive. Also, fluid behavior in the elbows was not a topic of interest for this study. The inlet and outlet of this arrangement were inclined at 45 degrees with a water depth of one foot. The wave developed downstream of the channel, and, velocity sensors were used to capture high velocities. The components were put together using PVC primer and glue for intact connections and prevention of leaks. A layout of the apparatus, with all components connected, is shown in Figure 18.

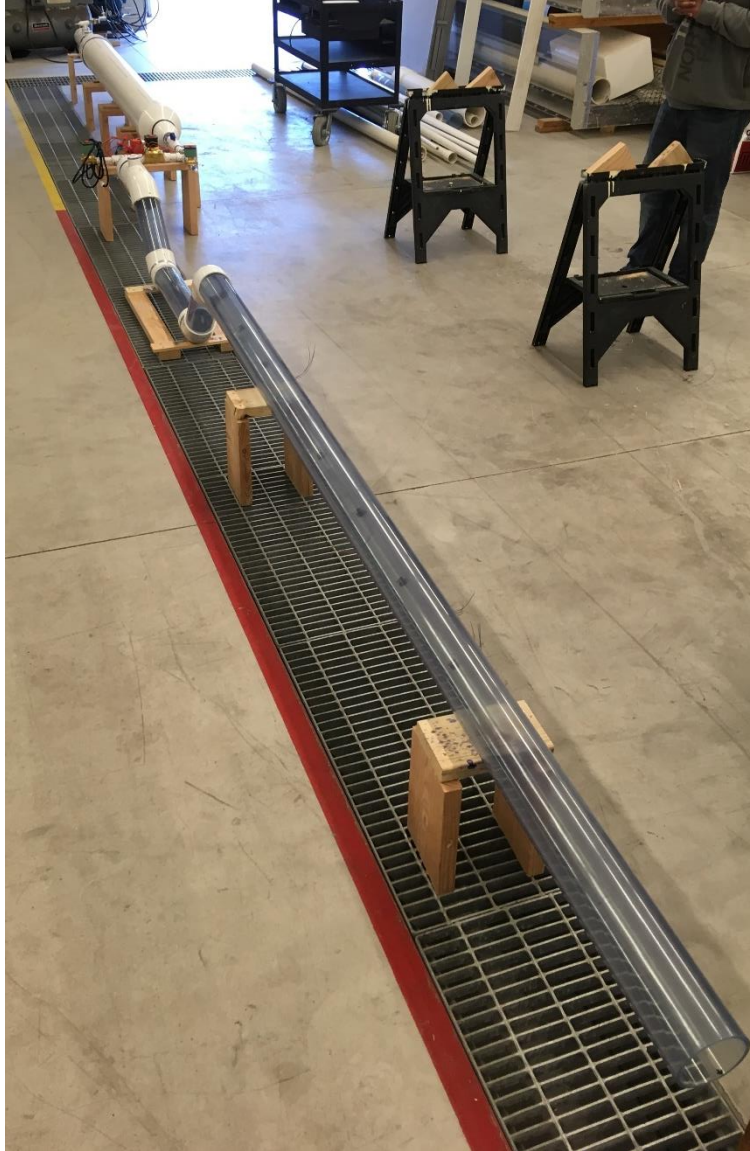


Figure 18: Layout of the physical experiment study

The apparatus consisted of three components: 1) Air pressure chamber, 2) Solenoid Valves and, 3) U-tube.

Component 1 (Air pressure chamber):

The air pressure chamber was constructed with a schedule 40 eight inch PVC pipe and was eight feet long. The main purpose of using a chamber instead of a large compressor was to supply a sufficient volume of air into the third component. Large compressor could be used to

supply air pressure into the U-tube, but most compressors would have a quarter inch outlet hose that would choke the airflow and limit the supply of air downstream. The volume within component one was enough to provide a constant volume of air downstream into the U-tube and the desired pipe size could be used in the outlet. Additional PVC Tee's were added on to this component for connecting pressure compressors to pressurize the chamber and a transducer to measure the pressure. Details on the pressure transducer are included in Appendix C. A ball valve was installed downstream to stop the air flow while pressurizing the tank. Figure 19 is a snapshot of the air pressure chamber. The Tee's can be observed on the left-hand side of the picture.



Figure 19: Component 1- Air pressure chamber

Component 2 (Solenoid Valves)

Kinematic theories suggested that a pressure of 1.09 psig would need to be applied, then removed in 0.53 seconds to produce a steady 11.36 feet per second velocity wave. The valves controlling the pressure would, therefore, need to be fast-acting, actuated valves as manually opening and closing the valves could not be accomplished in a sufficient timeframe. Solenoid valves with response time less than 50 milliseconds were chosen for the task. The following diagrams illustrate the concept chosen by the team for applying the air pressure to the pipe model, (see Figure 20). Valves one and three are normally open (NO) solenoid valves that close when energized. Valve 2 is a normally closed (NC) solenoid valve that opens when energized.

Power to all three valves is controlled by a multifunction timer relay. Figure 21 is a snapshot of the solenoid valves (Nichols, 2018).

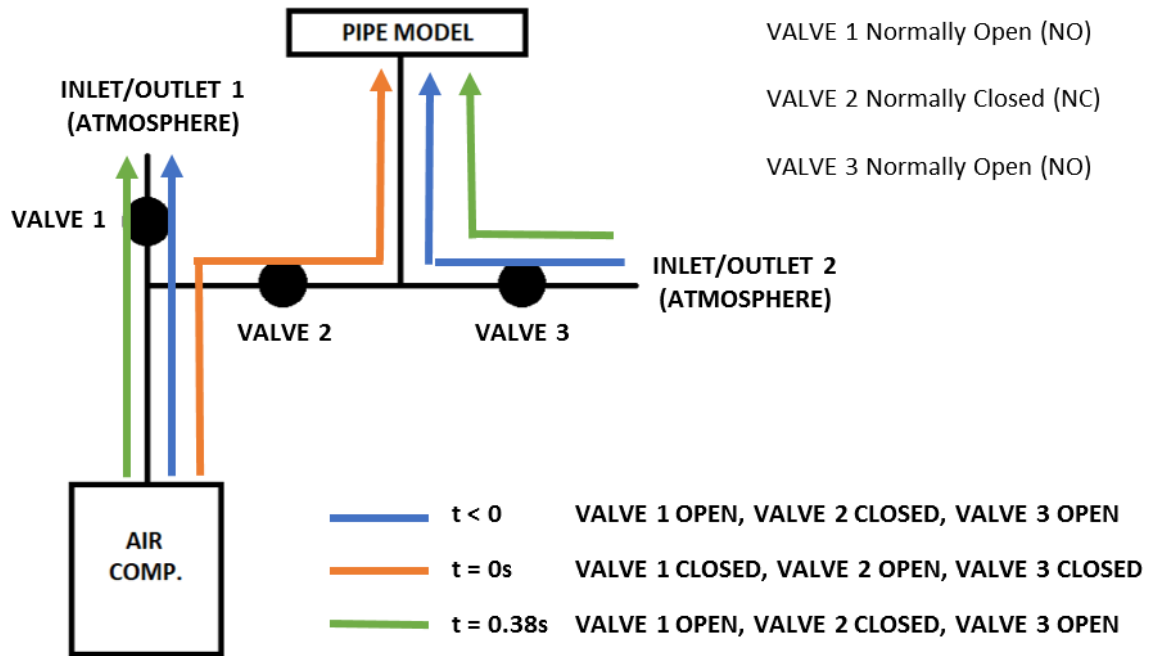


Figure 20: Diagram of pneumatic system for pipe model.



Figure 21: Solenoid valves arrangement

Component 3 (U-tube)

The U-tube was adopted in lieu of using gates in the system. Figure 22 is the side view drawing of the U-tube with dimensions in feet (hatched area represents water). Figure 23 is a snapshot of the U-tube from the laboratory and the downstream end of this component was ten feet long. The wave profile developed in this downstream section and various sensors were inserted in selected locations to measure the velocity of the wave. Jash (2018) programmed the pressure sensors to measure the velocity. Figure 24 shows the sensors located at every one foot along the length of the pipe. At the upstream section of this component, a tee was added for measuring pressure. A high-quality pressure transducer that could store a maximum of thousand numbers of data per second was used to record outlet pressures (Appendix C).

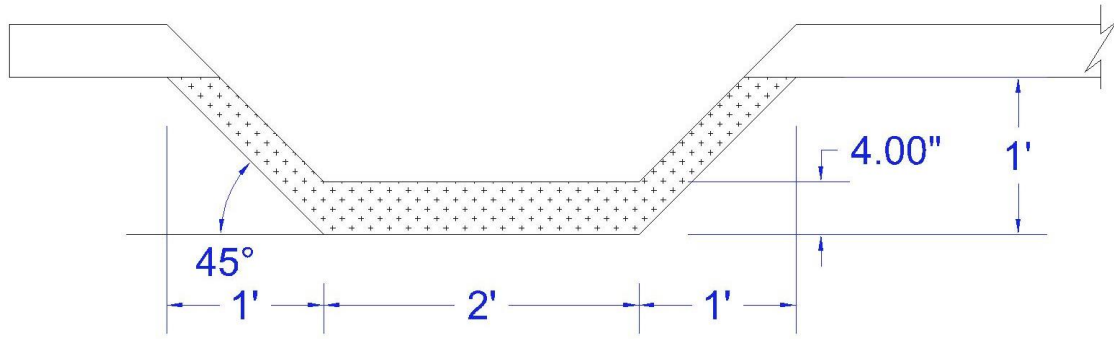


Figure 22: Physical experiment study (orthographic view)

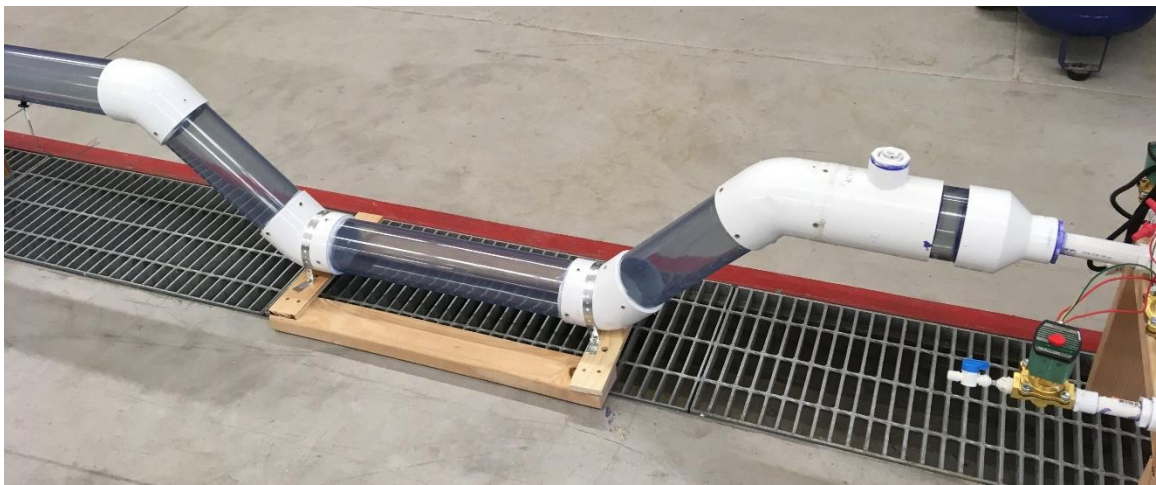


Figure 23: Component 3 (U-tube)

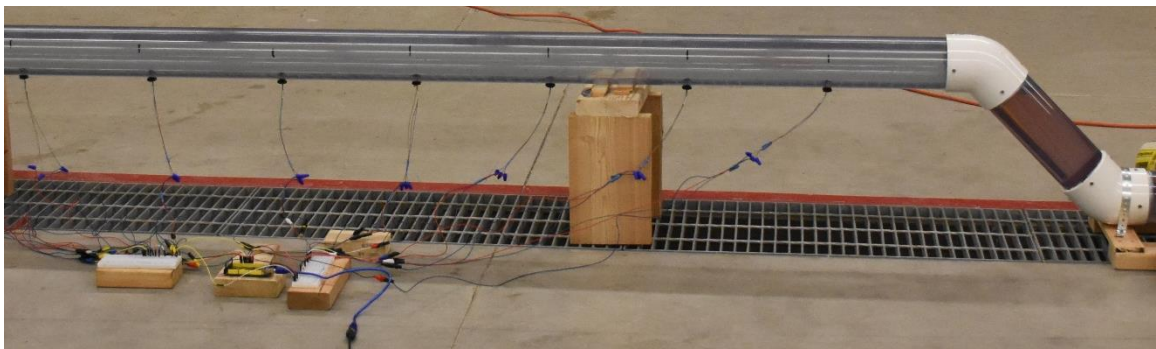


Figure 24: Velocity sensors

Results

A multitude of models was simulated in FLOW-3D to determine an ideal design for the WISD capable of creating a steady wave with a near vertical wave section. FLOW-3D models with different inlet angles, along with different fluid depths are presented in chronological order of development.

WISD (with gates)

Table 2 lists the designs simulated with a gate, their respective inlet angles, and fluid depths. For all models, the development length, the distance between the gate and the outlet was fixed to six feet, the length of the fluid chamber, from the gate to the start of the inclined inlet was set to 14 feet as shown in Figure 25. This particular figure depicts Design 8 (WD-25-2); dimensions are in feet. Also, a pressure of 625 pounds per square foot was used to displace the fluid as suggested by previous research (Roberts, 2017).

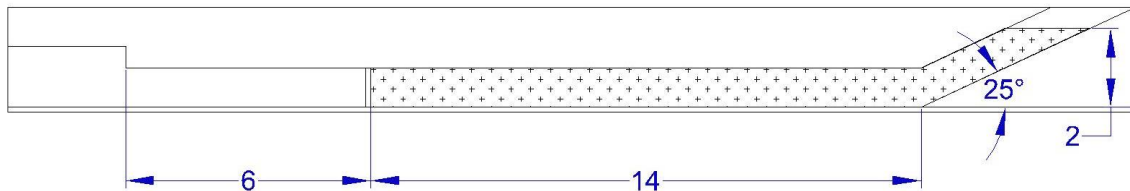


Figure 25: Design 8 (WD-25-2), orthographic view

The term “t” used in the comments below denote the simulation time. The simulation starts at time = zero seconds and ends at time = 1.5 seconds.

Design 1 (WD-45-1)

Model Description: 45 degrees inlet angle with a fluid depth of one foot (see Figure 26).

Comments: The fluid accelerated quickly at t=0.7 seconds up to 0.8 seconds but later continued steadily until t= 1.1 seconds. The highest velocity recorded was 29.5 feet per second. The velocity of the fluid generated by this model was

unsteady and the yielded wave profile was unsatisfactory (see Figure 27, color scale represents units in feet per second).

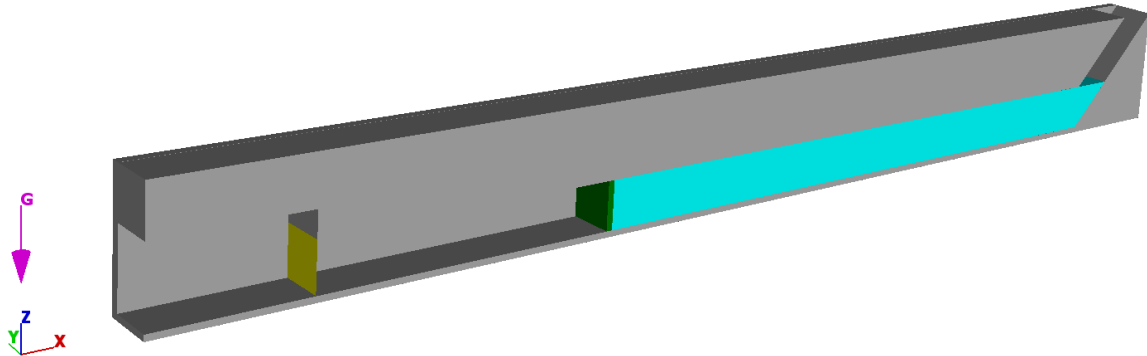


Figure 26: Design 1 (WD-45-1)

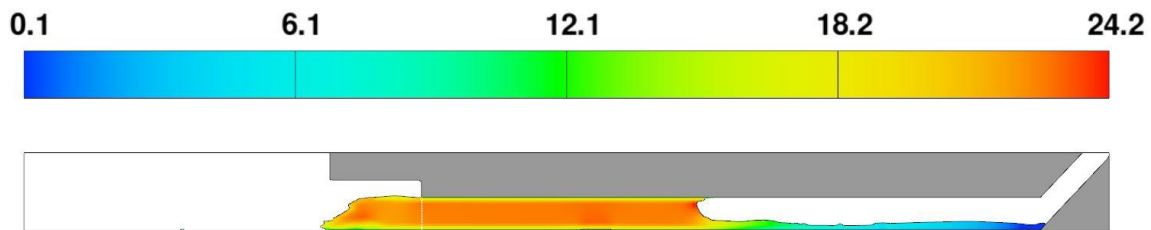


Figure 27: Design 1 (WD-45-1) – wave profile at $t = 0.8$ seconds

Design 2 (WD-45-2)

Model Description: 45 degrees inlet angle with a fluid depth of two feet (see Figure 28).

Comments: The fluid accelerated rapidly at $t=0.7$ seconds up to 0.8 seconds but later accelerated steadily until $t= 1.2$ seconds. With a higher volume of water than Design 1, it carries a higher momentum resulting in a peak velocity of 32 feet per second. The model is unsteady but produced an acceptable wave profile (see Figure 29, color scale represents units in feet per second).

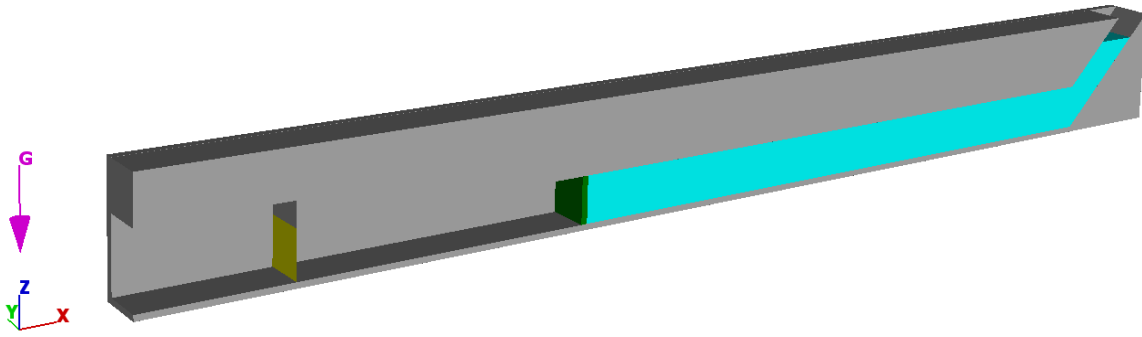


Figure 28: Design 2 (WD-45-2)

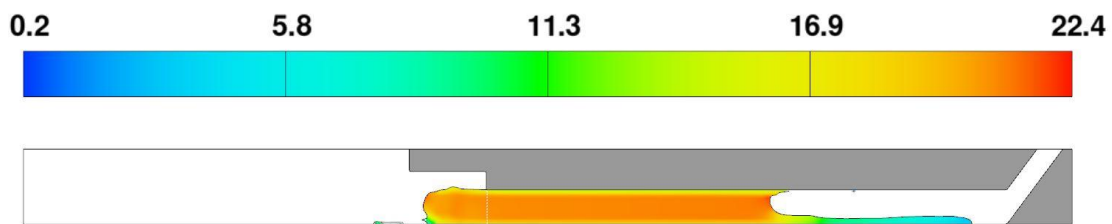


Figure 29: Design 2 (WD-45-2) – wave profile at t = 0.8 seconds

Design 3 (WD-45-3)

Model Description: 45 degrees inlet angle with a fluid depth of three feet (see Figure 30).

Comments: At t=0.7 seconds, water accelerated rapidly up to 0.9 seconds and later steadily accelerated until t= 1.3 seconds. With a higher volume of water than Design 1 and 2, its higher momentum resulted in a peak velocity of 36 feet per second. The results conclude the system to be unsteady but produced an acceptable wave profile (see Figure 31, color scale represents units in feet per second).

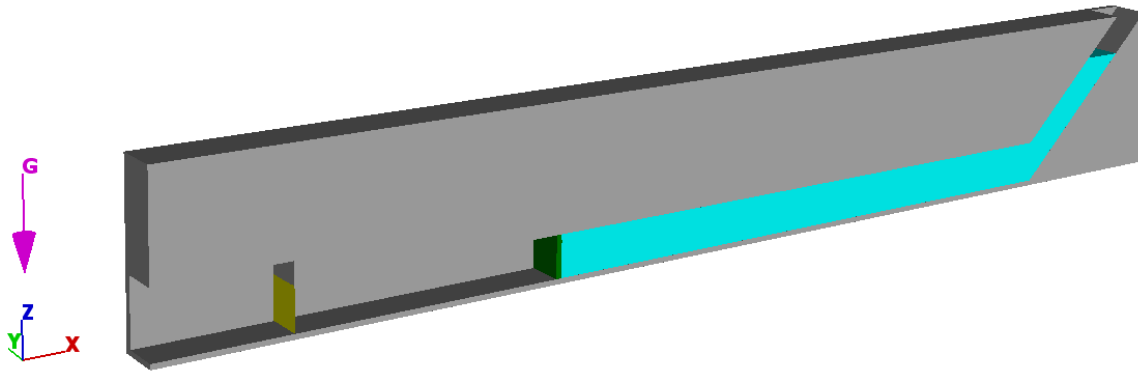


Figure 30: Design 3 (WD-45-3)

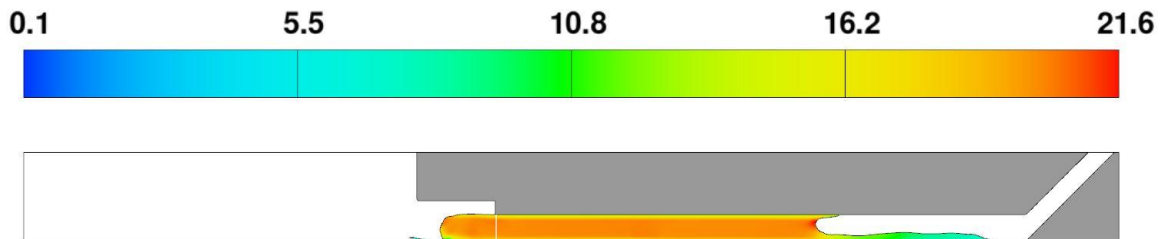


Figure 31: Design 3 (WD-45-3) – wave profile at $t = 0.8$ seconds

Design 4 (WD-35-1)

Model Description: 35 degrees inlet angle with a fluid depth of one foot (see Figure 32).

Comments: At $t=0.7$ seconds, water accelerated rapidly up to 0.8 seconds and later steadily accelerated until $t= 1.1$ seconds. This model resulted in a peak velocity of 38.6 feet per second. This model has a relatively higher cross-sectional area for the initial air pressure than the 45 degrees model, which would produce a higher motive force resulting in a larger peak velocity. The results show the system to be unsteady with a rather undesirable wave profile (see Figure 33, color scale represents units in feet per second).

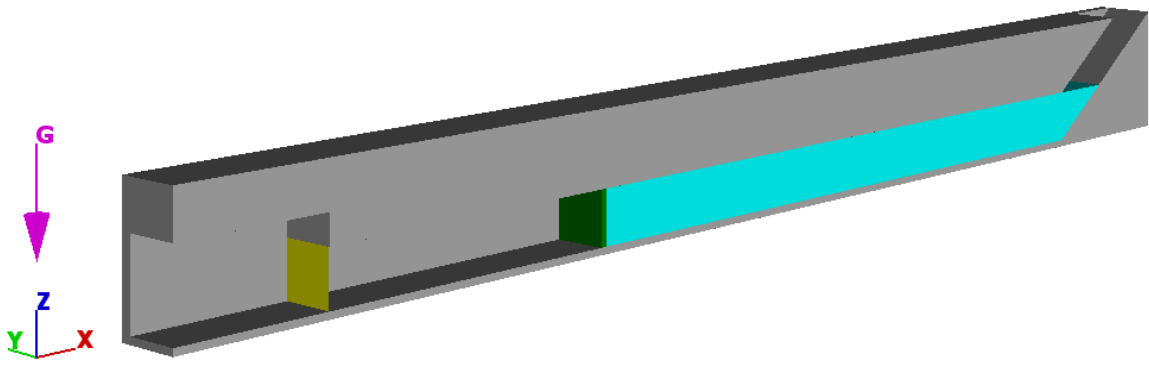


Figure 32: Design 4 (WD-35-1)

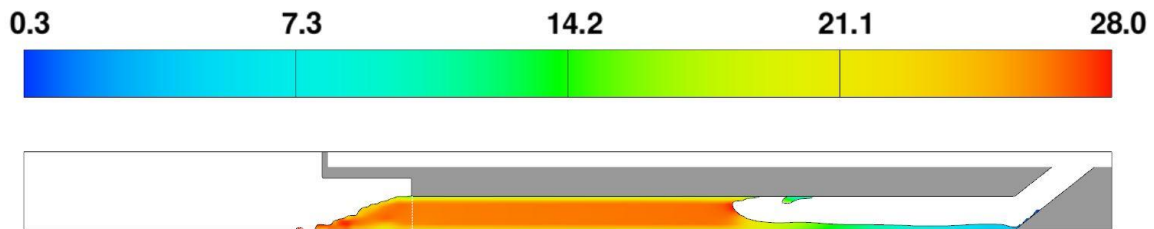


Figure 33: Design 4 (WD-35-1) – wave profile at $t = 0.4$ seconds

Design 5 (WD-35-2)

Model Description: 35 degrees inlet angle with a fluid depth of two feet (see Figure 34).

Comments: At $t=0.7$ seconds, water accelerated rapidly up to 0.8 seconds and later steadily accelerated until $t= 1.2$ seconds. This model resulted in a peak velocity of 34.2 feet per second. Unlike the 45 degrees model, the peak velocity is smaller than Design 4 (WD-35-1) that has a depth of 1 ft. The velocity is not constant over the time period and the wave profile does not meet the expectations of the study (see Figure 35, color scale represents units in feet per second).

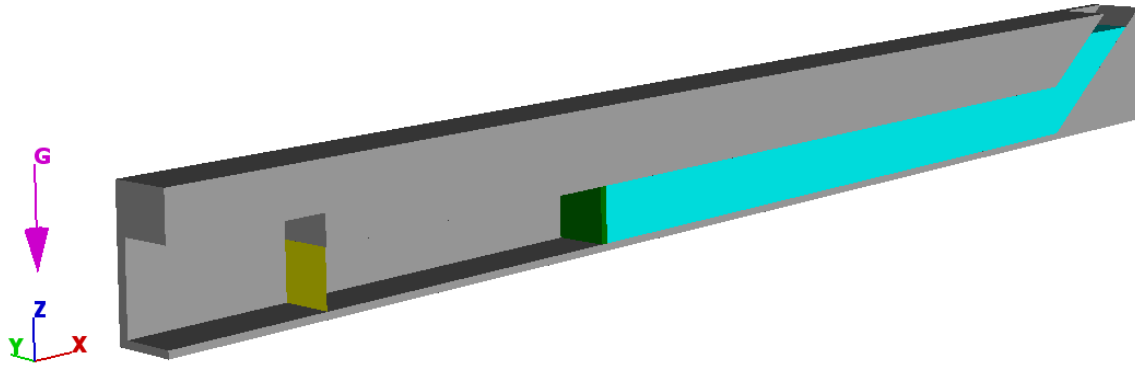


Figure 34: Design 5 (WD-35-2)

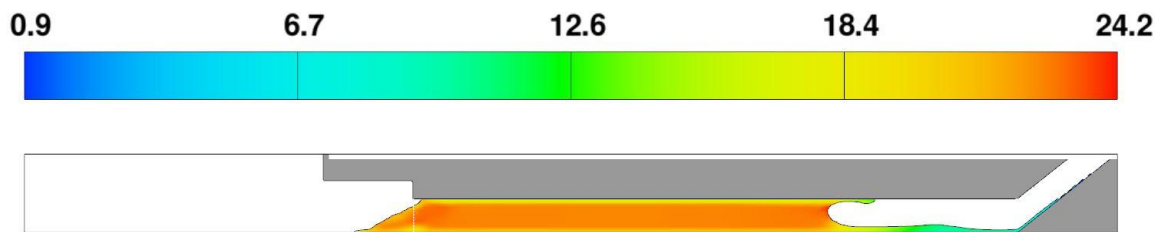


Figure 35: Design 5 (WD-35-2) – wave profile at t = 0.4 seconds

Design 6 (WD-35-3)

Model Description: 35 degrees inlet angle with a fluid depth of three feet (see Figure 36).

Comments: At t=0.7 seconds, water accelerated rapidly up to 0.9 seconds and later steadily accelerated until t= 1.3 seconds. This model resulted in a peak velocity of 33.7 feet per second. The velocity is not constant over a time period and the wave profile does not meet the expectations of the study (see Figure 37, color scale represents units in feet per second).

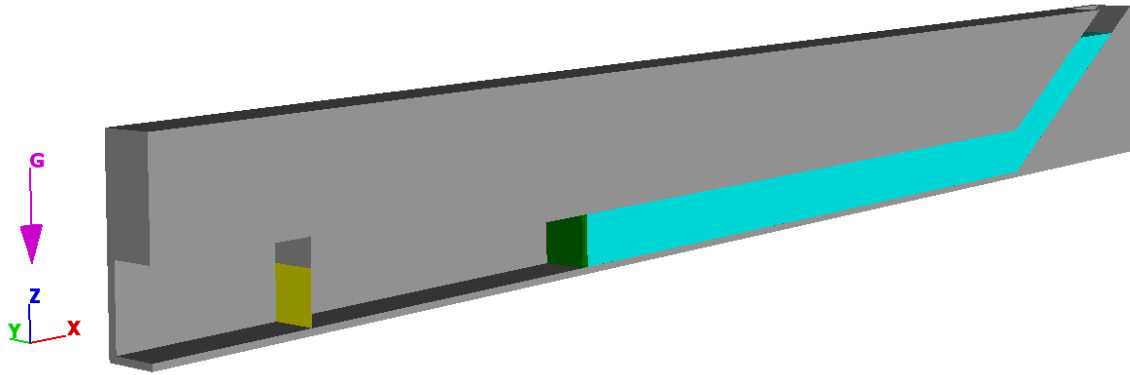


Figure 36: Design 6 (WD-35-3)

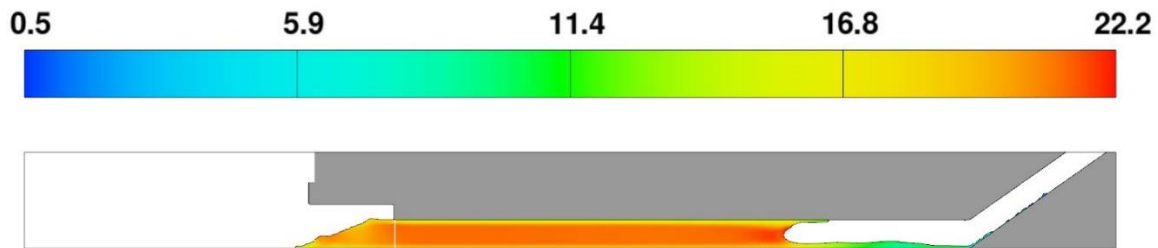


Figure 37: Design 6 (WD-35-3) – wave profile at t = 0.6 seconds

Design 7 (WD-25-1)

Model Description: 25 degrees inlet angle with a fluid depth of one foot (see Figure 38).

Comments: Water accelerated rapidly at t=0.7 seconds up to 0.8 seconds and later steadily accelerated until t= 1.1 seconds. This model resulted in a peak velocity of 33 feet per second. Unexpectedly, this model did not follow the trend set by previous simulations; the increased surface area for the initial pressure of this simulation compared to 25 and 35 degrees inlet should have produced a higher peak velocity due to the increased force. However, the peak velocity for this model is lesser than the 35 degrees geometry with one foot of depth. The velocity is unsteady and the wave profile does not meet the expectations of the study (see Figure 39, color scale represents units in

feet per second). Unusually, the top portion of the wave is ahead of the bottom portion, unlike previous model results.

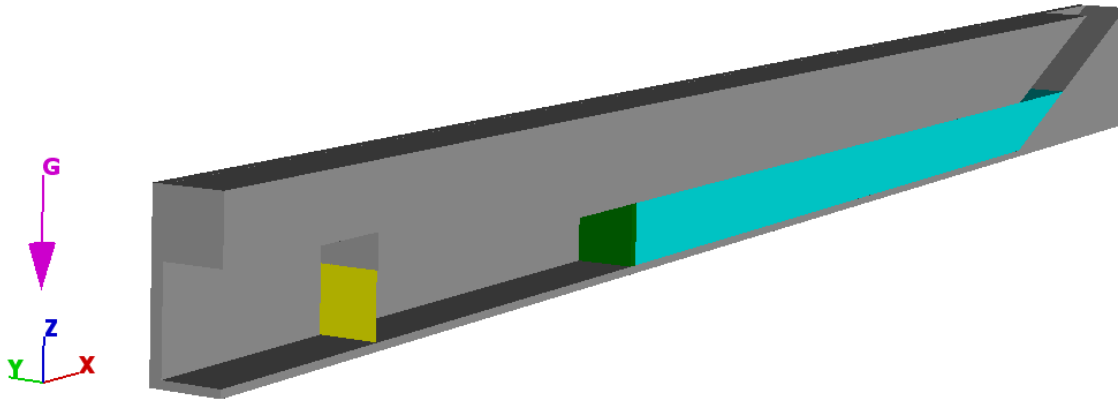


Figure 38: Design 7 (WD-25-1)

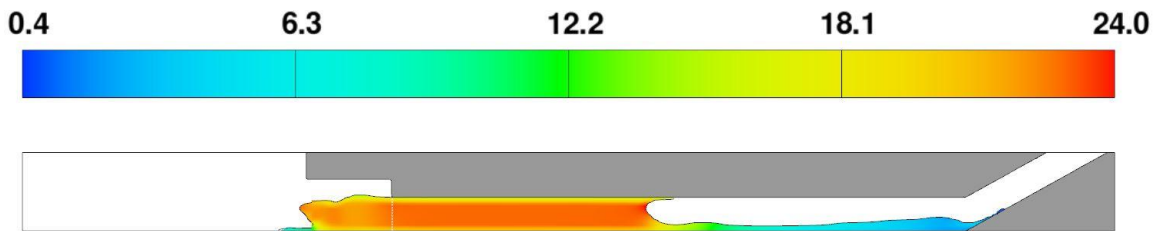


Figure 39: Design 7 (WD-25-1) – wave profile at t = 0.8 seconds

Design 8 (WD-25-2)

Model Description: 25 degrees inlet angle with a fluid depth of two feet (see Figure 40).

Comments: Water accelerated rapidly at t=0.7 seconds up to 0.8 seconds, followed by a rather steady acceleration until t= 1.3 seconds. This model resulted in a peak velocity of 38.4 feet per second. The velocity is unsteady and the observed wave profile is acceptable (see Figure 41, color scale represents units in feet per second).

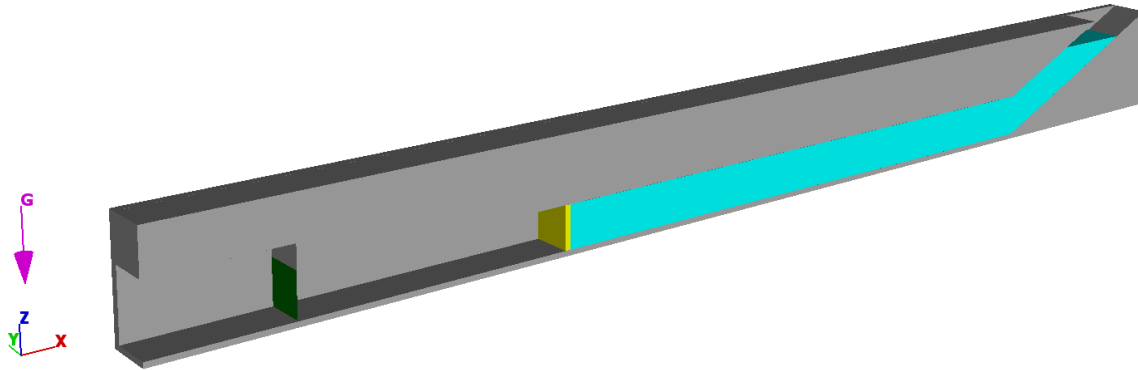


Figure 40: Design 8 (WD-25-2)

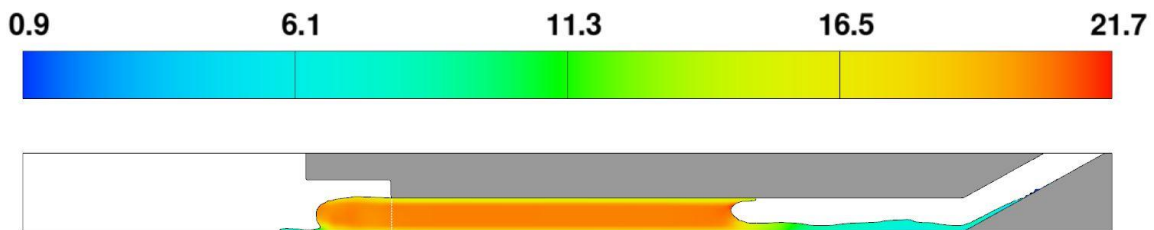


Figure 41: Design 8 (WD-25-2) – wave profile at $t = 0.85$ seconds

Design 9 (WD-25-3)

Model Description: 25 degrees inlet angle with a fluid depth of three feet (see Figure 42).

Comments: The fluid accelerated steadily at $t=0.7$ seconds up to 0.8 seconds, followed by a rapid acceleration until $t= 1.4$ seconds. This model has the highest volume of water resulting in a peak velocity of 36.2 feet per second which is quite strange as it was expected this model would have the highest peak velocity. The velocity is not constant but the wave profile is good enough (see Figure 43, color scale represents units in feet per second).

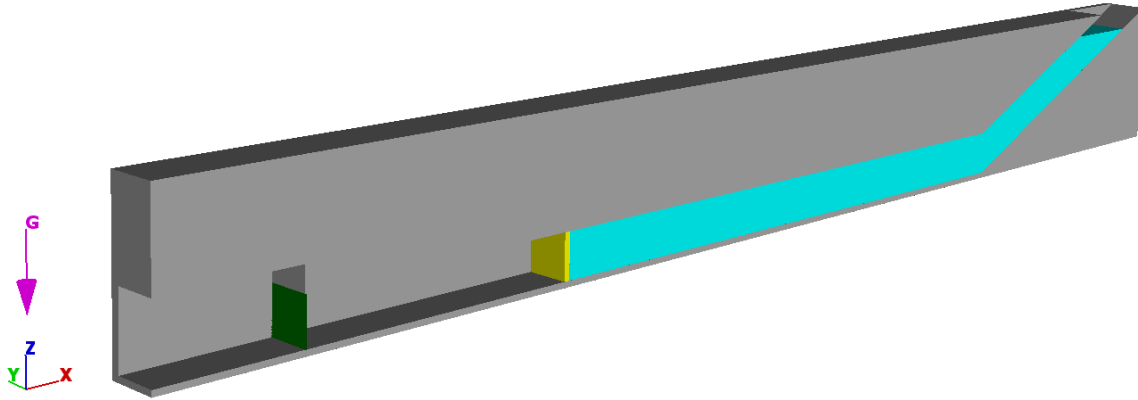


Figure 42: Design 9 (WD-25-3)

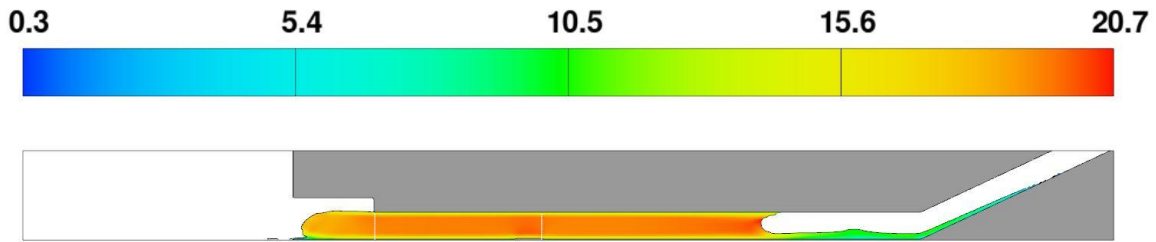


Figure 43: Design 9 (WD-25-3) – wave profile at $t = 0.9$ seconds

The mass flux/velocity for several arrangements listed in Table 2 was recorded with respect to time and compared in Figure 44. The simulation configurations included inlet angles at 25, 35, and 45 degrees with upstream depths ranging from one to three feet. All the simulations had similar behavior; the velocities would sharply increase at 0.7 seconds and then gradually increase for a range from 0.8 seconds to 1.3 seconds followed by a sudden decrease as the water exited the flow chamber, except for the setup with 25 degrees of inlet angle with a fluid depth of one foot, which would gradually increase from 0.7 seconds to 0.8 seconds followed by a steep increase up to 0.9 seconds. For the remaining timeframe, it follows the same behavior as other simulations.

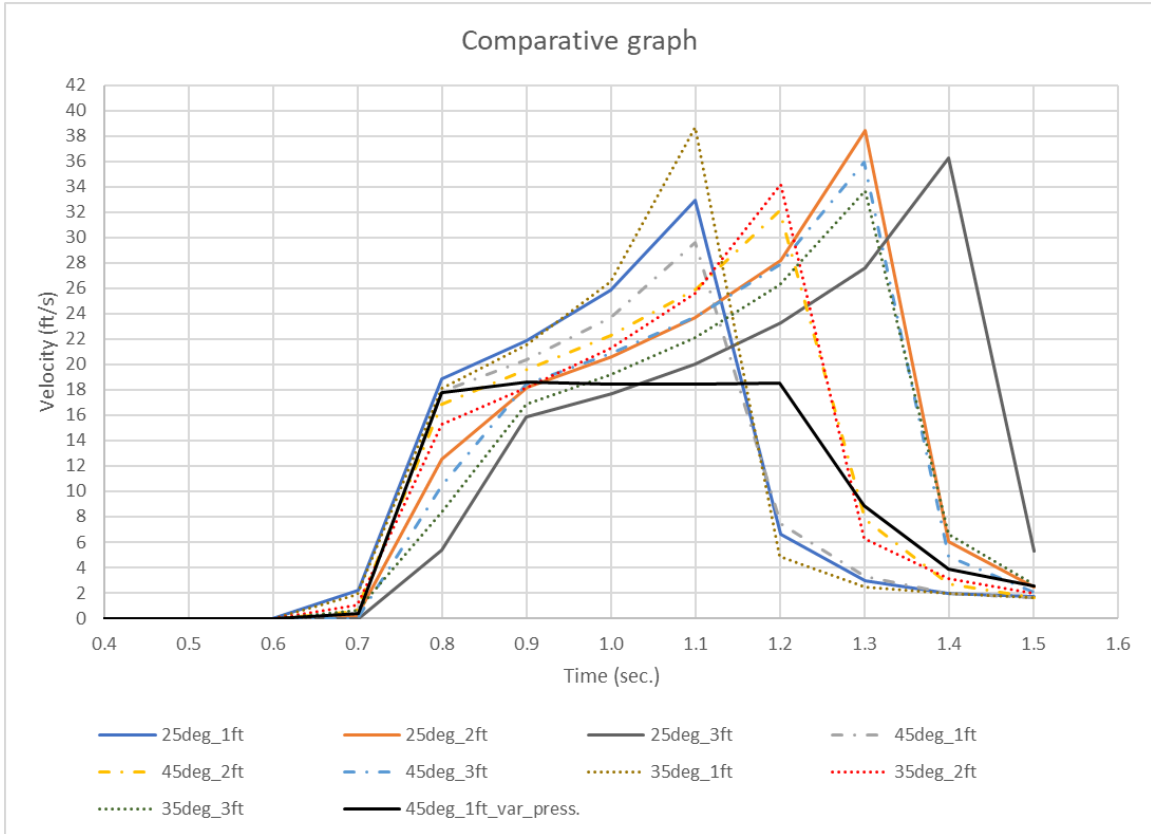


Figure 44: Velocity vs time

Comparing the one-foot depth inlet for angles 25, 35, and 45 degrees, the results show that the inlet angle does increase the motive force, moving the water through the chamber with a slightly higher initial response at 0.8 seconds and a larger peak at 1.1 seconds. This is expected since the initial pressure force is pressure multiplied by the area and the 25 degrees inlet provides more area. Figure 44 also shows that increasing the inlet depth slows the initial response at 0.7 seconds but produces a higher peak that is delayed. The higher peak is attributed to the increase in the initial inlet depth and the time delay is created by the change in inertia required to move the additional mass.

Initially, a trial and error process was used to select the air pressure that was applied to the static water to obtain a steady state velocity. To help understand this process better, analytical kinematic theories outlined in literature were adapted to compute the ideal variation in the air

pressure. Theoretically, the fluid should maintain a steady velocity if it maintains its initial geometry similar to a solid block. However, a real fluid does not follow this assumption, and thus, as expected, the numerical simulations using FLOW-3D has slight differences in its results compared to the theoretical values, when the variation in air pressure was applied to the system rather than a constant air pressure behind the system. The applied variation in air pressure allowed the fluid to maintain velocities ranging from 27.8 feet per second to 28.8 feet per second for a duration of 0.4 seconds instead of the expected velocity of 25.4 feet per second for the geometry with 25 degrees inlet and a fluid depth of 2 feet. Figure 45 shows a plot of velocity (feet per second) and time (seconds) for the geometry with a 25 degrees inlet angle and a fluid depth of 2 feet for the CFD simulation. The results with the variable pressure are also shown in Figure 44 for a 45 degrees inlet angle and a fluid depth of 1 foot. These results satisfy the expectations of the WISD, with a fairly constant velocity from 0.8 seconds to 1.2 seconds.

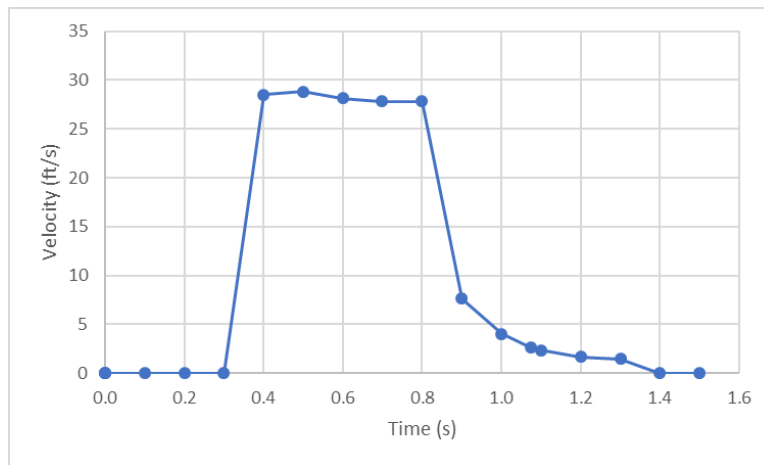


Figure 45: Velocity vs time (25 degrees inlet – 2 ft. depth)

WISD (without gates)

As the total volume of water in the domain varied with changes in the inlet/outlet angles and the fluid depth, the required air pressure variation was calculated in a spreadsheet for each

model. The base of the U-tube was fixed at two feet for all simulations and a baffle was placed at the same location for all models to record mass flux/velocity. The air pressure used for each simulation is shown in Table 7.

Table 7: Motive pressures for each simulation

| Design No. | Design ID | Motive Pressure (psf.) |
|------------|----------------|------------------------|
| 10 | WD-45-1-WG | 1997 |
| 11 | WD-45-2-WG | 2246 |
| 12 | WD-35-1-WG | 2050 |
| 13 | WD-35-2-WG | 2407 |
| 14 | WD-25-1-WG | 2140 |
| 15 | WD-25-2-WG | 2675 |
| 16 | WD-55-1-WG | 1960 |
| 17 | WD-45-1-WG-1C | 1997 |
| 18 | WD-45-1-WG-2C | 1997 |
| 19 | WD-45-1-WG-3C | 1997 |
| 20 | WD-45-1-WG-PHY | 157 |

Design 10 (WD-45-1-WG)

Model Description: 45 degrees inlet and outlet angle with a fluid depth of one foot (see Figure 46). A pressure of 1997 psf. was applied for 0.39 secs after which the pressure was reduced to zero as friction was not considered for the geometry.

Comments: Water accelerated rapidly at tentatively t=0.42 seconds up to 0.45 seconds, followed by a deceleration until t= 0.5 seconds. The velocity is almost constant at around 25 feet per second from t=0.5 seconds to t=0.98 seconds. This model has a peak velocity of 31.7 feet per second. The velocity is almost constant and the wave profile looks good except for the tongue generated on the bottom portion of the wave (see Figure 47, color scale represents units in feet per second).



Figure 46: Design 10 (WD-45-1-WG)

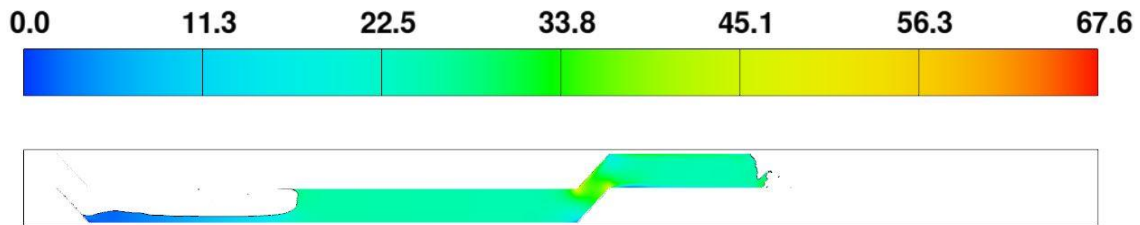


Figure 47: Design 10 (WD-45-1-WG) – wave profile at t = 0.4 seconds

Design 11 (WD-45-2-WG)

Model Description: 45 degrees inlet and outlet angle with a fluid depth of two feet (see Figure 48). A pressure of 2246 psf. was applied for 0.39 secs after which the pressure was reduced to zero as friction was not considered for the geometry.

Comments: Water accelerated rapidly at tentatively t=0.35 seconds up to 0.38 seconds, and maintained a velocity of about 25 feet per second but started to decelerate from t= 0.7 seconds. The velocity is not steady and the wave profile did not meet the expectations (see Figure 49, color scale represents units in feet per second).



Figure 48: Design 11 (WD-45-2-WG)

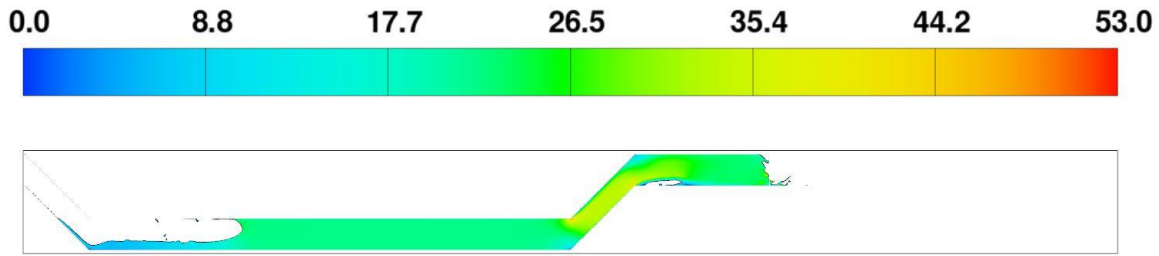


Figure 49: Design 11 (WD-45-2-WG) – wave profile at t = 0.4 seconds

Design 12 (WD-35-1-WG)

Model Description: 35 degrees inlet and outlet angle with a fluid depth of one foot (see Figure 50). A pressure of 2050 psf. was applied for 0.39 secs after which the pressure was reduced to zero as friction was not considered for the geometry.

Comments: The fluid accelerated rapidly at t=0.4 seconds up to 0.42 seconds, decelerated to a velocity of about 25 feet per second at t=0.45 seconds and maintained the velocity up to t=0.97 seconds. The velocity is fairly steady but the wave profile could not maintain a near vertical wavefront (see Figure 51, color scale represents units in feet per second).



Figure 50: Design 12 (WD-35-1-WG)

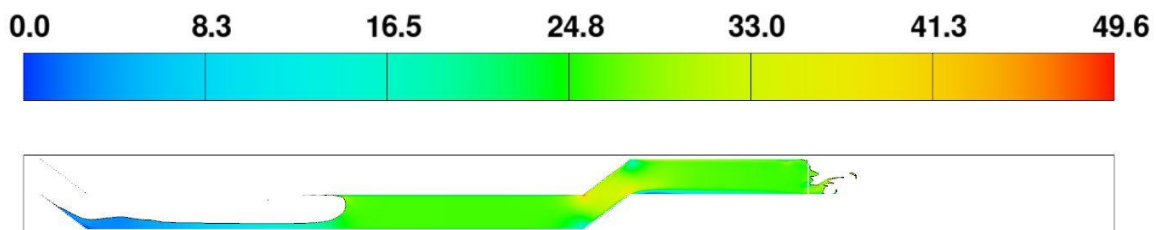


Figure 51: Design 12 (WD-35-1-WG) – wave profile at t = 0.45 seconds

Design 13 (WD-35-2-WG)

Model Description: 35 degrees inlet and outlet angle with a fluid depth of two feet (see Figure 52). A pressure of 2407 psf. was applied for 0.39 secs after which the pressure was reduced to zero as friction was not considered for the geometry.

Comments: The fluid accelerated rapidly at $t=0.4$ seconds up to 0.43 seconds, decelerated quickly to a velocity of about 20 feet per second at $t=0.5$ seconds and maintained the velocity in the range of 19 to 23 feet per second up to $t=1.2$ seconds. The velocity was somewhat steady but the wave profile could not maintain a near vertical wavefront (see Figure 53, color scale represents units in feet per second).



Figure 52: Design 13 (WD-35-2-WG)

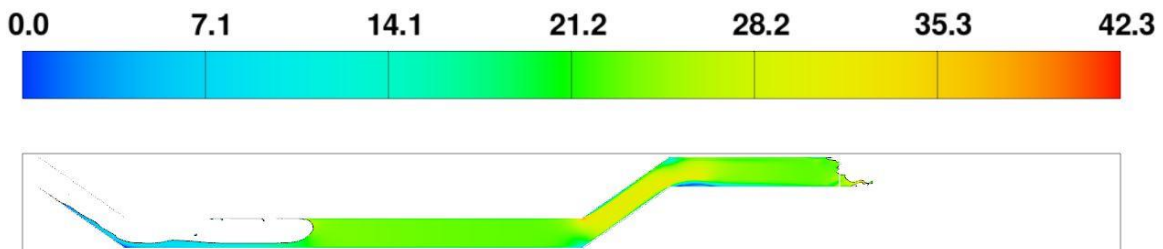


Figure 53: Design 13 (WD-35-2-WG) – wave profile at $t = 0.48$ seconds

Design 14 (WD-25-1-WG)

Model Description: 25 degrees inlet and outlet angle with a fluid depth of one foot (see Figure 54). A pressure of 2140 psf. was applied for 0.39 secs after which the

pressure was reduced to zero as friction was not considered for the geometry.

Comments: The fluid accelerated rapidly at $t=0.35$ seconds up to 0.4 seconds, maintained a velocity of about 25 feet per second up to $t=0.92$ seconds. The velocity was conserved and the wave profile was satisfactory (see Figure 55, color scale represents units in feet per second).



Figure 54: Design 14 (WD-25-1-WG)

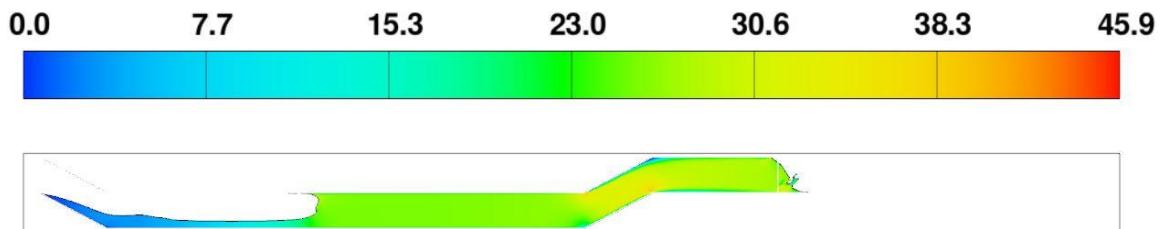


Figure 55: Design 14 (WD-25-1-WG) – wave profile at $t = 0.4$ seconds

Design 15 (WD-25-2-WG)

Model Description: 25 degrees inlet and outlet angle with a fluid depth of two feet (see Figure 56). A pressure of 2675 psf. was applied for 0.39 secs after which the pressure was reduced to zero as friction was not considered for the geometry.

Comments: The fluid accelerated rapidly at $t=0.4$ seconds up to 0.42 seconds, decelerated steadily with alternating velocities up to $t=0.8$ seconds and maintained 20 feet per second velocity up to $t=1.25$ seconds. The velocity was conserved for a considerable time period and the wave profile was

unsatisfactory (see Figure 57, color scale represents units in feet per second).



Figure 56: Design 15 (WD-25-2-WG)

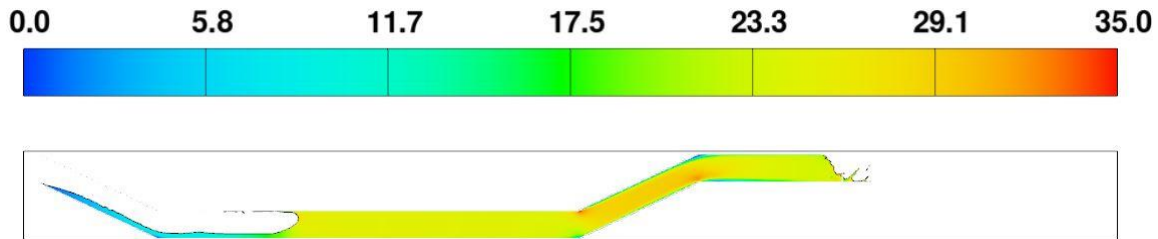


Figure 57: Design 15 (WD-25-2-WG) – wave profile at $t = 0.45$ seconds

Design 16 (WD-55-1-WG)

Model Description: 55 degrees inlet and outlet angle with a fluid depth of one foot (see Figure 58). A pressure of 1960 psf. was applied for 0.39 secs after which the pressure was reduced to zero as friction was not considered for the geometry.

Comments: The fluid accelerated rapidly at $t=0.41$ seconds up to $t=0.45$ seconds, it could maintain its velocity at 30 feet per second for one-tenth of a second but significantly decelerated later in the simulation. Water was forced out of the inclined outlet creating a huge air pocket below the jet which ultimately produced an unsatisfactory wave profile (see Figure 59, color scale represents units in feet per second).



Figure 58: Design 16 (WD-55-1-WG)

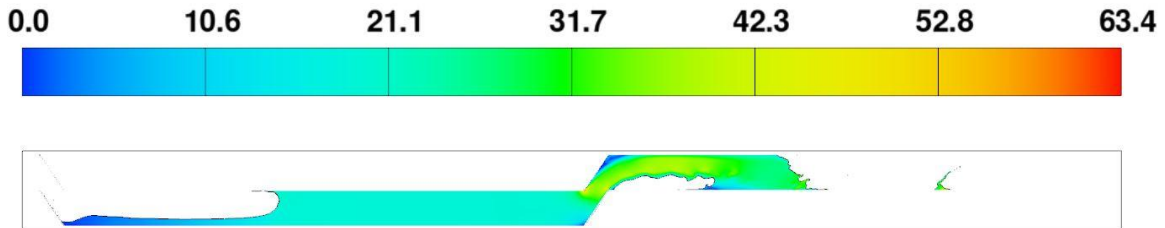


Figure 59: Design 16 (WD-55-1-WG) – wave profile at $t = 0.42$ seconds

The velocities were recorded via a baffle placed at the same location for all simulations. The results were plotted on a graph with velocity (feet per second) on the y-axis and time (seconds) on the x-axis as shown in Figure 60. It can be observed that most geometries with a depth of one foot have a near constant velocity of approximately 25 feet per second starting within $t = 0.4$ to 0.5 seconds that is conserved for almost $t = 1$ seconds. Whereas, the geometry with 55 degrees and the 25 degrees inlet-outlet have not produced acceptable results as shown in Figure 60 (c). The initial bump on the graphs is believed to appear from splashing and turbulent nature of water.

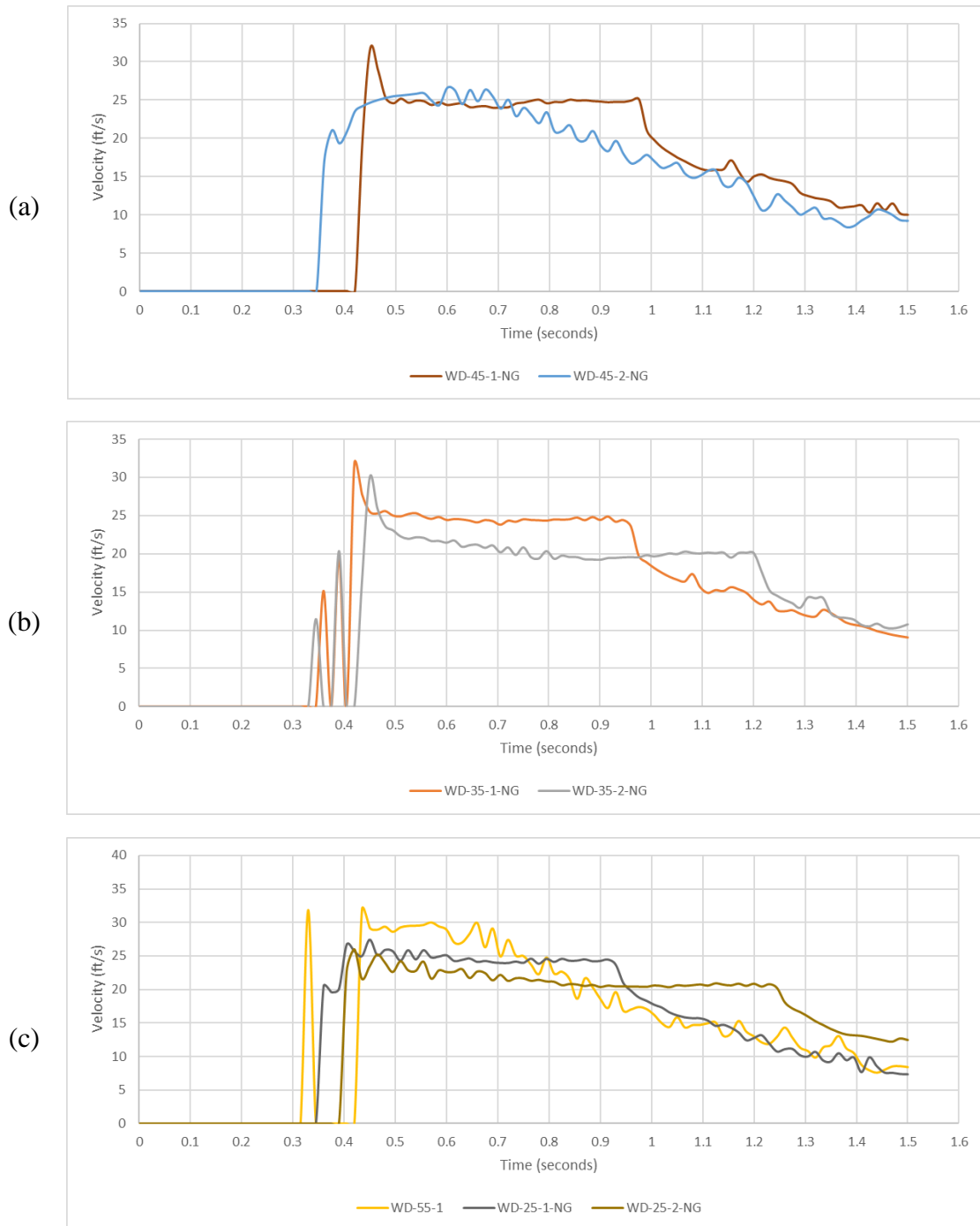


Figure 60: Velocity – vs – time (without gates) for geometries with: (a) 45 degrees; (b) 35 degrees; (c) 55 degrees and 25 degrees

Design 17, 18, & 19 (WD-45-1-WG-1C, 2C, & 3C)

Figure 61, Figure 62, Figure 63, and Figure 64 show the wave profiles for Design 10 (WD-45-1-WG), Design 17 (WD-45-1-WG-1C), Design 18 (WD-45-1-WG-2C), and Design 19

(WD-45-1-WG-3C), respectively. Each design is differentiated with thin films of water with one, two, and three cell thicknesses, respectively. The results for Design 17 met the expectations of the study creating a nearly vertical wavefront. In the physical experimentation, when the tests are carried out, a thin film of water is left out by the previous test which is believed to act as the same thin film of water considered in the numerical simulation.



Figure 61: Wave profile at t = 0.39 seconds



Figure 62: Wave profile at t = 0.39 seconds with 1 cell of fluid depth downstream



Figure 63: Wave profile at t = 0.39 seconds with 2 cell of fluid depth downstream



Figure 64: Wave profile at t = 0.39 seconds with 3 cell of fluid depth downstream

Design 20 (WD-45-1-WG-PHY)

Model Description: Four-inch pipe, 45 degrees inlet, and outlet angle with a fluid depth of one foot (see Figure 65). A pressure of 157 psf. was applied for 0.53 secs after which the pressure was reduced to six psf. to overcome shear stress acted upon the water by the solid geometry.

Comments: The fluid accelerated rapidly and peaked at a velocity of 8 feet per second. Figure 67 shows that the wave tried to maintain its velocity for three-tenths of a second with a gradual decrease in value till almost 6.5 feet per second. The expected velocity according to the adopted kinematic theories is 11.3 feet per second. This behavior was unlikely compared to other simulations which yielded desired results in terms of steadiness and velocity magnitudes. The wave, however, is near vertical and considered to be acceptable (see Figure 66, color scale represents units in feet per second).

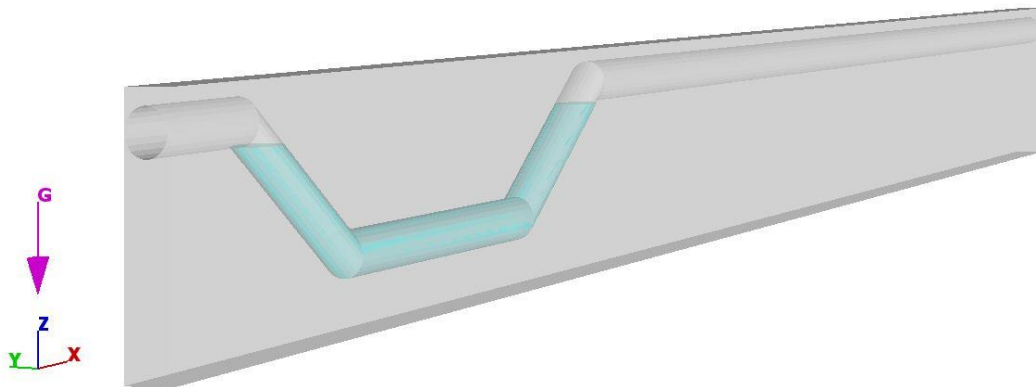


Figure 65: Design 20 (WD-45-1-WG-PHY)

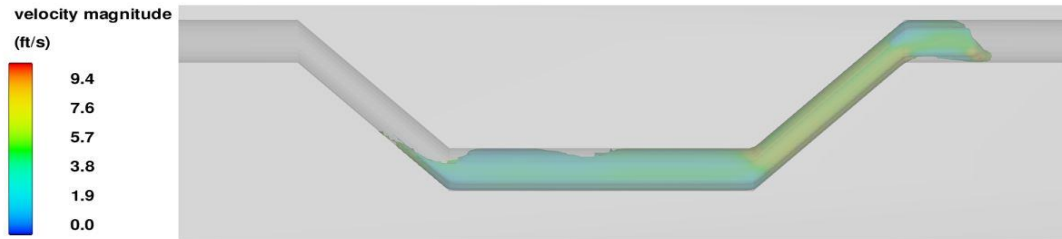


Figure 66: Design 20 (WD-45-1-WG-PHY) – wave profile at t = 0.42 seconds

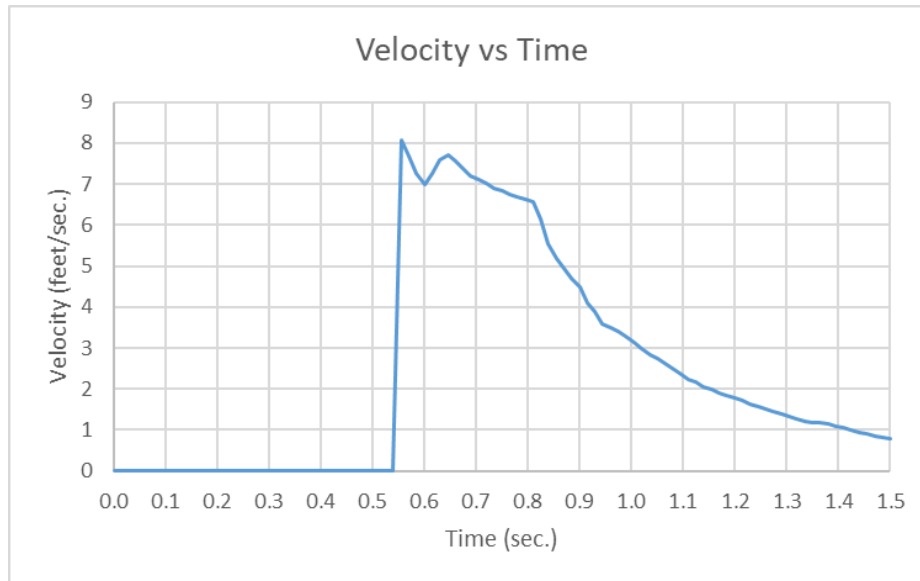


Figure 67: Velocity vs time – Design 20 (WD-45-1-WG-PHY)

Physical Experimental Study

Primarily, three parameters were focused in the physical experimental test:

1) U-tube Pressure, 2) Wave velocity and, 3) Wave profile. The U-tube pressures and wave velocities were adjusted by controlling the chamber pressure (listed in Table 8). The wave profiles generated by all test configurations were near vertical, which was one of the major objectives of this study. Among a number of test configurations, a chamber pressure of 2.75 psig yielded an almost constant velocity and a U-tube pressure of 1.1 psig. The target velocity was 11.3 feet per second and the adopted kinematics suggested a U-tube pressure of 1.09 psig would be required to displace the water in motion for the mentioned velocity. The wave profile produced by this configuration was acceptable (see Figure 68).

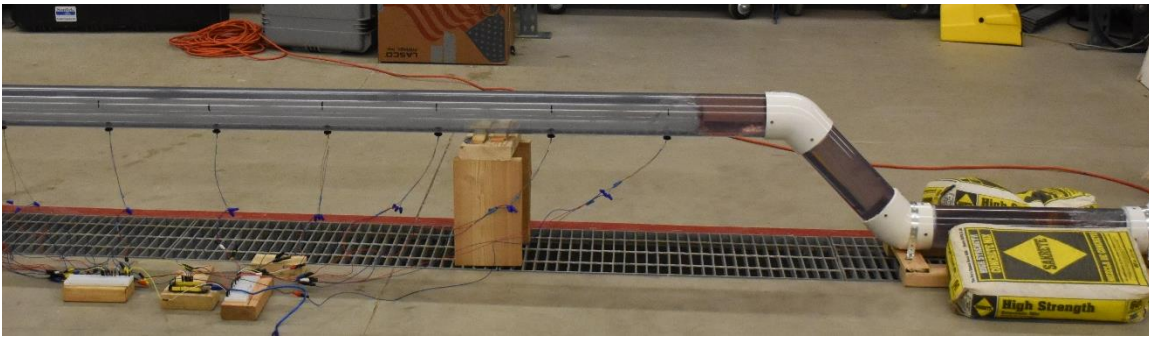


Figure 68: Wave profile generated by an inlet pressure of 2.75 psi

The results from the physical experimental study are shown in Table 8. The target velocity was 11.3 feet per second generated by a U-tube pressure of 1.09 psig within 0.53 seconds for a development length of three feet as indicated by adopted kinematic theories.

Table 8: Results from the physical experimental study

| Run | Chamber Pressure (psig.) | DL (ft.) | Time(s.) | Velocity at locations: (ft./s) | | | | | Average U-tube Pressure (psig.) |
|-----|--------------------------|----------|----------|--------------------------------|-------|-------|-------|--------|---------------------------------|
| | | | | 2 ft. | 4 ft. | 6 ft. | 8 ft. | 10 ft. | |
| 1 | 10 | 3 | 0.53 | 22.73 | 12.05 | 38.46 | 27.78 | 25.94 | 2.89 |
| 2 | 5 | 2 | 0.4 | 15.63 | 16.95 | 11.36 | 13.70 | 14.56 | 2.22 |
| 3 | 5 | 3 | 0.53 | 28.57 | 11.36 | 16.95 | 16.67 | 16.60 | 1.85 |
| 4 | 4 | 3 | 0.53 | 20.00 | 12.99 | 16.13 | 14.08 | 10.78 | 1.56 |
| 5 | 3 | 2 | 0.4 | 12.35 | 12.50 | 12.99 | 12.82 | 14.56 | 1.6 |
| 6 | 3 | 3 | 0.75 | 8.26 | 15.15 | 11.49 | 9.52 | 8.06 | 0.4 |
| 7 | 3 | 3 | 0.75 | 13.70 | 13.25 | 10.42 | 12.50 | 11.53 | 1.1 |
| 8 | 3 | 2.5 | 0.5 | 16.67 | 10.42 | 10.20 | 12.35 | 11.22 | 1.3 |
| 9 | 3 | 3 | 0.58 | 16.13 | 11.49 | 12.20 | 10.10 | 11.22 | 1.1 |
| 10 | 3 | 3 | 0.58 | 18.87 | 15.63 | 12.35 | 12.20 | 9.43 | 1.2 |
| 11 | 3 | 3 | 0.53 | 14.08 | 15.63 | 9.71 | 12.20 | 11.53 | 1.2 |
| 12 | 2.75 | 3 | 0.53 | 10.10 | 12.82 | 10.64 | 10.64 | 10.25 | 1.09 |
| 13 | 2.75 | 3 | 0.53 | 11.63 | 12.82 | 12.35 | 10.10 | 8.30 | 1.11 |
| 14 | 2.75 | 3 | 0.53 | 11.49 | 14.08 | 11.11 | 11.36 | 10.64 | 1.13 |
| 15 | 2.75 | 3 | 0.53 | 11.24 | 12.20 | 11.76 | 9.35 | 12.39 | 1.09 |
| 16 | 2.75 | 3 | 0.53 | 11.57 | 11.24 | 10.63 | 11.11 | 10.57 | 1.11 |
| 17 | 2.75 | 3 | 0.53 | 11.76 | 13.16 | 10.42 | 10.35 | 9.71 | 1.14 |
| 18 | 2.5 | 2 | 0.4 | 21.74 | 12.50 | 12.82 | 10.53 | 6.97 | 1.41 |
| 19 | 1.5 | 3 | 0.63 | 6.25 | 10.87 | 10.20 | 8.26 | 15.37 | 0.82 |
| 20 | 1.5 | 3 | 0.75 | 11.63 | 14.49 | 12.35 | 11.49 | 9.76 | 1.19 |
| 21 | 1.5 | 3 | 0.75 | 7.75 | 7.94 | 7.63 | 6.49 | 6.10 | 0.5 |
| 22 | 1.5 | 3 | 0.58 | 8.33 | 8.06 | 8.33 | 7.19 | 7.76 | 0.68 |

It can be observed that using an inlet pressure of 2.75 psig yielded a nearly constant velocity (S.no. 16), which is pretty close to what was expected. Figure 69 shows the velocities yielded by a chamber pressure of 2.75 psig at selected locations on the downstream pipe. The fifth test simulation with a chamber pressure of 2.75 psig yielded the best result with near constant velocities at all locations. For this simulation, it can be observed that water accelerated with a peak velocity of around 11.5 ft. /s at the location of two feet and then decelerated slowly. Another small peak velocity is observed at the location of eight feet. Gravity acts on the

wavefront and produces a tongue in the bottom portion as shown in Figure 70 which might be a reason for the peak velocity as water is accelerated by gravity. In another perspective, as the tongue is produced, the wetted perimeter of the water jet is reduced, when compared with the jet with a vertical wavefront, as the top portion of the wave is dragged down by gravity. With the smaller surface area in contact, water might have been additionally accelerated due to the acting pressure.

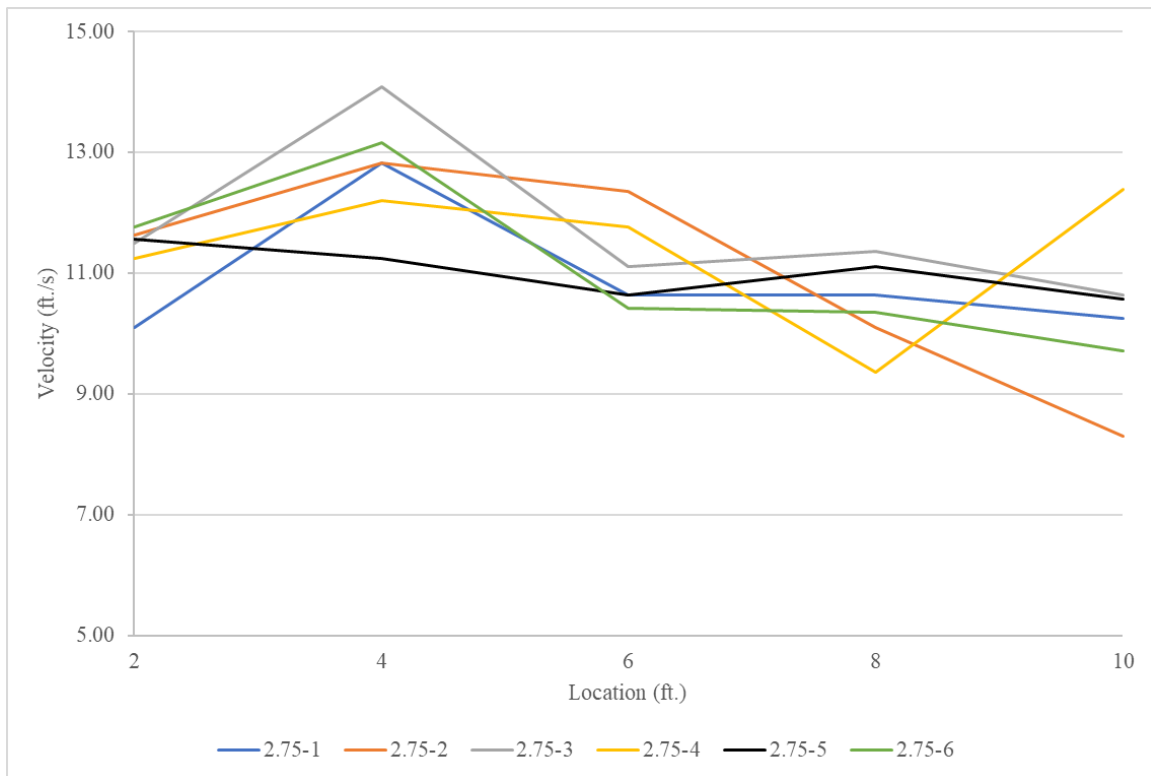


Figure 69: Velocity Results

The chamber pressures and their respective U-tube pressures are compared and presented in Figure 71. A relation between these pressures can be generated almost accurately with an equation and additionally, a correlation coefficient has been generated as shown in the figure. The correlation coefficient is quite close to unity indicating that the regression line almost perfectly fits the data.



Figure 70: Tongue produced by the wave

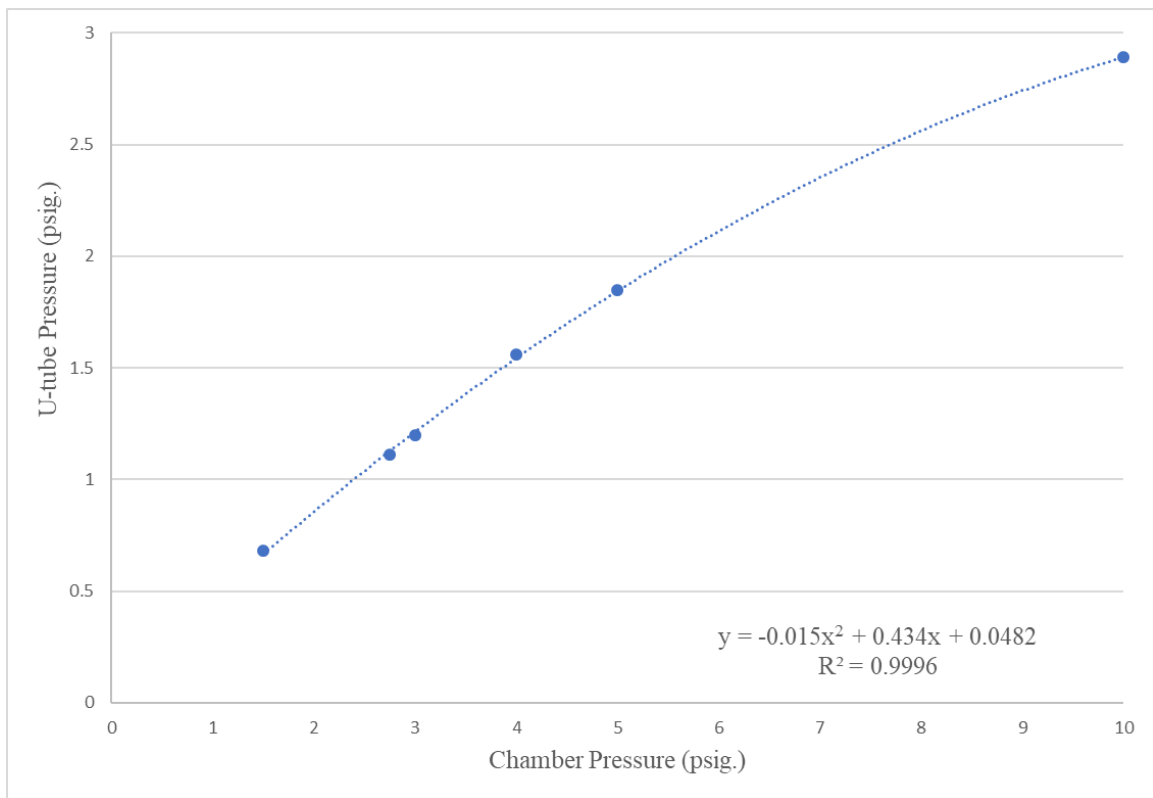


Figure 71: Chamber pressure vs U-tube pressure

These results indicate that the physical and theoretical experiments are similar to one another as shown in Table 9. This verifies the workability of air pressure to generate the motive force on the water, and, similarly, the velocity sensors proved to work very well with the ability to records velocities up to 28 feet per second.

Table 9: Physical vs theoretical results for a chamber pressure of 2.75 psig (run 5)

| Results | Theoretical | Physical |
|-------------------------------|--------------------|--------------------------------------|
| U-tube pressure (psig) | 1.09 | 1.11 |
| Velocity (ft. /s) | 11.3 | 11.57, 11.24, 10.63, 11.11,and 10.57 |

Conclusions and Future work

Wave impact testing capability for CFEL was developed further by improving past designs and conducting a physical experimental study. Numerical modeling using FLOW-3D provided insight into the behavior of water under various pressured conditions and adaptation of different geometries. Results from theoretical kinematic analysis were well matched and verified by the physical experimental study. Also, air pressure proved to be a suitable motive force, controlled by solenoid valves, and as a result, produced steady near vertical wave profiles that can be used to replicate a tsunami wave.

Numerical modeling for the designs with gates produced satisfactory wave profiles for all tested geometries, however, under the action of a constant air pressure, they failed to generate steady waves. Results show that upon adopting kinematic theories from the literature and using variable air pressure, these designs produced steady waves. WISD designs without gates were explored, which is considered to provide some flexibility during construction of the full-scale model. Numerical modeling of these configurations yielded good results producing steady waves with near vertical wave profiles. Design 10 (WD-45-1-WG) is proposed as the most viable WISD option for validation and further studies.

The physical experimental study results were identical with the theoretical kinematic approach. The waves were almost vertical and the velocity was fairly conserved. However, the numerical model of this physical experimentation, Design 20 (WD-45-1-WG-PHY), failed to achieve steady waves and the target velocity. In the physical model, a four-inch circular pipe was used with a fluid depth of one foot, which does not resemble geometric similarity with any other numerical simulations. In addition, the hydrostatic pressure within the static fluid was not considered in the theoretical kinematic approach. Additional research is required for further

improvement on this identified flaw. Moreover, the physical model developed the wave profile and attained a peak velocity ahead of the locations predicted by the kinematic theory. Further research is required to understand this behavior resulted from the physical experiments.

In the physical experiment, it was observed that the wave moved opposite to the direction of the flow for a small fraction of simulation, probably due to negative pressures in the upstream of the U-tube component. Valve 3 of the solenoid valve component provides access for the U-tube to the atmosphere to neutralize any negative or vacuum pressures. But, it could be that the flow was choked by the diameter of the pipe used. Hence, higher diameter pipes are suggested so that enough volume of air could quickly enter the U-tube and prevent negative pressures.

Future work includes the small scaled testing of prototypes that will help to identify probable design weaknesses or unexpected design complications. Once a design is finalized, full-scale WISD can perform idealized wave impacts. Data gathered from full-scale prototype testing will be used to test components for the CFEL program and hence, produce fragility data to develop probabilistic risk assessment models for NPP components and facilities.

References

- Apelt, C.J., & Piorewicz, J. (1987). Laboratory studies of breaking wave forces acting on vertical cylinders in shallow water. *Coastal Engineering*, 11, 263-282.
- Babaali, H., Shamsai, A., & Vosoughifar, H. (2015). Computational modeling of the hydraulic jump in the stilling basin with convergence walls using CFD codes. *Arabian Journal for Science and Engineering*, 40(2), 381-395.
- Dhatt, G., Touzot, G., & Lefrançois, E. (2012). *Numerical Methods, in Finite Element Method*. Hoboken, NJ, USA: John Wiley & Sons, Inc. doi: 10.1002/9781118569764.ch5
- “Directional Wave Basin.” Oregon State University, College of Engineering O. H. Hinsdale Wave Research Laboratory, Facilities. (2017) [Online] Available: http://wave.oregonstate.edu/sites/wave.oregonstate.edu/files/hwrl_data_sheet_dwb_2015_for_website.pdf
- Flammer, G. H., Jeppson, R. W., & Keedy, H. F. (1986). *Fundamental principles and applications of fluid mechanics*. Logan, Utah: Utah State University.
- Flow Science, Inc. (2017), FLOW-3D user manual: Excellence in flow modeling software, v 11.1. Santa Fe, New Mexico, USA: Flow Science, Inc.
- Goseberg, N., Wurpts, A., & Schlurmann, T. (2013). Laboratory-scale generation of tsunami and long waves. *Coastal Engineering*, 79, 57-74.
- Harlow, F. H., & Nakayama, P. I. (1968). *Transport of turbulence energy decay rate*. Los Alamos Scientific Lab., New Mexico.
- Hirt, C. W., & Nichols, B. D. (1981). Volume of fluid (VOF) method for the dynamics of free boundaries. *Journal of computational physics*, 39(1), 201-225.

- Hirt, C. W., & Sicilian, J. M. (1900). A porosity technique for the definition of obstacles in rectangular cell meshes. *International Conference on Numerical Ship Hydrodynamics, 4th.*
- Jash, S. (2018). *High-Speed Velocity Measurement Instrumentation of Air-Driven Water Jet for a Wave Impact Simulation Device* (Unpublished Master's thesis). Idaho State University, Pocatello, Idaho.
- Kirby, J. T., Özkan-Haller, H. T., & Haller, M. C. (2007). Seiching in a large wave flume. *Coastal Engineering*. 1159-1171.
- Kraatz, W. (1965). Flow characteristics of a free circular water jet. *Proceedings of the 11th Congress of the International Association for Hydraulic Research*, (1).
- Kundu, P. K., & Cohen, I. M. (2008). *Fluid mechanics*. USA: Elsevier Academic Press.
- “Large Wave Flume.” Oregon State University, College of Engineering O. H. Hinsdale Wave Research Laboratory, Facilities. (2017) [Online]. Available: http://wave.oregonstate.edu/sites/wave.oregonstate.edu/files/hwrl_data_sheet_lwf_2015_for_website.pdf
- Madsen, P. A., Fuhrman, D. R., & Schäffer, H. A. (2008). On the solitary wave paradigm for tsunamis. *Journal of Geophysical Research: Oceans*, 113(C12).
- Mayo, N. (1997). Ocean Waves-Their Energy and Power. *The Physics Teacher* 35, 352-356. doi: 10.1119/1.2344718
- Monaghan, J. J. (1992). Smoothed particle hydrodynamics. *Annual review of astronomy and astrophysics*, 30(1), 543-574.

- Nichols, L. (2018). *The Structural Design, Simulation, and Analysis of a Wave Impact Simulation Device for the Component Flooding Evaluation Laboratory* (Unpublished Master's thesis). Idaho State University, Pocatello, Idaho.
- Nimmala, S. B., Yim, S. C., & Grilli, S. T. (2013). An efficient three-dimensional FNPF numerical wave tank for large-scale wave basin experiment simulation. *Journal of Offshore Mechanics and Arctic Engineering*, 135(2), 1-10.
- Pool, R. (2011). Life begins at forty. *Engineering & Technology*, 6(9), 62-65.
doi:10.1049/et.2011.0909
- Qu, K., Ren, X. Y., & Kraatz, S. (2017). Numerical investigation of tsunami-like wave hydrodynamic characteristics and its comparison with solitary wave. *Applied Ocean Research*, 63, 36-48.
- Rabinovich, A. B., Geist, E. L., Fritz, H. M., & Borrero, J. C. (2015). Introduction to "Tsunami Science: Ten Years after the 2004 Indian Ocean Tsunami. Volume I". *Pure and Applied Geophysics*, 172(3), 615-619.
- Rabinovich, A. B., Geist, E. L., Fritz, H. M., & Borrero, J. C. (2015). Introduction to "Tsunami Science: Ten Years after the 2004 Indian Ocean Tsunami. Volume II.". *Pure and Applied Geophysics*, 172(12), 3265-3270.
- Roberts, G. D. (2017). *Research and development of a wave impact simulation device for the Idaho State University component flooding evaluation laboratory* (Unpublished Master's thesis). Idaho State University, Pocatello, Idaho.
- Savage, B. M., & Johnson, M. C. (2001). Flow over ogee spillway: Physical and numerical model case study. *Journal of Hydraulic Engineering*, 127(8), 640-649.

- Taghavi, M., & Ghodousi, H. (2016). A Comparison on Discharge Coefficients of Side and Normal Weirs with Suspended Flow Load using FLOW3D. *Indian Journal of Science and Technology*, 9(3).
- Van Gent, M.R.A. (2015, July). The New Delta Flume for Large Scale Testing. *Hydrolink*, 48-50. Retrieved from <https://www.deltares.nl/app/uploads/2015/02/THE-NEW-DELTA-FLUME-FOR-large-scale-testing.pdf>
- Versteeg, H. K., & Malalasekera, W. (2007). *An introduction to computational fluid dynamics: The finite volume method*. England: Pearson Education.
- Yakhot, V., & Smith, L. M. (1992). The renormalization group, the ϵ -expansion, and derivation of turbulence models. *Journal of Scientific Computing*, 7(1), 35-61.

Appendix A : Artificial wave generation references



O. H. HINSDALE

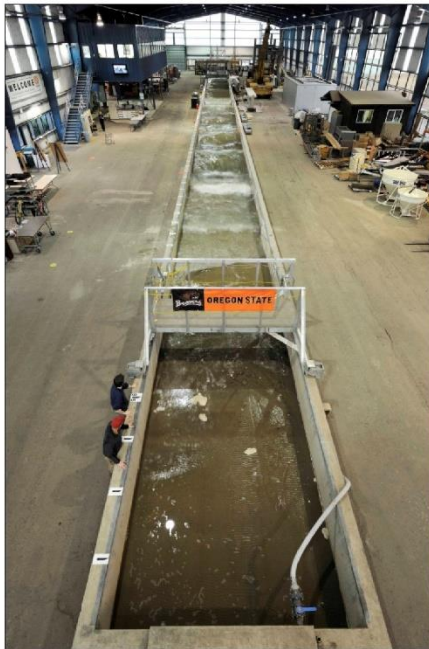
WAVE RESEARCH LABORATORY

O R E G O N S T A T E U N I V E R S I T Y

Large Wave Flume

The Large Wave Flume is the largest of its kind in North America. Because of its size and ability to operate in high Reynolds regimes, the flume is ideally suited for:

- Scaled shallow water hurricane and storm wave conditions
- Long wave and tsunami generation
- Active wave absorption for large reflected waves
- Minimizing tank seiche for long duration studies



Wave Flume

- Length: 104 m 342 ft
- Width: 3.7 m 12 ft
- Depth: 4.6 m 15 ft

Wavemaker

- Type: Piston-type, Hydraulic Actuator Assembly
- Wave Types: Regular, Irregular, Tsunami, User Defined
- Period Range: 0.8 to 12 seconds
- Max Wave: 1.7 m (5.6 ft) @ 5 sec in max 2.7 m water
1.4 m (3.9ft) tsunami in max 2.0 m water
- Max Stroke: 4 m (13.1 ft) at 4 m/s (13.1 ft/s)

Instrumentation Carriage

- Powered carriage with full cross-shore traverse
- Carriage-mounted vertical instrument deployment frame
- Lightweight carriage for video and lighting applications





O. H. HINSDALE

WAVE RESEARCH LABORATORY

O R E G O N S T A T E U N I V E R S I T Y

Directional Wave Basin

Previously known as the Tsunami Wave Basin, was designed to understand the fundamental nature of tsunami inundation, tsunami-structure impact, harbor resonance and to improve the numerical tools for tsunami mitigation.

In addition to tsunami research, the facility is particularly suited for general testing of coastal infrastructures, nearshore processes research, wave hydrodynamics, floating structures and renewable energy devices.

The wave machine is a unique powerful snake-type system made of 29 boards with up to 2.1 m long stroke. It has been designed to generate short- and long-period multidirectional high quality waves.



Wave Basin Dimensions

- Length: 48.8 m 160 ft
- Width: 26.5 m 87 ft
- Max depth: 1.37 m 4.5 ft
- Freeboard: 0.6 m 2.0 ft

Wavemaker

- Type: Piston-type, Electric motor
- Waveboards: 29 boards, 2.0 m (6.6 ft) high
- Wave types: Regular, Irregular, Tsunami, Multidirectional, User defined
- Period range: 0.5 to 10 seconds
- Max. Wave: 0.75 m (2.5 ft) in 1.37 m (4.5 ft) depth
- Max. Stroke: 2.1 m (6.9 ft)
- Max. Velocity: 2.0 m/s (6.6 ft/s)

Supporting infrastructure

- 7.5 T capacity bridge crane
- Instrumentation carriage, spans 26.5 m
- Unistrut installed in floor and sides to secure models
- Two access ramps, 14 ft width (4.2 m)
- Steady flow currents installed on project-by-project basis



THE NEW DELTA FLUME FOR LARGE-SCALE TESTING

BY MARCEL R.A. VAN GENT

The new Delta Flume in Delft was constructed to facilitate large-scale physical model testing. The new Delta Flume has a length of about 300m, a width of 5m and a height of 9.5m. The maximum significant wave height that can be generated is about $H_s = 2.2\text{m}$ and maximum individual wave heights in the range between $H_{\text{max}} = 4\text{m}$ and 4.5m . This unique facility enables physical modelling at prototype-scale or at close-to-prototype scale. Preventing or diminishing scale-effects is especially important for coastal structures in which sand, clay, grass or other natural construction material is being applied. Besides projects with dikes and dunes, structures such as breakwaters, bed protections, monopiles, offshore wind farms, and storm surge barriers are scheduled to be tested. Along with new facilities also new measurement techniques have been developed, both for the new Delta Flume and for the other wave facilities (e.g. wave basins). The new Delta Flume completes a set of wave facilities for physical model testing consisting of small and large-scale test facilities and 2D (wave flumes) and 3D (wave basins) facilities.

Introduction

To determine the response of coastal structures such as dikes, dunes, dune-revetments, breakwaters, cobble & gravel beaches, intake & outfall structures, offshore windfarms and bed protections, under loading of waves and/or currents physical model testing is an essential part of the design and evaluation process of such structures. Some aspects require modelling at a large scale since the materials and/or physical processes cannot be modelled properly on a small scale using Froude's scaling law.

Examples of materials that cannot be modelled properly at a small-scale are sand, clay, grass or natural construction material (e.g. brushwood). Physical processes that cannot be modelled properly at a small-scale are often related to flow characteristics that do not scale according to Froude's scaling law, e.g. for structures in which laminar (porous) flow plays an important role results may be affected by scale-effects. Nevertheless, tests at small-scale can provide valuable indicative results although for accurate quantitative results large scale models are still

Figure 1 - Examples of projects in the Delta Flume



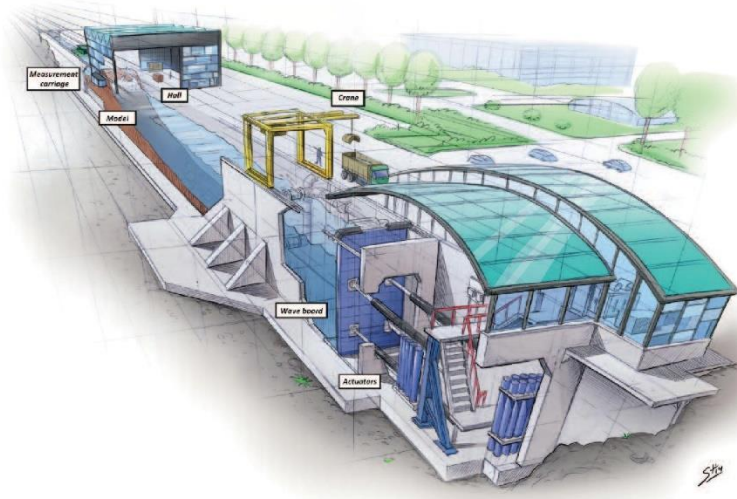


Figure 2 - Impression of the new Delta Flume (courtesy mr Stephan Timmers)

required. Many types of coastal structures can be modelled sufficiently accurate at small scales, e.g. most rubble mound breakwaters.

Besides the scale of models it is important to determine whether the structures can be modelled in a 2D model (wave flumes) or need to be modelled in a 3D model (wave basins). Often combinations of 2D and 3D models are applied, e.g. where cross-sections of structures are optimized in a wave flume, while 3D aspects are studied afterwards in a separate 3D model. Also the combination of small-scale tests and large-scale tests may be an efficient way to determine the performance of coastal structures for those structures in which some of the characteristics would be affected by scale-effects in smaller models. Therefore, it is essential to have a set of small-scale and large-scale facilities available, as well as 2D (wave flumes) and 3D facilities (wave basins). Not only the facilities are important, also the measurement equipment and experienced staff are key factors of the success of physical model tests. In Van Gent (2014) an overview of projects in the various physical model facilities is given.

Projects In The Old Delta Flume

In the old Delta Flume (240m*5m*7m) a large number of projects has been performed in the last 35 years. In these projects the choice for this facility has been based mainly on the need to limit or avoid scale-effects in physical model tests. The new Delta Flume in Delft (300m*5m*9.5m) has been constructed to facilitate measurements at an even larger scale. Figure 1 shows examples of projects performed in the old Delta Flume: Wave impacts on vertical walls, wave overtopping at dikes with grass, the dynamic behaviour of cobble beaches, the stability of placed-block revetments, the residual strength of clay-dikes, breakwater stability, dune erosion, and wave damping by brushwood mattresses. Other typical studies in the Delta Flume are related to for instance the validation of numerical models, testing and calibration of field measurement equipment, and the stability of pipeline covers.

Besides consultancy projects many research projects in the Delta Flume

have been performed and resulted in information on the performance of coastal structures, for instance:

- Placed-block revetments
- Grass slopes under wave attack
- Residual strength of dikes
- Dune erosion
- Gravel and cobble beaches
- Wave impacts on vertical walls
- Geotubes and geocontainers.

The New Delta Flume

The main characteristics of the new Delta Flume compared to the old Delta Flume are that the maximum wave height that can be generated is higher, the length is increased, tidal water level variations can be generated, and the new Delta Flume is close to the other wave facilities in Delft. One of the main advantages of the new Delta Flume over the old Delta Flume is that scale-effects are further reduced; a larger portion of the projects can be performed at (close-to) prototype scale. Figure 2 provides an impression of the new Delta Flume.

Flume dimensions The flume has a total length of about 300m. The size was determined based on tests that have been performed in the old Delta Flume. The modelling area has a total depth of 9.5m for a length of 183m, and an extra 75m section of 7m deep. The deep part has a length that is sufficient to model structures such as dikes while the combination with a shallower section allows for modelling of gentle foreshores over a length of about 250m in combination with for instance dunes. For the majority of the projects the water depth at the wave board will be between 2.5m and 8m. The flume is 5m wide.

Wave conditions The maximum wave heights that can be generated are about $H_{m0} = 2.2m$ and maximum individual wave heights in the range between $H_{max} = 4m$ and $4.5m$. The optimal water depth at the wave board for reaching the highest significant wave height for which also the wave height distribution is modelled accurately, is estimated at 6.9m. Spectral significant wave heights larger than $H_{m0} = 2.2m$ can be generated but these will cause some side wall overtopping. Irregular and regular waves, as well as some more special wave conditions can be generated (e.g. for

Tsunami modelling and focussed waves). It is expected that irregular wave conditions with standard spectral shapes (e.g. Jonswap) will be generated in the majority of experiments, so that during the design of the wave generator emphasis was put on precise specification of this type of wave conditions. Increasing wave height, wave period and water depth require more wave generating power, more wave board stroke and larger flume depths. In Hofland et al (2013) the percentage of water defences in The Netherlands that can be modelled at full scale is discussed. It is estimated that the new Delta Flume is capable of generating sufficiently large wave heights to cover about 85% of the Dutch sea dikes at prototype scale under design conditions. This means an increase in number of Dutch dike sections that can be tested at full scale of about 50% compared to the old Delta Flume.

To generate the large wave heights (e.g. $H_{m0} = 2.2\text{m}$) with the corresponding wave periods (e.g. $T_p = 9.4\text{s}$), a certain wave board stroke is needed. However, waves will reflect from the structures in the wave flume. To absorb these reflected waves with our active reflection compensation system (ARC, see also Wenneker et al, 2010), also a part of the wave board stroke is needed. The stroke of the new wave board is 7m, allowing for the mentioned significant wave height in combination with space to absorb waves that are reflected by structures in the flume.

Wave generator To generate the waves that are required a piston-type wave board was selected because of its good performance for coastal applications. The wave board is of the dry-back type. A hydraulic system was opted for. Four actuators are applied to better distribute the forces that the board will experience. The wave generator utilizes Degree of Freedom (DOF) control on the four actuators to accurately control the linear motion of the board while zeroing out unwanted board deflections such as twisting or bending due to hydrodynamic forces and board compliance. The length of an actuator is 24.5m when fully extended. A novelty in the new Delta Flume is that a tidal variation in the water level is possible by filling and emptying the flume during an experiment. The maximum filling discharge is $1\text{ m}^3/\text{s}$.

Measurements Various measurement techniques are acquired and developed to extract data from the experiments in the flume (Hofland et al,

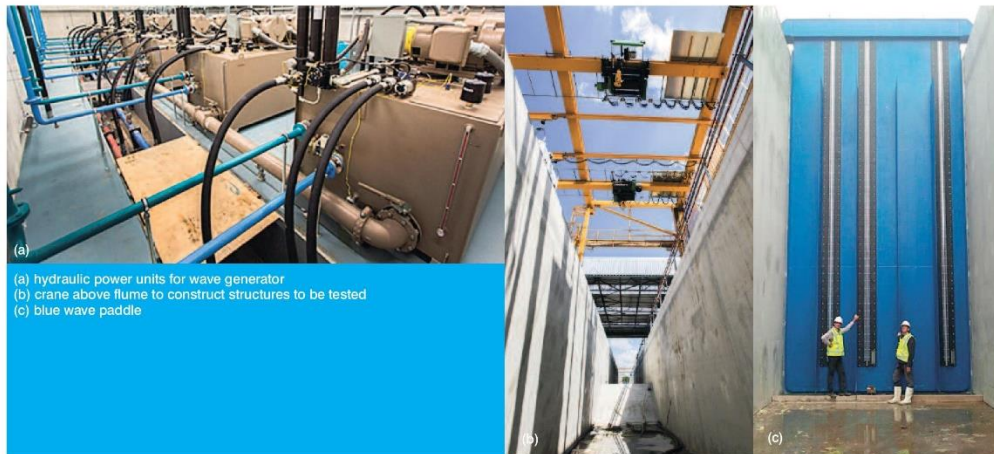


Dr Marcel R.A. van Gent is a specialist in the field of coastal engineering, in particular coastal structures, wave modelling, dikes and dunes. He obtained his PhD at the Delft University of Technology in 1995 on the modelling of reshaping rubble mound coastal structures and gravel beaches. Dr Marcel van Gent is now head of the department 'Coastal Structures & Waves' at Deltares, Delft. His is leading a group that consists of about 35 scientists and assistants for performing physical model tests in wave flumes and wave basins, developing numerical wave models, and providing specialist consultancy services. Since 1991 Marcel van Gent participated in various research projects, including projects for the European Union, for the Dutch Government, and in co-operation with Universities, Consultancy firms, and Contractors. Dr Marcel van Gent published about 100 international scientific papers on coastal structures, wave modelling and dune erosion.

2012). Besides classic point measurements, also synoptic measurement techniques (i.e. high resolution measurements of time-varying spatial fields) have been developed. For the measurements of waves (at the wall) the proven resistance-type wave probes are used. Radars will be used to obtain wave height measurements at any location. In addition, the use of laser scanners and stereo matching of video images can be used to obtain spatially distributed information of waves and/or (deformed) structures. Also good visual observation of the tests is ensured using for instance a central video observation system and many (flush) cavities in the wall near the location of most models to install instruments.

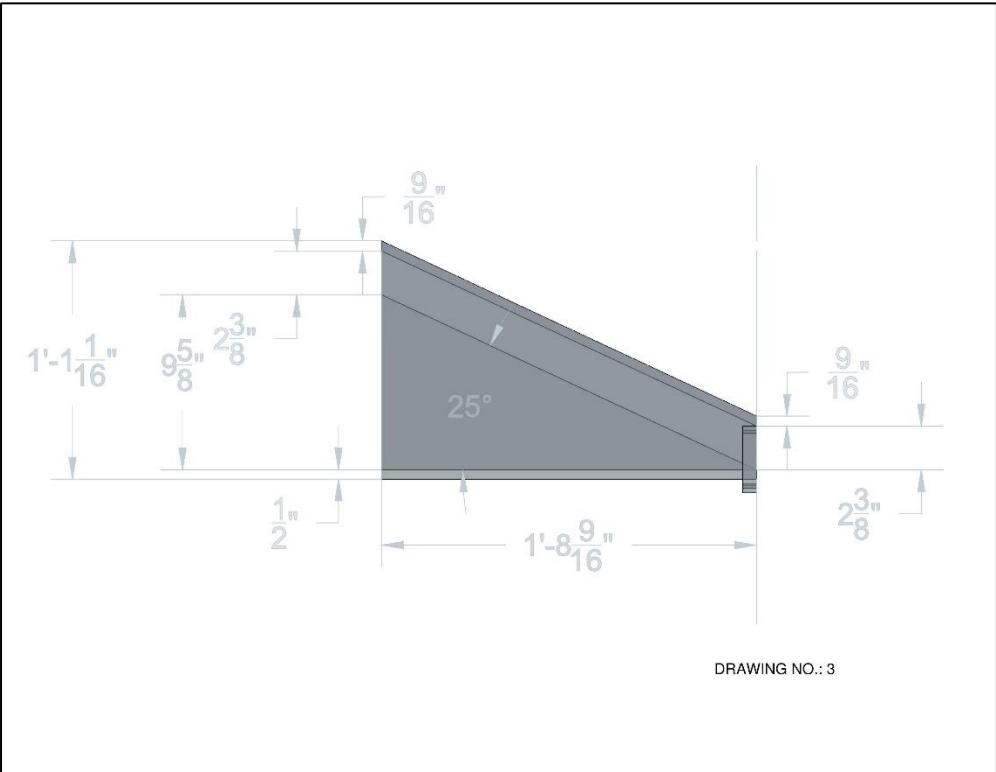
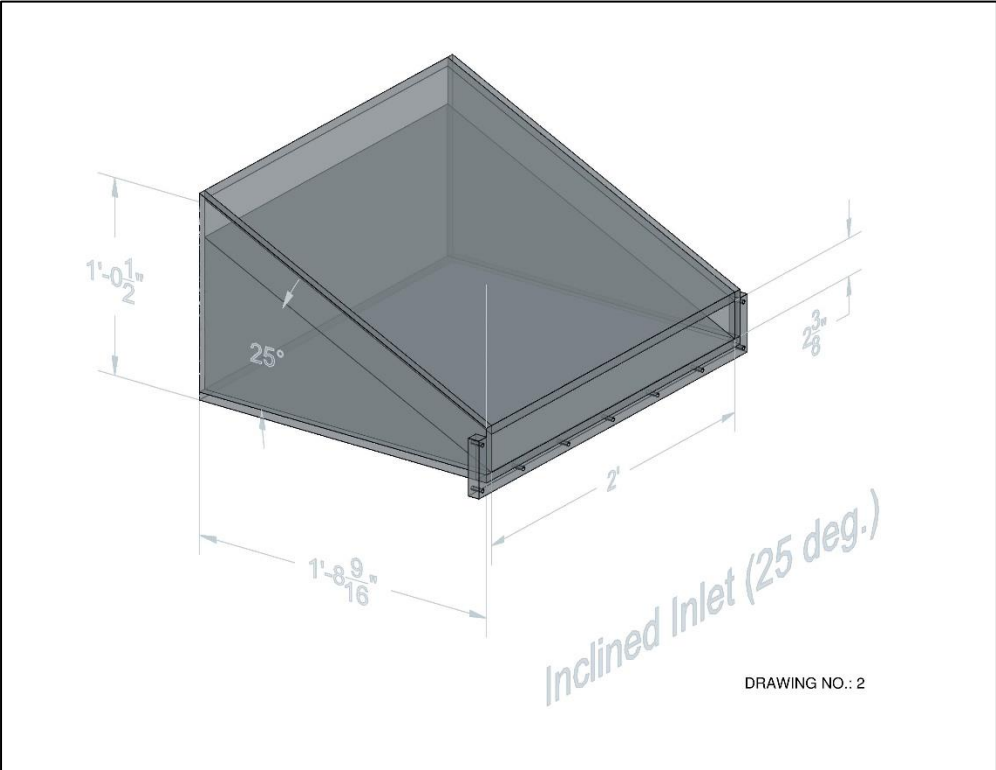
REFERENCES

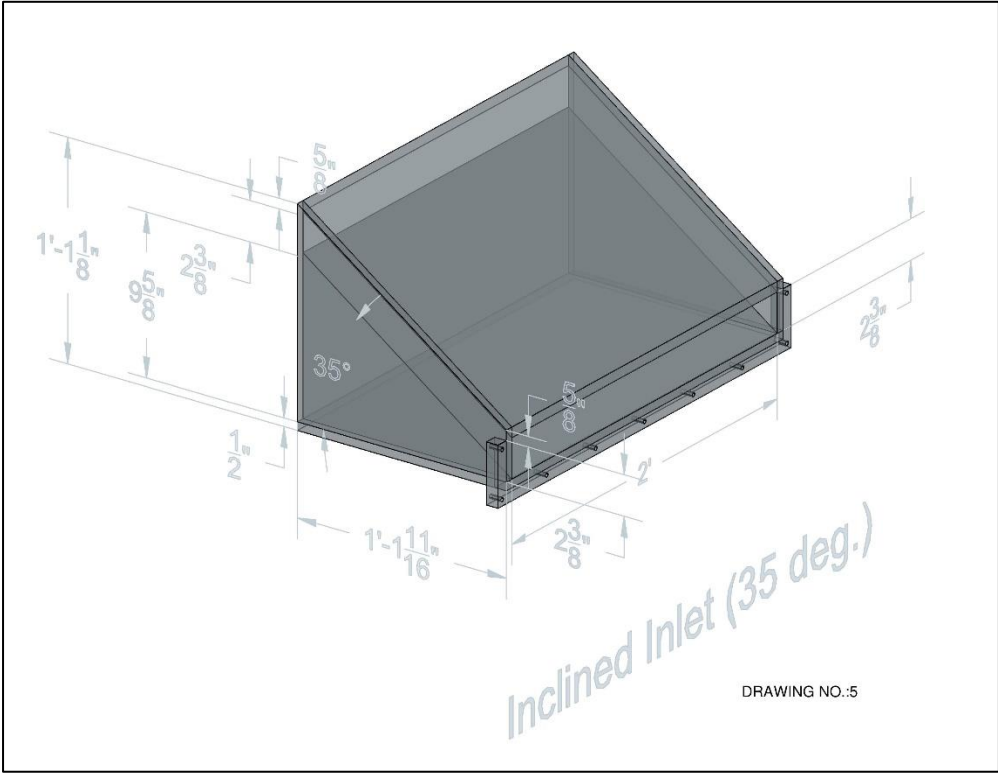
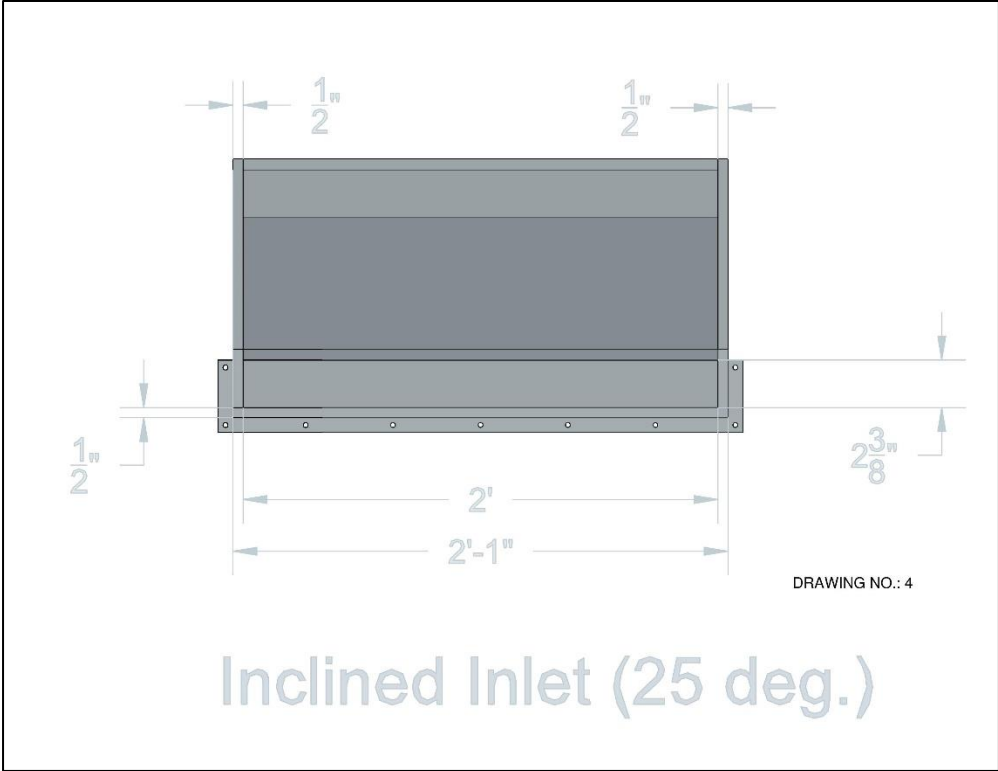
- Hofland, B., R. Hoffmann and R. Lindenberg (2012), Wave measurement techniques for the new large-scale Delta Flume. Proc. Coastlab2012, Gent.
 Hofland, B., I. Wenneker and M. van Gent (2013), Description of the new Delta Flume. Proc. Coastlines, Marne.
 Van Gent, M.R.A. (2014), Overview of physical modeling at Deltares including the new Delta Flume, Keynote, Proc. Coastlab 2014.
 Wenneker, I., J. Meesters, R. Hoffmann and D. Francissen (2010), Active Wave Absorption System ARCH, Proc. Coastlab 2010, Barcelona.

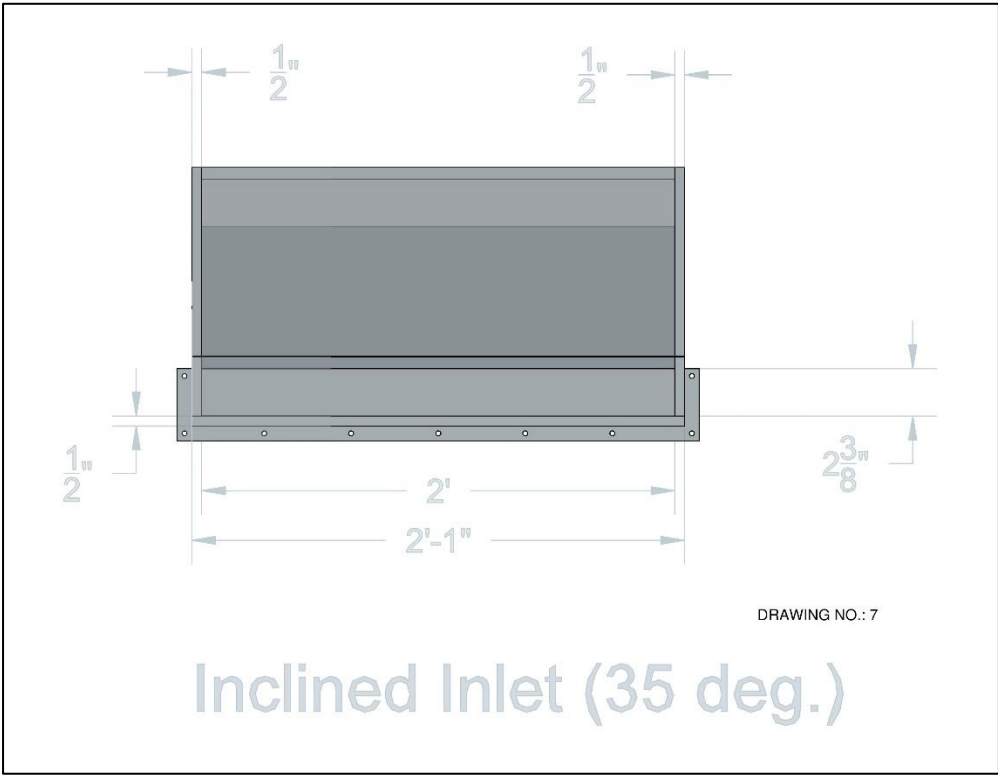
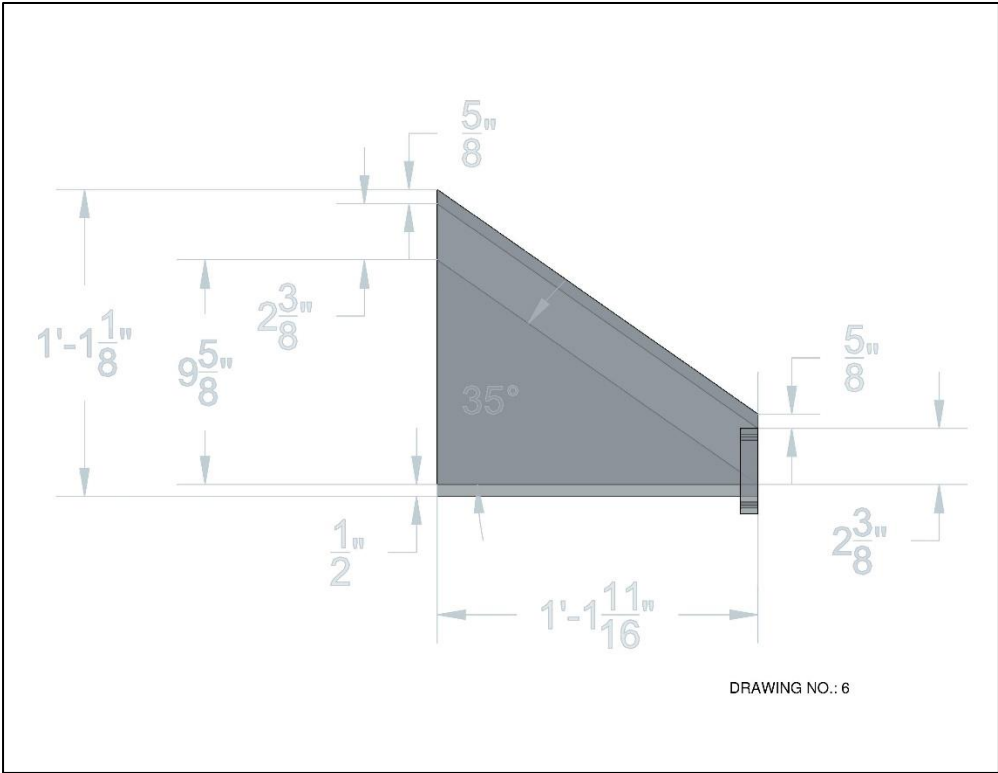


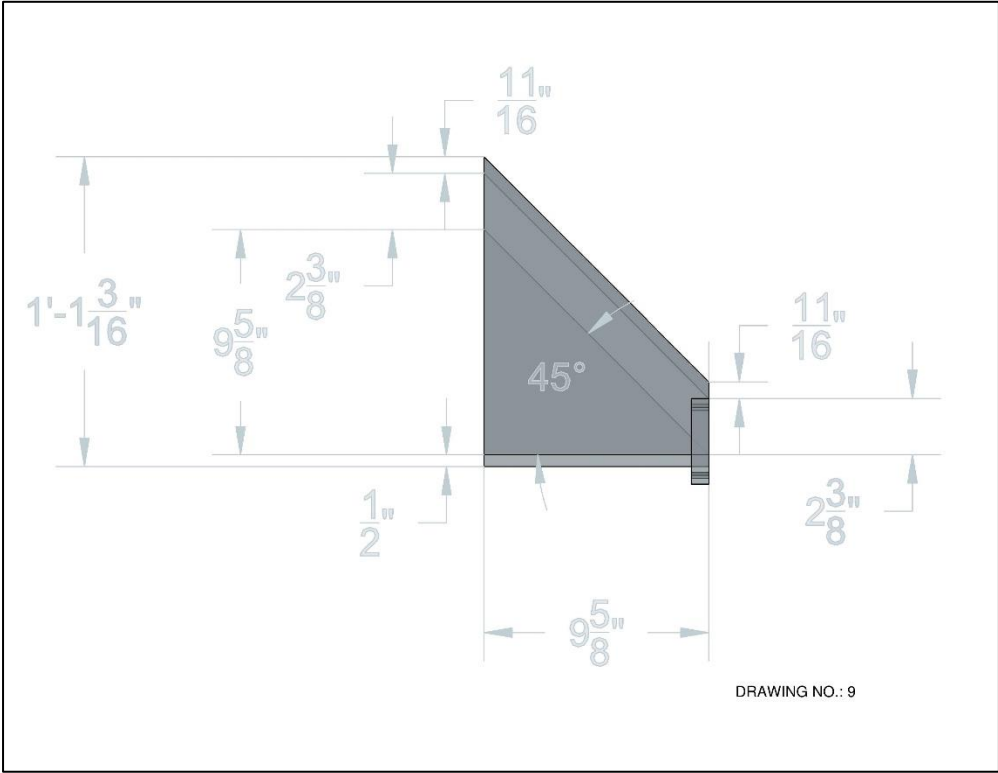
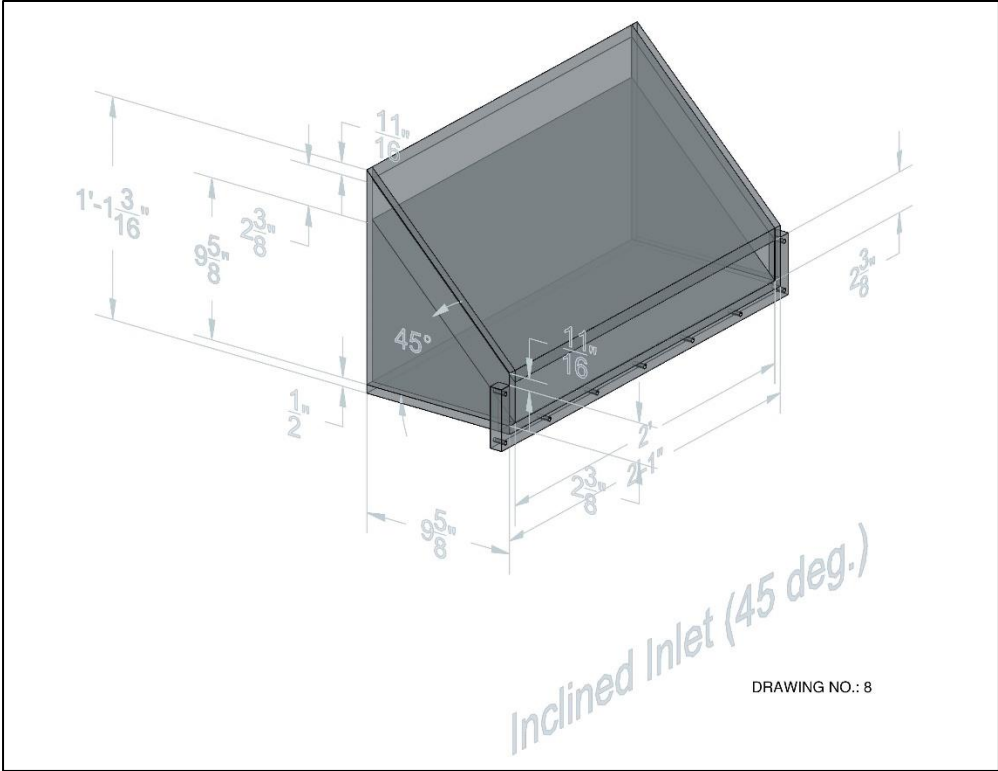
(a) hydraulic power units for wave generator
 (b) crane above flume to construct structures to be tested
 (c) blue wave paddle

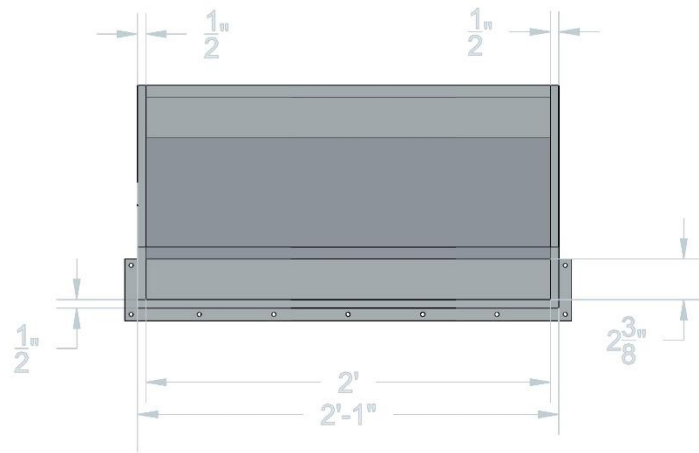
Appendix B: Drawings for sectional physical model





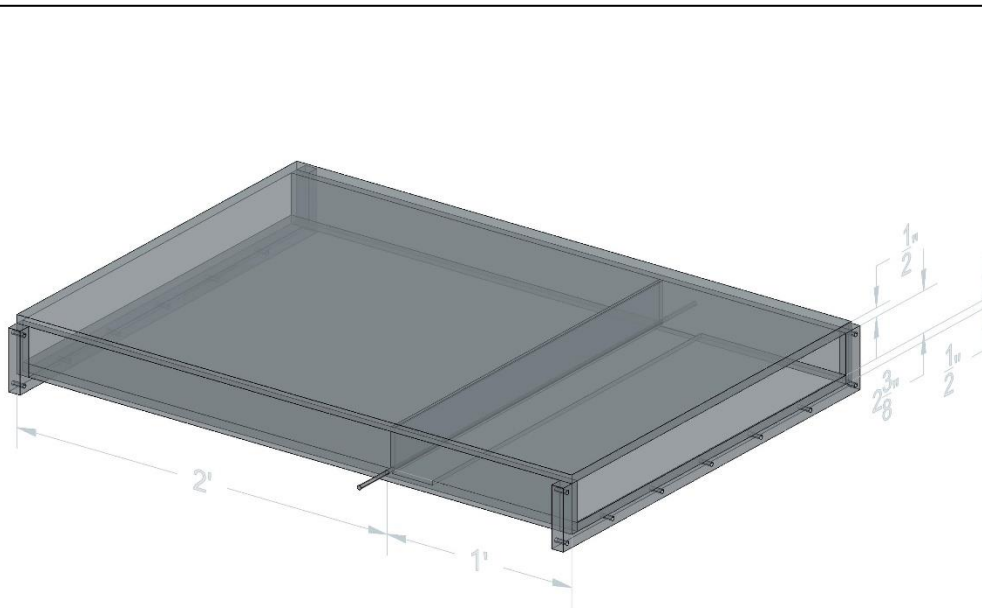




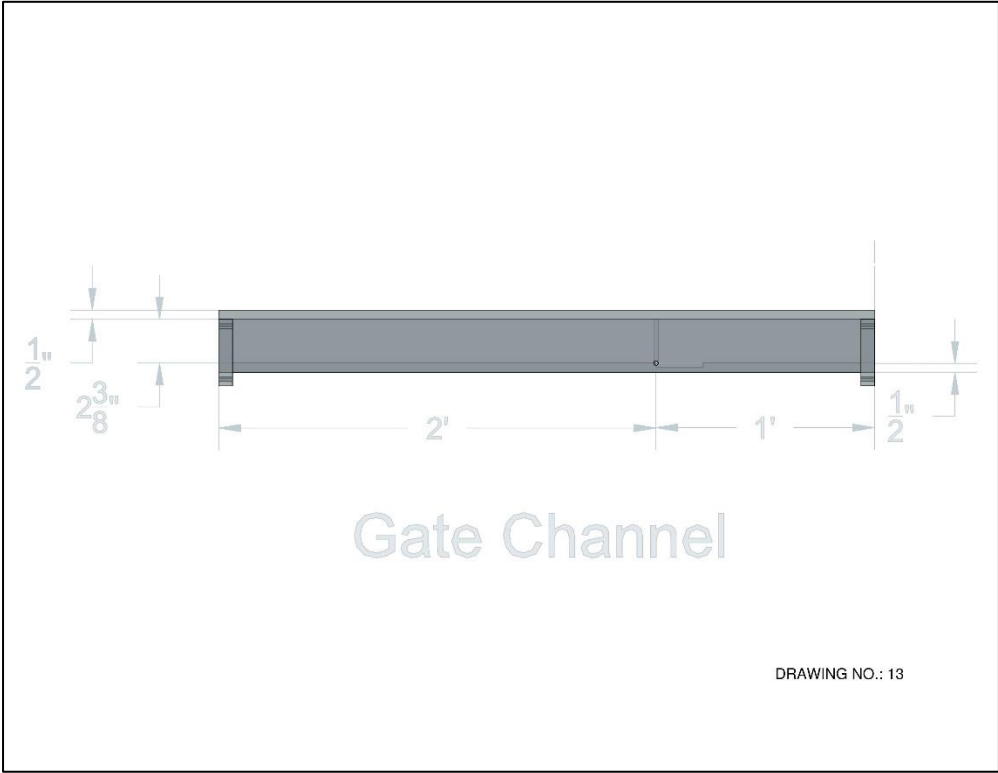
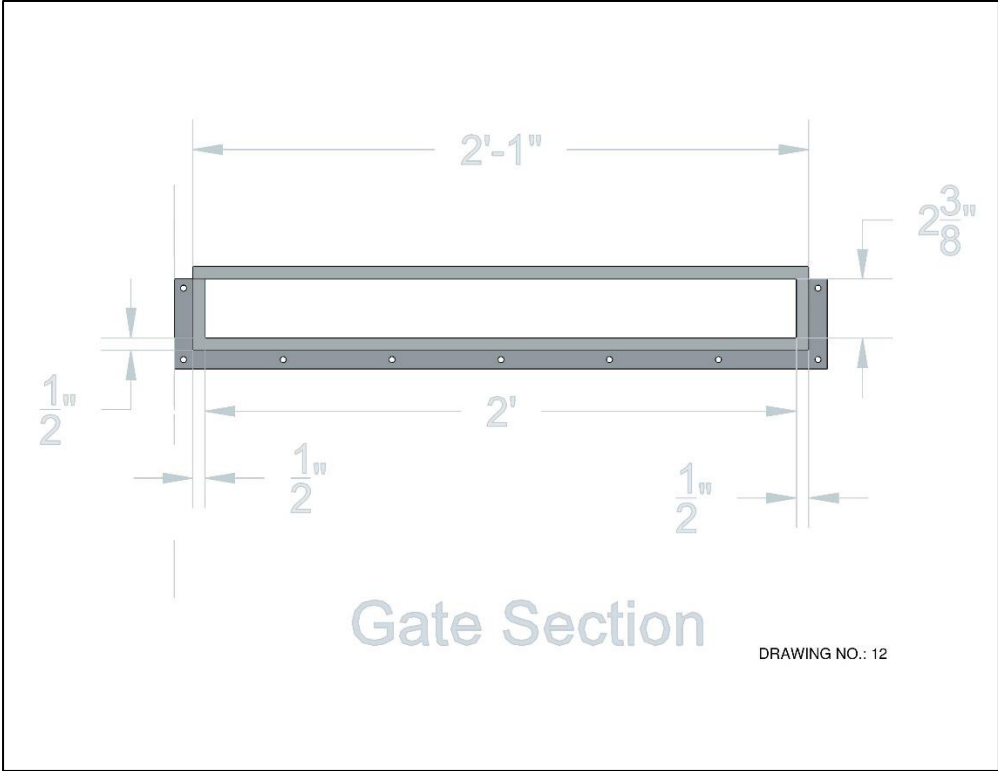


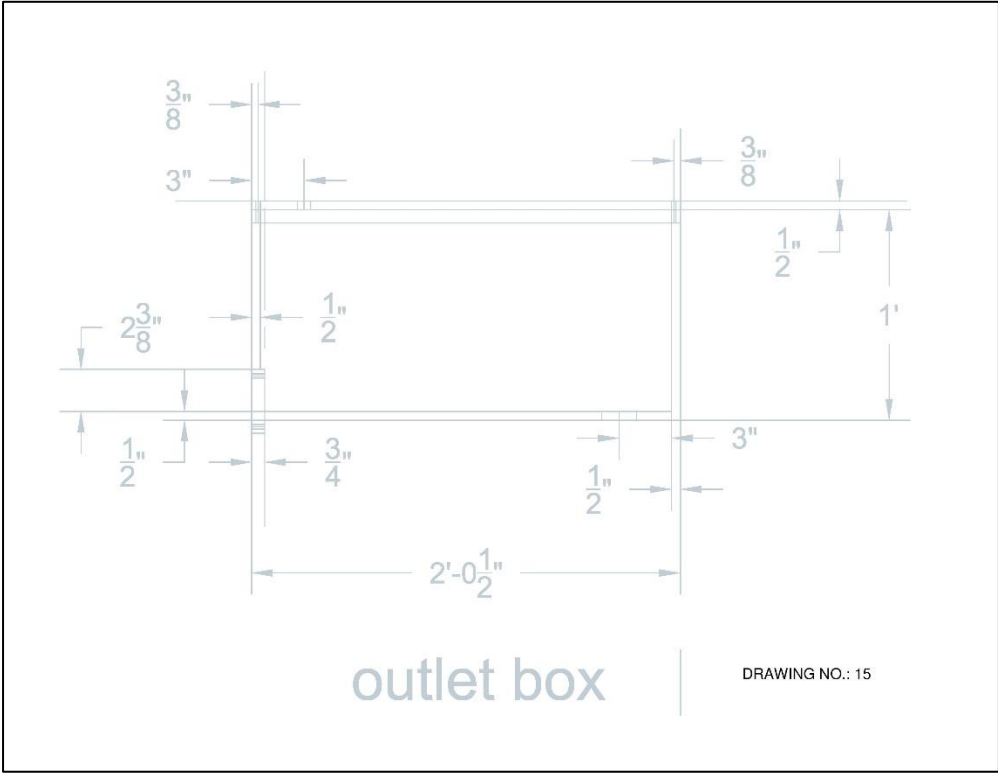
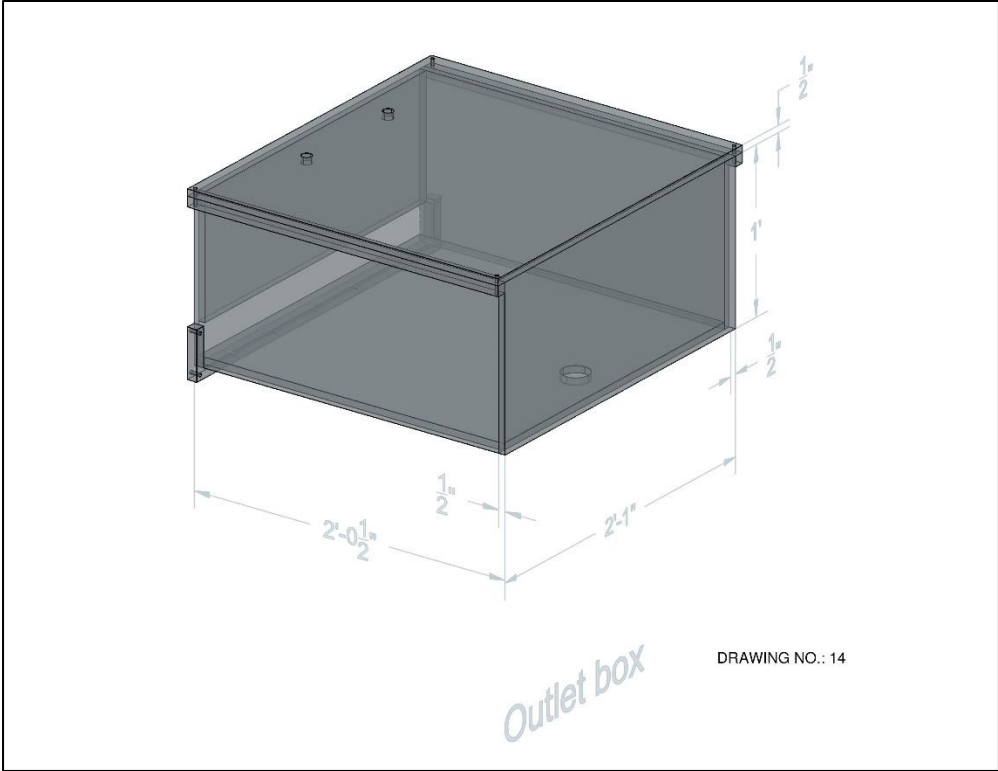
DRAWING NO.: 10

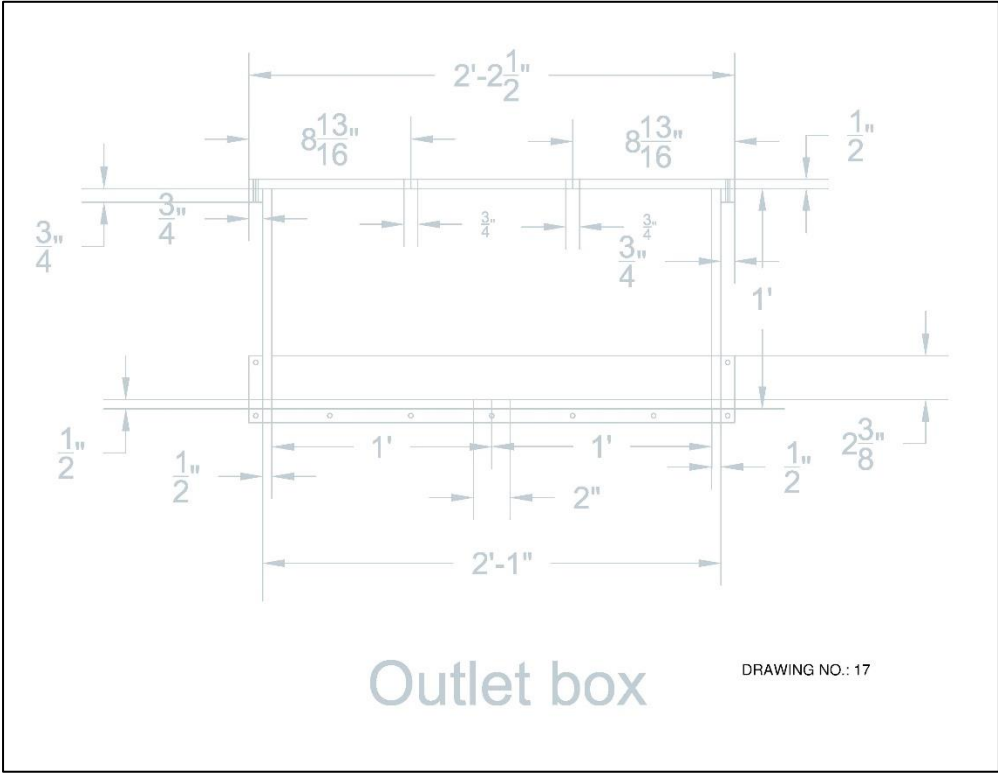
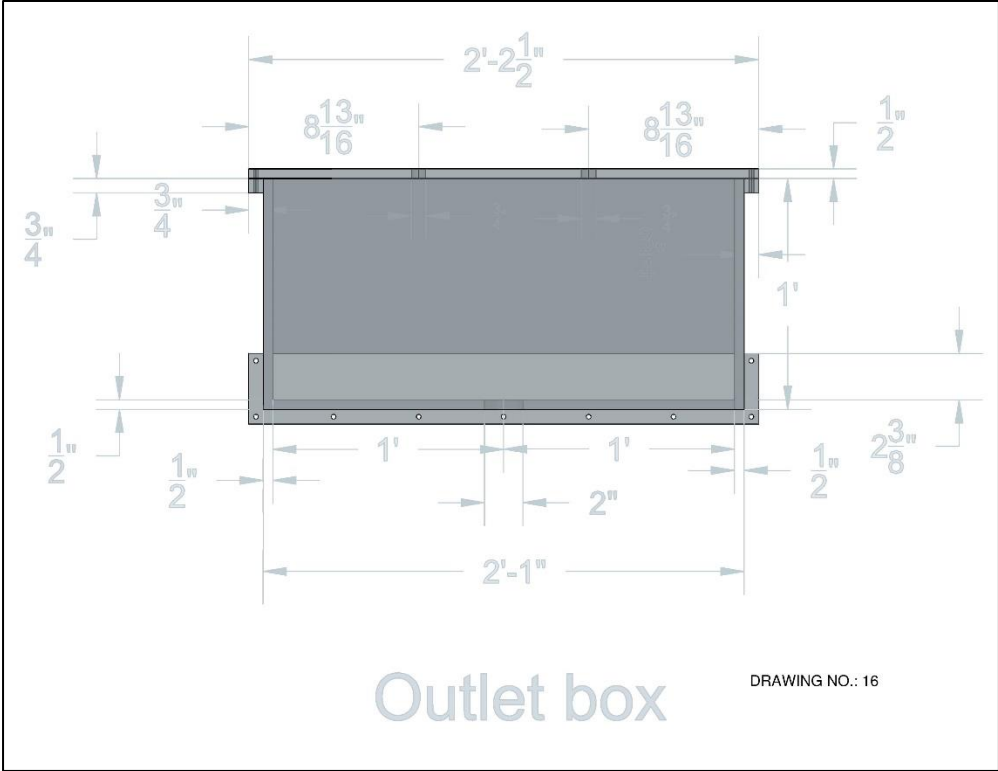
Inclined Inlet (45 deg.)

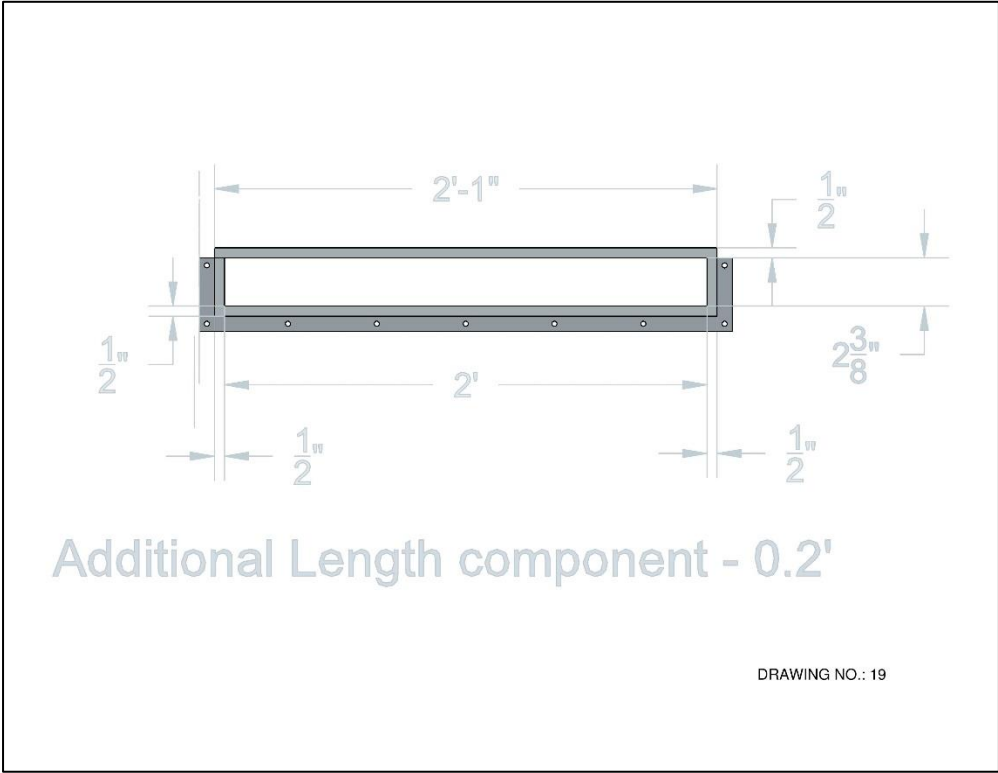
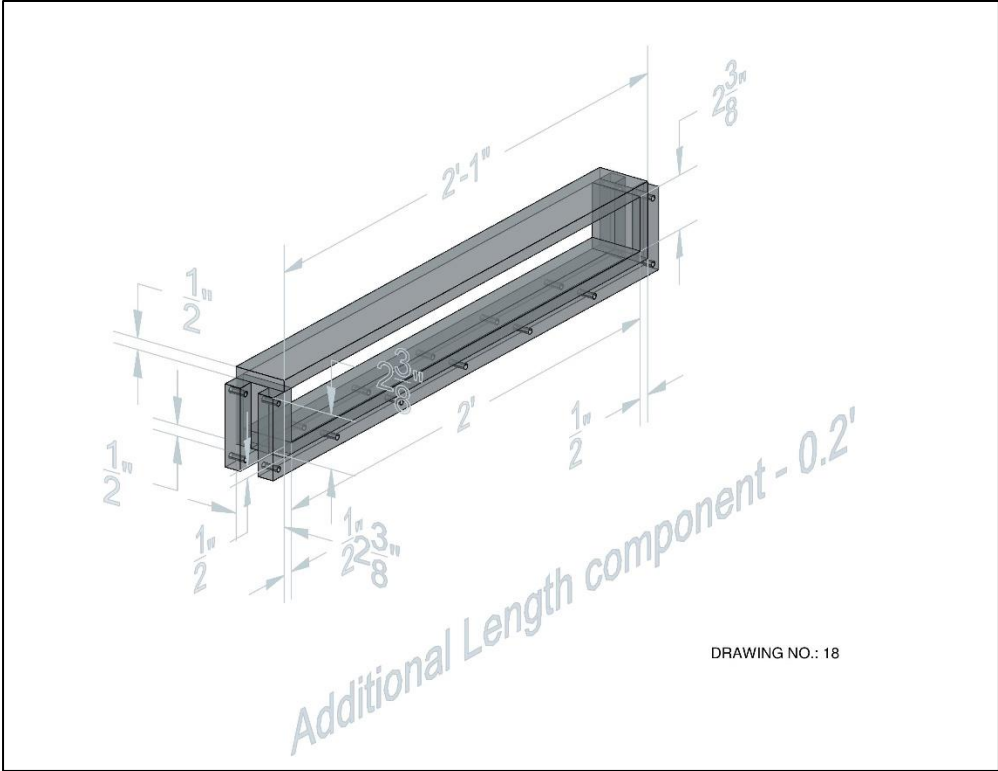


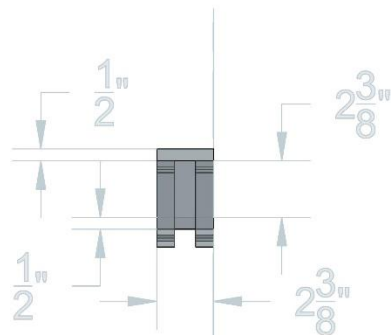
GATE CHANNEL [DRAWING NO.: 11]





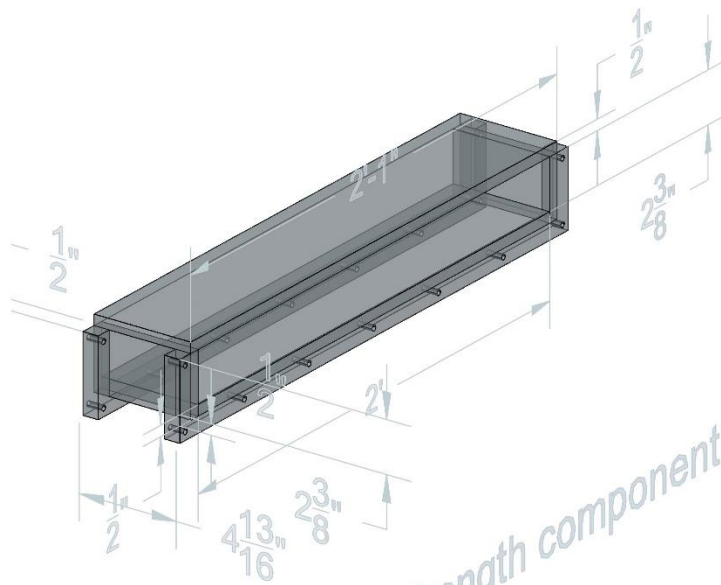






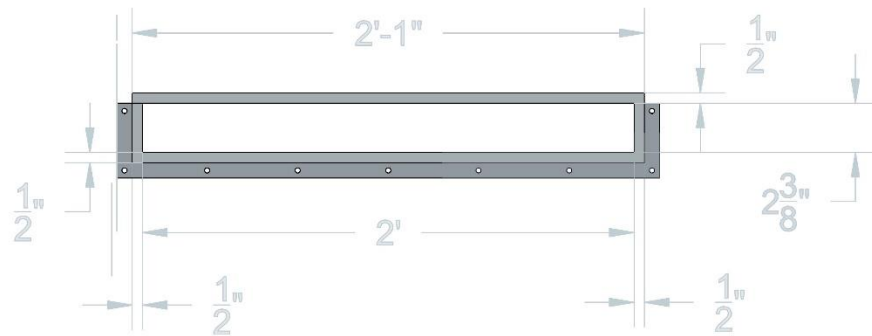
Additional Length component - 0.2'

DRAWING NO.: 20



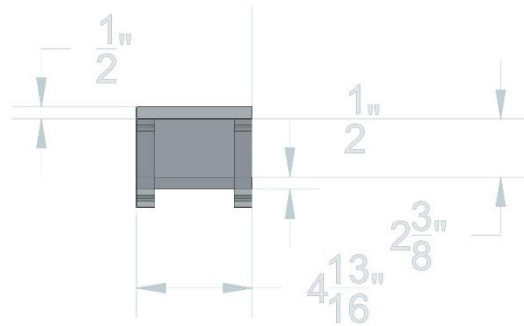
Additional Length component - 0.4'

DRAWING NO.: 21



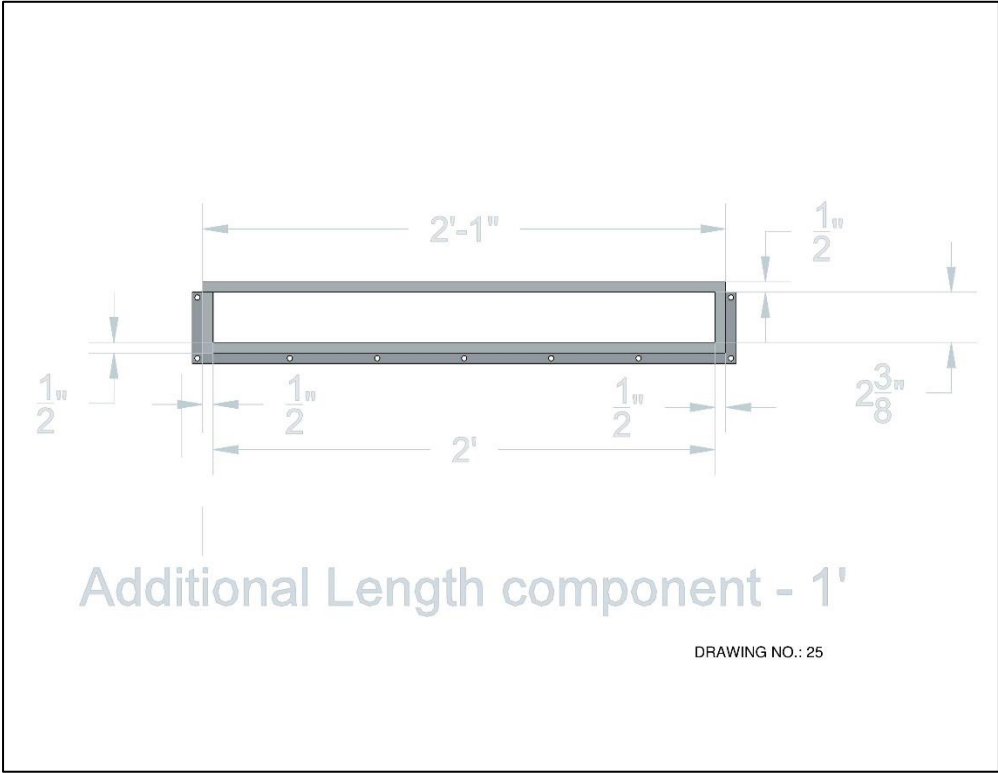
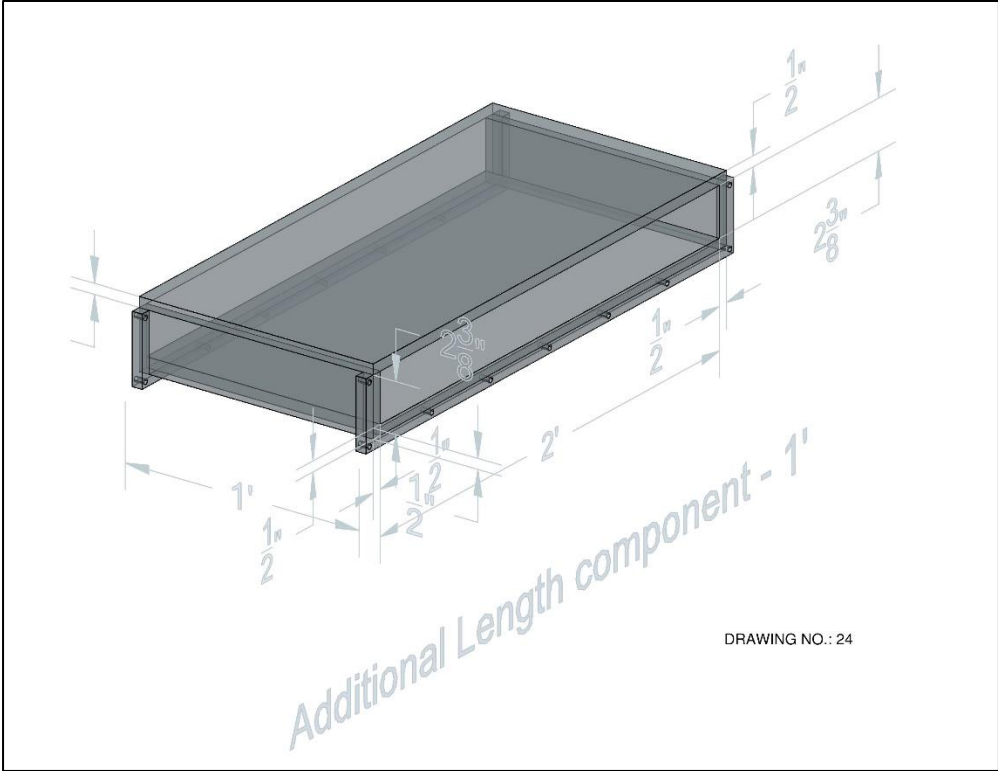
Additional Length component - 0.4'

DRAWING NO.: 22



Additional Length component - 0.4'

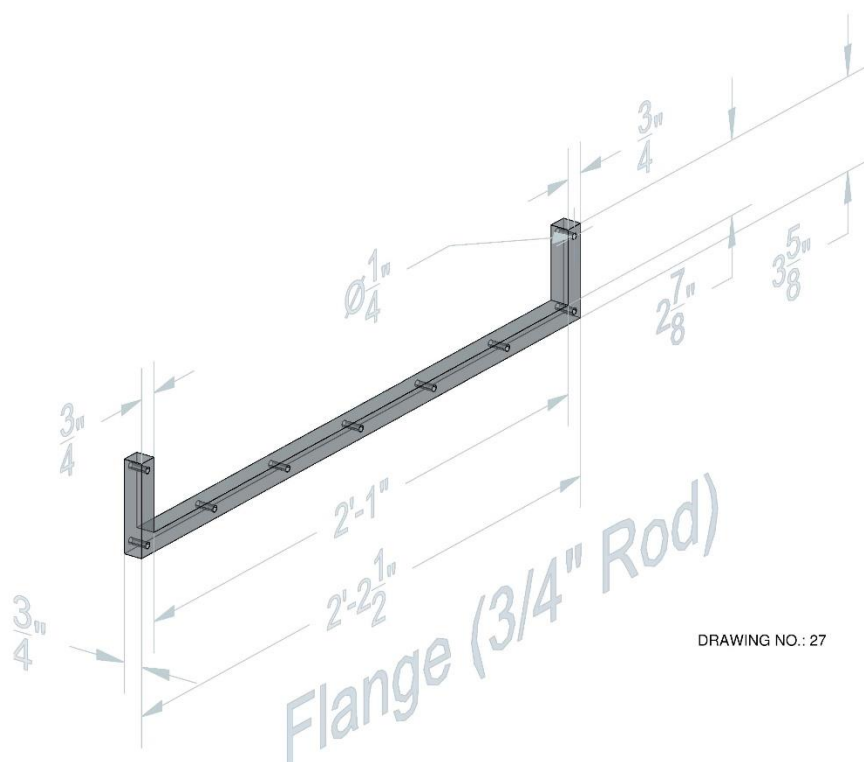
DRAWING NO.: 23



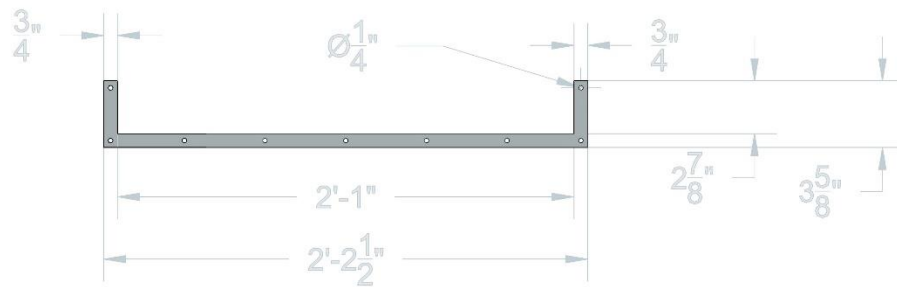


Additional Length component - 1'

DRAWING NO.: 26



DRAWING NO.: 27



Flange (3/4" Rod)

DRAWING NO.: 28

Appendix C: Pressure transducers



| Specifications | |
|-------------------------|---|
| Product Type | Digital Pressure/Vacuum Gauge |
| Temperature range (° F) | 14 to 122 |
| Temperature range (° C) | -10 to 50 |
| Media compatibility | Gas |
| Wetted materials | 316 SS |
| Enclosure rating | IP67 |
| Unit of Measurement | psi, in .Hg, mm Hg, kPa, mPa, Pa, mbar, bar, kg/cm ² , in. WC, mm WC, oz/in ² , plus six customizable units |
| Range | Vac to 30 psi |
| Output | Wireless frequency: 2.4 G ISM bands, 20 meter range; chanel 1 to 15 Software: wireless network demo software included |
| Process connection | 1/4" NPT(M) |
| Accuracy | ±0.25% full-scale |
| Dial size (" Dia) | 4" |
| Case | ABS plastic |
| Power | Two AA batteries (included); 3000 hour life at 3 readings per second |
| Lens material | Polycarbonate |
| Qty/ea | 1 |
| Manufacturer number | ADT680W-25-CP30-PSI-N |
| Brand | Additel |
| CE Compliance | Yes |
| Display | 5-digit LCD, 1/2" (15 mm) H; 7-segment bar graph scaled 0 to 100% full-scale |

HIGH SPEED USB OUTPUT PRESSURE TRANSDUCER CONNECT DIRECTLY TO YOUR COMPUTER

High Speed
1000 Updates/second

Gage and Absolute Pressures
10 inH₂O to 5000 psi (25 mb to 345 bar)
Vacuum and Compound Ranges
10 inH₂O to 15 psi
Barometric and Differential Pressure Ranges

Fast
Delivery!

PX409-015GUSBH
shown actual size.

PX409-USBH Series



Standard

- ✓ 1000 Readings/Second
- ✓ Micro-Machined Silicon Sensor
- ✓ 316L SS Wetted Parts
- ✓ High $\pm 0.08\%$ BSL Accuracy
- ✓ Excellent Long Term Stability
- ✓ USB 2.0 and Below Compatible
- ✓ Standard USB Connector Termination
- ✓ Shock and Vibration Rated
- ✓ Ruggedized with Secondary Containment

The PX409 High Speed USBH Series connects directly to your computer. Free PC software enables you to chart, log, display, and output data for analysis. Also included are .NET APIs, and a command set for command-line access. The micro-machined silicon design is ideal for pressure or level applications in laboratory, test platforms, or bio/pharmaceutical applications as well as industrial applications that require a rugged, high accuracy transducer. The micro-machined silicon sensor provides a very stable transducer with exceptional high accuracy of $\pm 0.08\%$ and a broad compensated range of -29 to 85°C (-20 to 185°F). The modular construction allows for fast delivery of most configurations and fittings. Delivery is typically stock to 1 week!

SPECIFICATIONS

Accuracy: 0.08% BSL (linearity, hysteresis and repeatability combined)

Resolution: Up to 5.5 significant figures

Temperature Compensation (Over Compensated Range):

Span: Range > 5 psi: $\pm 0.5\%$

Range ≤ 5 psi: $\pm 1.0\%$

Zero: Range > 5 psi: $\pm 0.5\%$

Range ≤ 5 psi: $\pm 1.0\%$

Minimum Isolation:

100 M Ω @ 50 Vdc case to sensor

2 M Ω @ 50 Vdc case to output terminations

Pressure Cycles: 1 million, minimum

Long Term Stability (1-Year): $\pm 0.1\%$ full scale typical

A to D Conversion: 24-bit

Shock: 50 g, 11 ms half sine, vertical and horizontal axis

Vibration: 5-2000-5 Hz, 30 minute cycle, Curve L, Mil-Spec 810 figure 514-2-2, vertical and horizontal axis

Bandwidth: DC to 1000 updates per second typical ($\pm 3\%$)



2 m (6') integral
USB cable connects
directly to your PC.

PRESSURE TRANSDUCERS
USB OUTPUT
B

FREE OMEGA® USBH Downloadable Software!

OMEGA is excited to announce the release of a major software update for USB Transducers! The fresh look and added features add even more value and flexibility to your transducer's performance.

Free OMEGA PC software takes the data from the transducer directly to the digital domain, turning your laptop or Windows® tablet (with USB connection) into a virtual meter, chart recorder, or data logger.

Also included are .NET APIs and a set for command-line access. Visit <ftp://ftp.omega.com/public/DASGroup/products/USBH/> to download your free copy.*

*Includes software to run TRH Central compatible devices.

Power Consumption: 0.35 W typical

CE Compliant: Meets industrial emissions and immunity EN61326

Environmental Protection: IP65

Secondary Containment

Gage/Vacuum/Compound Pressure:

10 inH₂O to 5 psi: to 1000 psi

15 to 1000 psi: to 3000 psi

1500 to 5000 psi: to 10,000 psi

Absolute/Barometric Pressure:

5 to 1000 psia: to 6000 psia

1500 to 5000 psia: to 10,000 psia

Overpressure

Gage/Vacuum/Compound Pressure:

10 inH₂O: 10 times span

1 psi: 6 times span

2.5 psi to 1000 psi: 4 times span

1500 psi to 5000 psi: 7250 psi maximum

Absolute/Barometric Pressure:

5 psia: 6 times span

15 psia to 1000 psia: 4 times span

1500 to 5000 psia: 7250 psia maximum

Wetted Parts: 316L stainless steel

Weight: 200 g (7 oz)

Operating Temperature Range: -40 to 85°C (-40 to 185°F)

Compensated Temperature:

Ranges >5 psi: -29 to 85°C (-20 to 185°F)

Ranges ≤ 5 psi: -17 to 85°C (0 to 185°F)

Metric threads and
ranges available.

B-1

Appendix D: Additional Wavefront Images from the physical experiment



1) 3 psi – Run 4



2) 3 psi – Run 6



3) 3 psi – Run 7



4) 4 psi – Run 1